WORLD METEOROLOGICAL ORGANIZATION

GLOBAL ATMOSPHERE WATCH

WORLD DATA CENTRE FOR GREENHOUSE GASES

WMO WDCGG DATA SUMMARY

WDCGG No. 44

GAW DATA

Volume IV-Greenhouse and Related Gases

PUBLISHED BY
JAPAN METEOROLOGICAL AGENCY
IN CO-OPERATION WITH
WORLD METEOROLOGICAL ORGANIZATION

NOVEMBER 2020

CONTENTS

PREFACE

Global observations of greenhouse gases are essential for understanding of the global carbon cycle and the roles they play in driving climate change. The results of observations demonstrate gradual increase of levels of various greenhouse gases in the atmosphere which is a result of the increased emissions of greenhouse gases to the atmosphere from anthropogenic activity (such as fossil fuel combustion and deforestation) since the beginning of the industrial era in around 1750. The increasing greenhouse gas concentrations are driving detectable tropospheric warming. To avoid negative consequences of climate change, urgent action should be taken toward the reduction of greenhouse gas emissions based on scientifically robust information. Against this background, there is increased demand for greenhouse gas data to meet scientific requirements and provide reliable information for use by policy makers.

The World Data Centre for Greenhouse Gases (WDCGG) has been operated by the Japan Meteorological Agency (JMA) since 1990 in response to a request from the World Meteorological Organization (WMO). It holds the status of a World Data Centre (WDC) under the WMO Global Atmosphere Watch (GAW) programme and provides critical services to the community through data collection, archiving and distribution of data on greenhouse and related gases (such as CO) in the atmosphere and oceans from surface stations, mobile platforms and satellites worldwide. WDCGG plays a critical role in the data management system of GAW. The data are provided online with a requirement for acknowledgment or co-authorship accreditation when used in publications (see the WDCGG website for details).

Information on the global state of major greenhouse gases in the atmosphere is regularly published in the WMO Greenhouse Gas Bulletin, to which WDCGG contributes via the calculation of related global mean mole fractions, long-term trends and growth rates. The WMO WDCGG Data Summary reports on global means covered in bulletins and on latitudinal or hemispheric means and individual observational data used in global analysis. In addition to the gases covered by bulletins, the Data Summary contains information on CO and certain halogenated species.

This issue of the Data Summary covers observational data collected at surface stations and on certain ships for the period from 1968 to 2018 based on monthly mean data submitted to WDCGG by September 2019. Observational data and the results of related analysis indicate that concentrations of major greenhouse gases (CO_2, CH_4, N_2O, SF_6 and certain HCFCs and HFCs) are increasing, while those of certain ozone-depleting substances (e.g., CFCs) are not. The global mean mole fractions of CO_2, CH_4 and N_2O reached new highs of 407.8±0.1 ppm, 1,869±2 ppb and 331.1±0.1 ppb in 2018, corresponding to 147, 259 and 123% of pre-industrial levels, respectively. More detailed information is provided in the main text. The value-added analytical information presented in this Data Summary is expected to support scientific research, assessment and policy-making in relation to environmental issues.

WDCGG thanks all data contributors worldwide for their efforts in maintaining accurate long-term observations and for their ongoing data submissions. Contributors include the National Oceanic and Atmospheric Administration (NOAA) Earth System Research Laboratory (ESRL) and its cooperative air-sampling network, the Advanced Global Atmospheric Gases Experiment (AGAGE), and a variety of other observational stations operating under the framework of GAW and other monitoring programmes as listed in Appendix D. All organizations submitting data to WDCGG are acknowledged as invaluable contributors to the Data Summary.

Mailing address:
WMO World Data Centre for Greenhouse Gases (WDCGG)
c/o Japan Meteorological Agency
1-3-4, Otemachi, Chiyoda-ku, Tokyo 100-8122, Japan
E-mail: wdcgg@met.kishou.go.jp
Telephone: +81-3-3287-3439
Facsimile: +81-3-3211-3047
Website: https://gaw.kishou.go.jp/

1.

CARBON DIOXIDE

(CO_2)

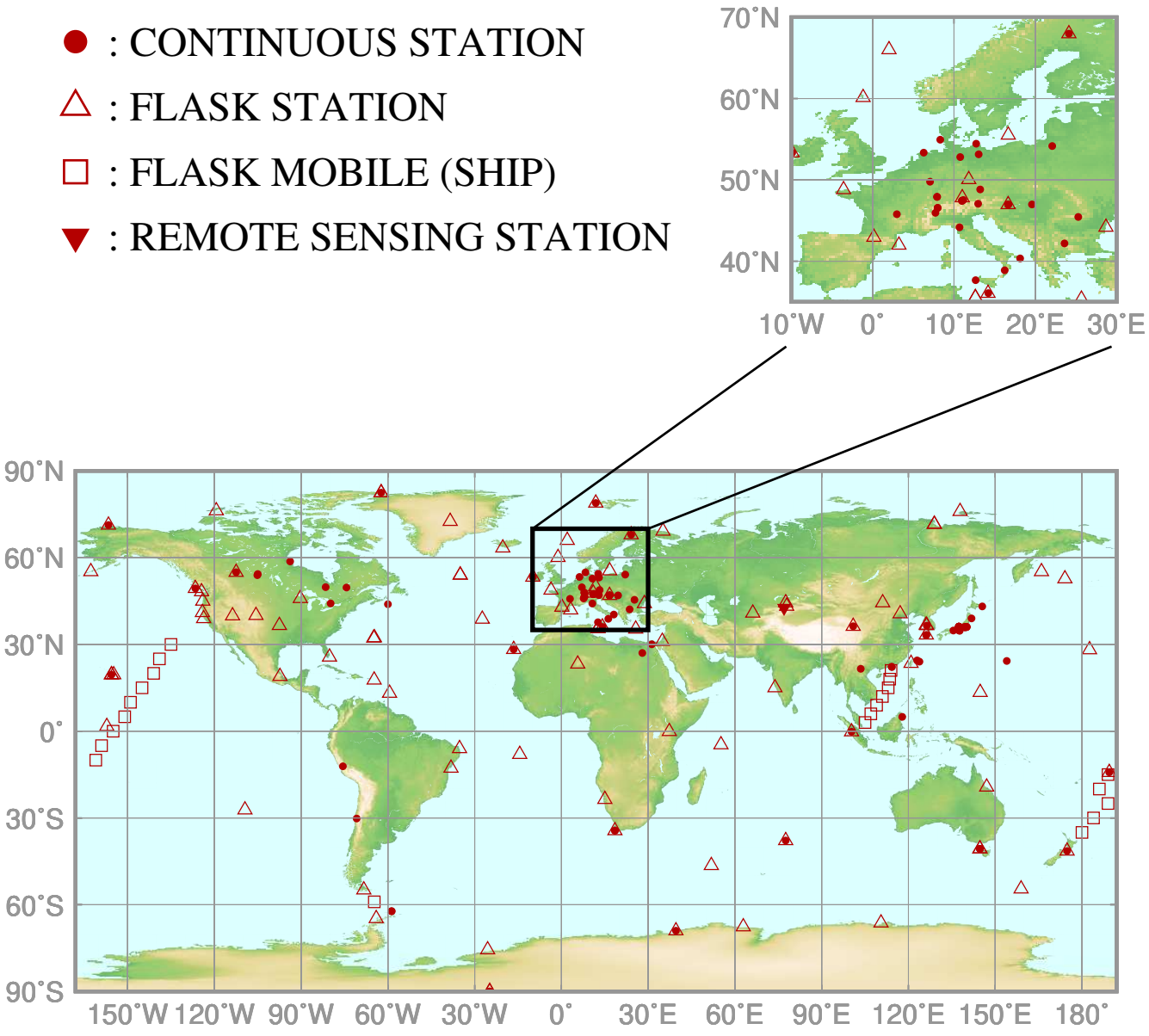

This map shows locations of the stations that have submitted data for monthly mean mole fractions.

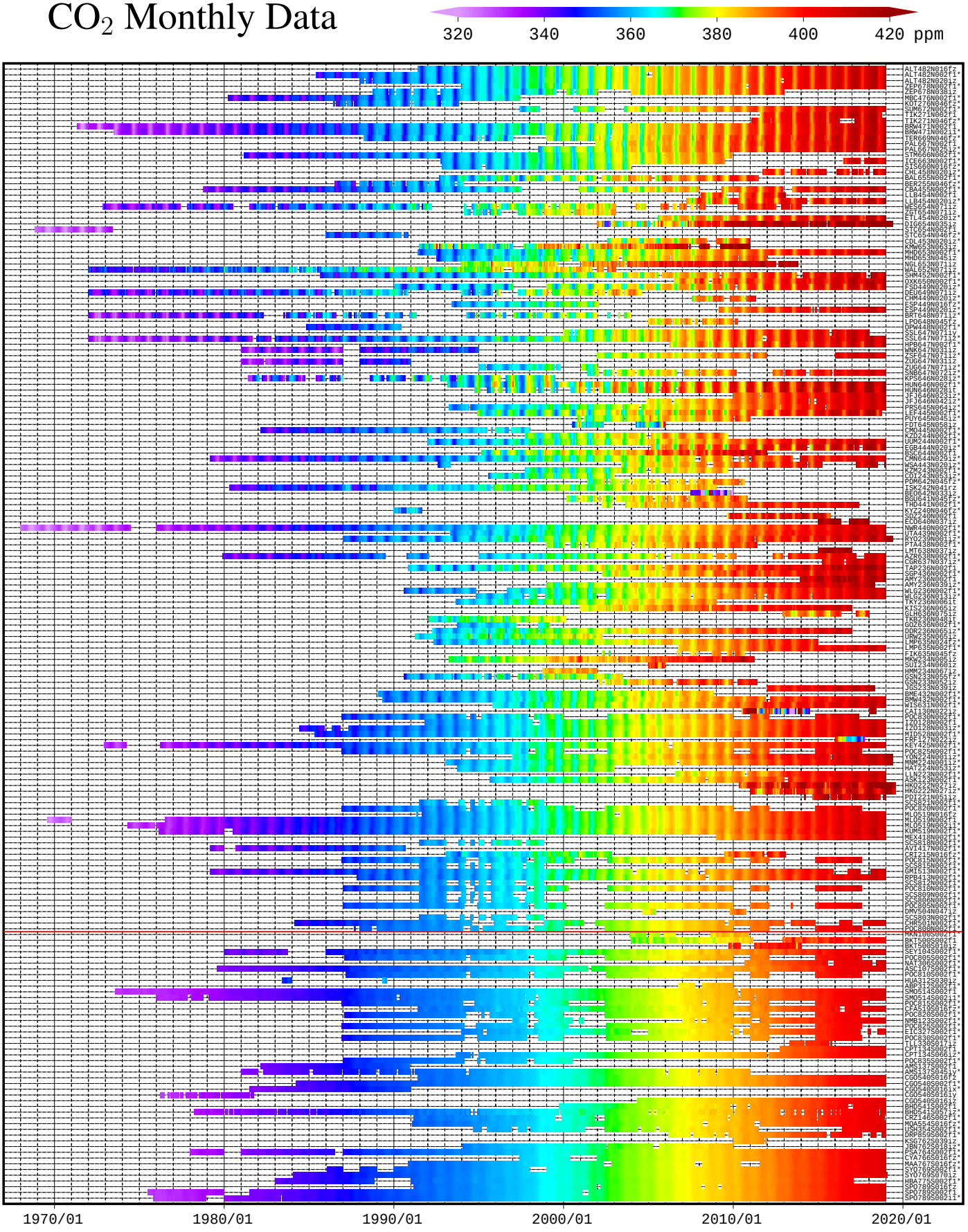

Plate 1.1 Monthly mean CO_2 mole fractions that have been reported to the WDCGG. The mole fractions are illustrated in different colors. The sites are listed in order from north to south. The red line indicates the equator. In cases where data are reported for two or three different altitudes, only the data at the highest altitudes are illustrated. In cases where monthly means are not reported, the WDCGG calculates them from hourly or other mole fractions reported to the WDCGG by simple arithmetic mean. The data from the sites with an asterisk at the end of the station index were used for the analyses shown in Plate 1.2 (see Appendix A).

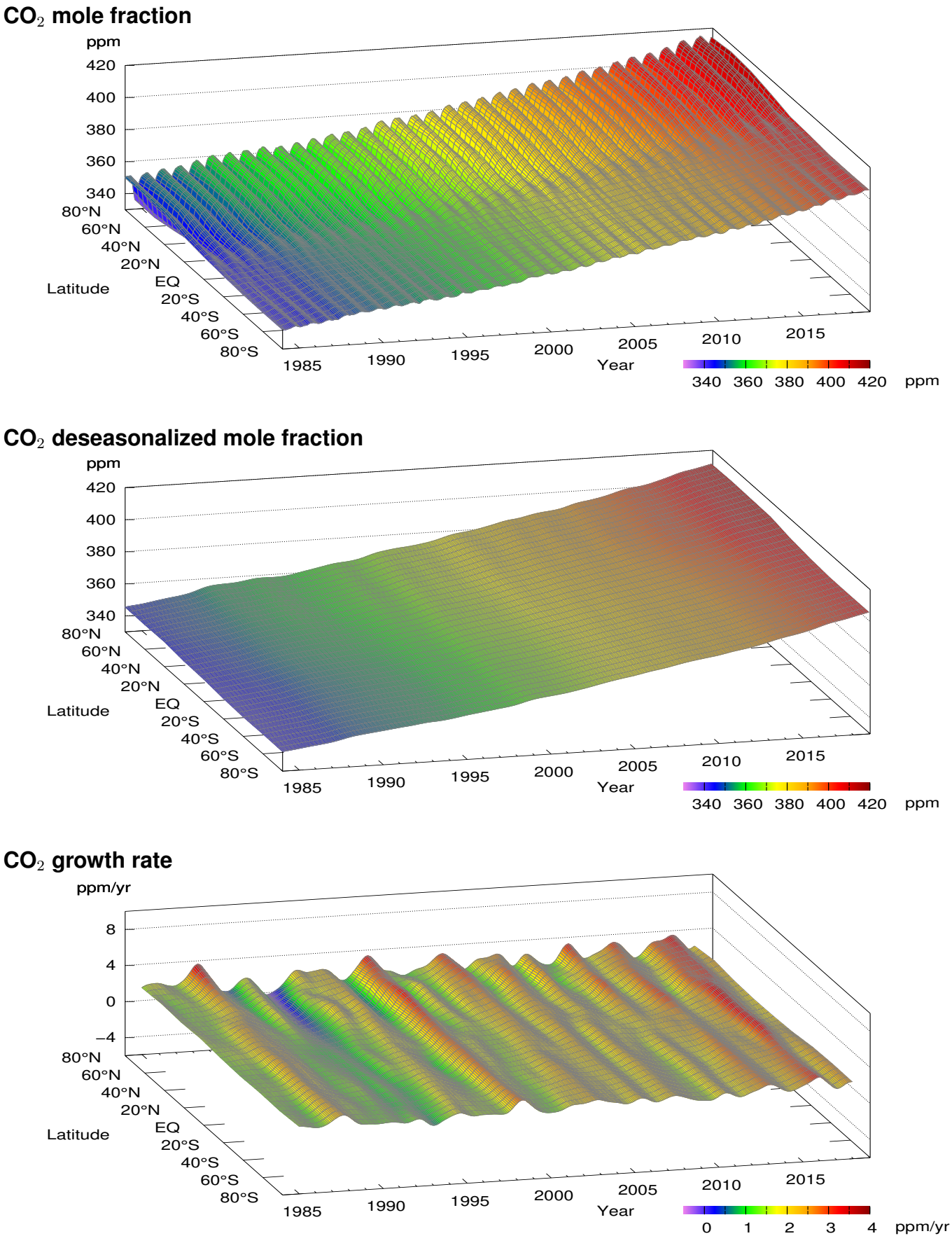

Plate 1.2 Variation of zonally averaged monthly mean CO_2 mole fractions (top), deseasonalized long-term trends (middle), and growth rates (bottom). The zonally averaged mole fractions were calculated for each 20° zone. The deseasonalized trends and growth rates were derived as described in Appendix A.

1. CARBON DIOXIDE (CO_2)

Atmospheric mole fractions of carbon dioxide (CO_2) – the most significant long-lived greenhouse gas related to anthropogenic activities – have been increasing since the beginning of the industrial era in around 1750. The global mean mole fraction of CO_2 reached a new high of 407.8±0.1 ppm in 2018, representing an increase of 2.3 ppm from the previous year. This mole fraction constitutes 147% of the pre-industrial level of 278 ppm as inferred from ice-core studies. CO_2 is responsible for around 66% of radiative forcing (relative to the pre-industrial era) caused by long-lived greenhouse gases (WMO, 2019).

The increase in CO_2 mole fractions is primarily attributable to human activity, particularly fossil fuel combustion, cement production and deforestation. Around half of anthropogenic CO_2 emissions are removed by the biosphere and oceans, and the rest remains in the atmosphere. The balance between emissions and sinks determines the annual CO_2 increment in the atmosphere. The red columns in Fig. 1.1 show the observed growth rate for atmospheric CO_2 dry mole fractions, and the green line shows theoretical growth rates for CO_2 based on the assumption that all annual anthropogenic carbon emissions remain in the atmosphere. The lack of correlation between these time-series representations suggests significant interannual variations in absorption via land and/or ocean sinks. A comprehensive understanding of the mechanisms that control various CO_2 sources/sinks and their current states is of key importance in providing a scientific foundation for strategies to combat climate change.

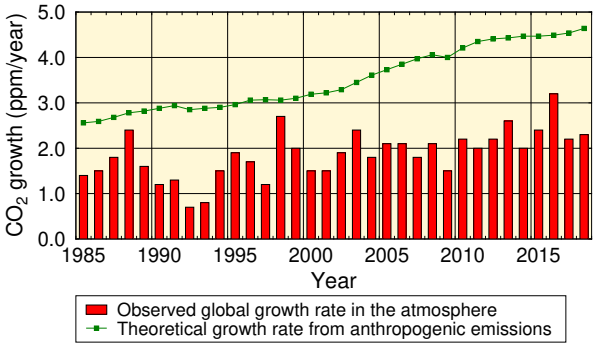

Fig. 1.1 Annual mean growth rates for CO_2 in the atmosphere calculated from observational data (red columns), and theoretical rates driven by anthropogenic emissions (green curve). The theoretical data were calculated taking CO_2 emissions as a proxy (from the Global Carbon Project (Friedlingstein *et al*., 2019)), expressed as moles divided by the total mass of gas in the atmosphere (5.2 petatonnes) converted to moles based on the mean molar mass of dry air (about 29.0 g/mol). The observed growth rates were calculated by WDCGG. CO_2 abundance from observational data is expressed as mole fractions with respect to dry air, while that estimated from anthropogenic emissions is based on atmospheric data, including water vapor, usually in a proportion less than 1%.

Global mean mole fractions

The blue dots in Fig. 1.2 show global mean CO_2 monthly averaged mole fractions (top) and related growth rates (bottom). The red line in the top panel shows the long-term trend after removal of seasonal cycles from the monthly averages shown by the blue. Details of the analysis are provided in Appendix A.

Throughout the period for which observation data are available, the CO_2 mole fraction shows a continuous increase accompanied by characteristic seasonal cycles, with higher values from boreal winter to spring and lower values in summer. The seasonal cycle of CO_2 mole fractions is mainly driven by activity in the terrestrial biosphere, where plant photosynthesis is active in summer and large amounts of CO_2 are consumed, while plant respiration and organic-matter decomposition in soil

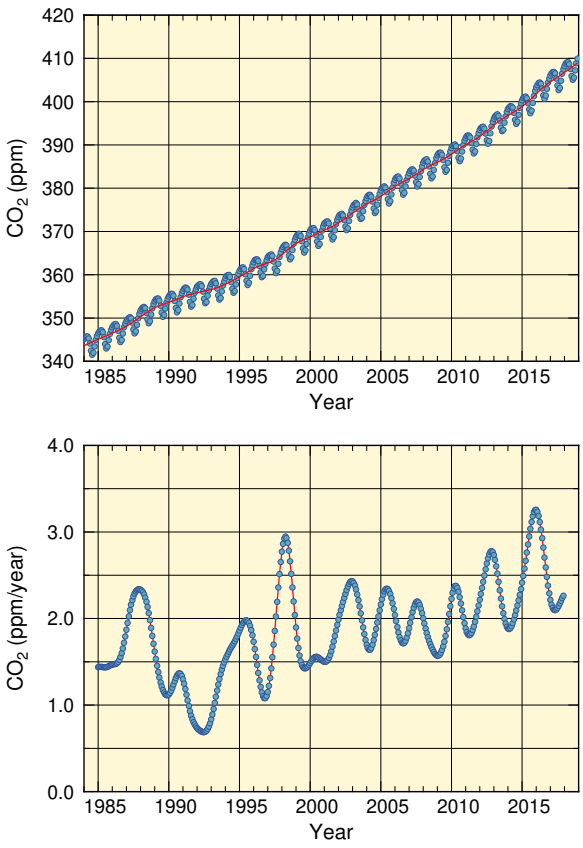

Fig. 1.2 Globally averaged monthly mean mole fraction of CO_2 from 1984 to 2018 and the deseasonalized long-term trend shown as a red line (top), and its growth rate (bottom).

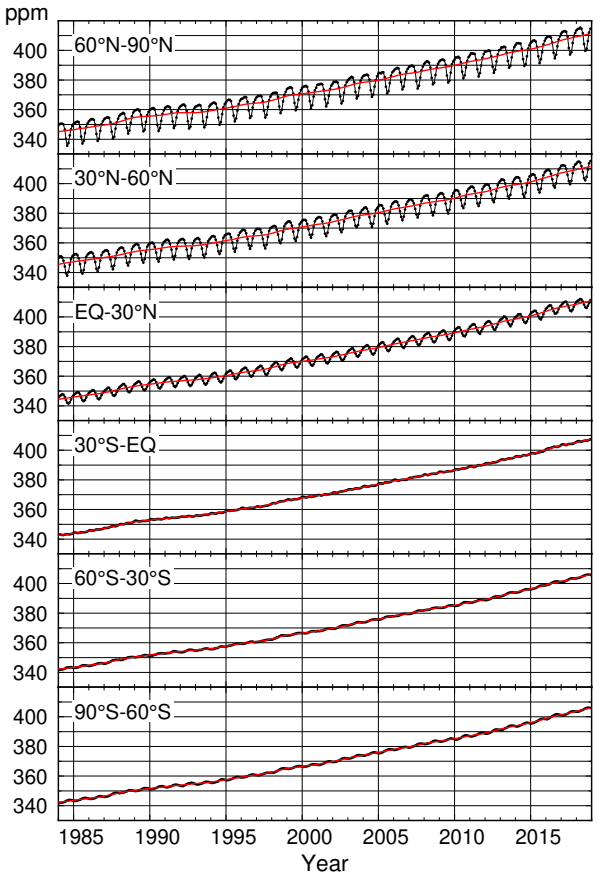

Fig. 1.3 Monthly mean mole fractions of CO_2 from 1984 to 2018 averaged over each 30° latitudinal zone (black) and their deseasonalized long-term trends (red).

become dominant in winter and emissions exceed the amount absorbed.

The activity of the terrestrial biosphere is characterized by significant interannual fluctuations, as reflected in the CO_2 growth rate variations shown in the bottom panel of Fig. 1.2. The growth rate has been particularly high during El Niño events, such as those of 1986 – 1988, 1997/1998, 2002/2003, 2009/2010 and 2014 – 2016. El Niño conditions are usually associated with high temperatures and droughts in tropical land areas. High temperatures enhance plant respiration and organic-matter decomposition in soil, thereby increasing CO_2 emissions, while droughts suppress CO_2 consumption via plant photosynthesis and induce forest/peat fires, which also increase CO_2 emissions. The CO_2 growth rate was exceptionally low during the El Niño event of 1991/1992. This is largely attributed to the eruption of Mt. Pinatubo in June 1991, which caused low-temperature anomalies on a global scale and a terrestrial biospheric change opposite to the one described above.

Latitudinal dependence of mole fractions

The black lines in Fig. 1.3 show CO_2 mole fractions averaged over six 30° latitudinal bands (60 – 90°N, 30 – 60°N, etc.). Long-term trends are shown by red lines in each panel, and are collectively shown in the top panel of Fig. 1.4. The bottom panel of Fig. 1.4 shows CO_2 growth rates in each latitudinal belt, and Fig. 1.5 shows average seasonal cycles of CO_2 mole fractions in the relevant six bands. Figure 1.6 presents monthly mean CO_2 mole fractions for specific months of 2018 at individual stations as included in calculation of the global average mole fraction as a function of latitude.

As shown in Fig. 1.4, CO_2 mole fractions are higher on average in the Northern Hemisphere, largely due to higher

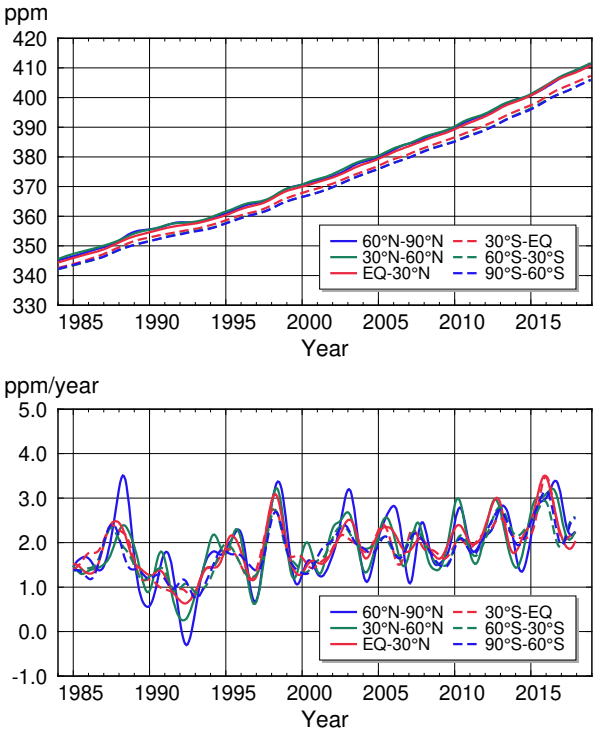

Fig. 1.4 Long-term trends of the CO_2 mole fractions for each 30° latitudinal zone (top) and their growth rates (bottom).

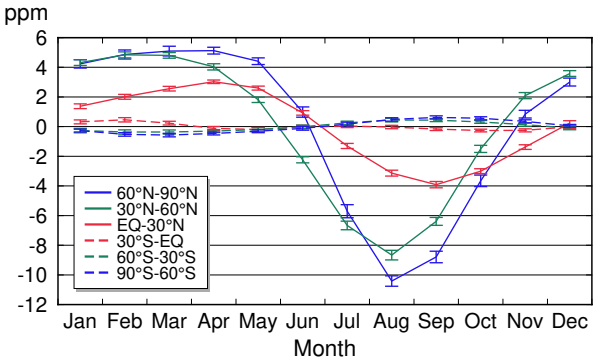

Fig. 1.5 Average seasonal cycles of the CO_2 mole fractions for each 30° latitudinal zone obtained by subtracting long-term trends from the zonal mean time series. Vertical error bars represent the range of ±1σ which was calculated for each month (period 1984 to 2018).

concentrations of human activity and the land mass areas there. However, the long-terms trends are the same in all latitudinal bands. This suggests that, although the major sources and sinks of CO_2 are located in the Northern Hemisphere, changes in mole fractions occur on a global scale due to atmospheric transport.

Figure 1.5 indicates that the seasonal cycles of CO_2 mole fractions have a large amplitude in northern regions, mainly because the Northern Hemisphere has larger continental areas and an extensive terrestrial biosphere. The pronounced lagging between the peak absorption in the different latitude belts is also seen on this figure. These large variations are also evident in Fig. 1.6. In contrast, low seasonal variability is observed in southern hemisphere. In the mid- and high southern latitudes, seasonal cycles of CO_2 mole fractions have an opposite phase to those of northern regions. In the low southern latitudes, however, their phase is similar to those of northern regions, suggesting that CO_2 mole fractions in the former are more readily affected by Northern Hemisphere air.

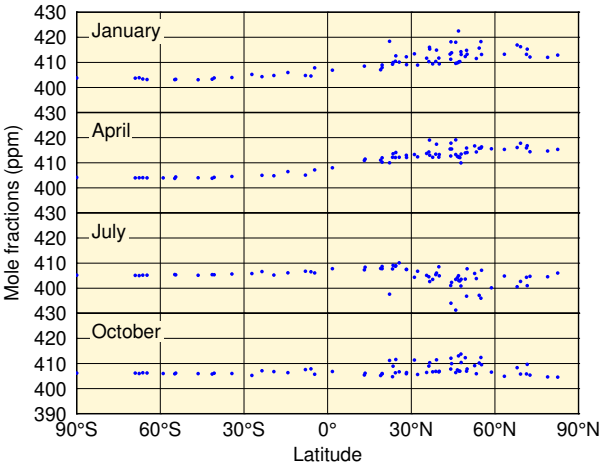

Fig. 1.6 Latitudinal distributions of the monthly mean mole fractions of CO_2 in January, April, July and October 2018 at individual stations.

2.

METHANE

(CH_4)

● : CONTINUOUS STATION

△ : FLASK STATION

□ : FLASK MOBILE (SHIP)

▼ : REMOTE SENSING STATION

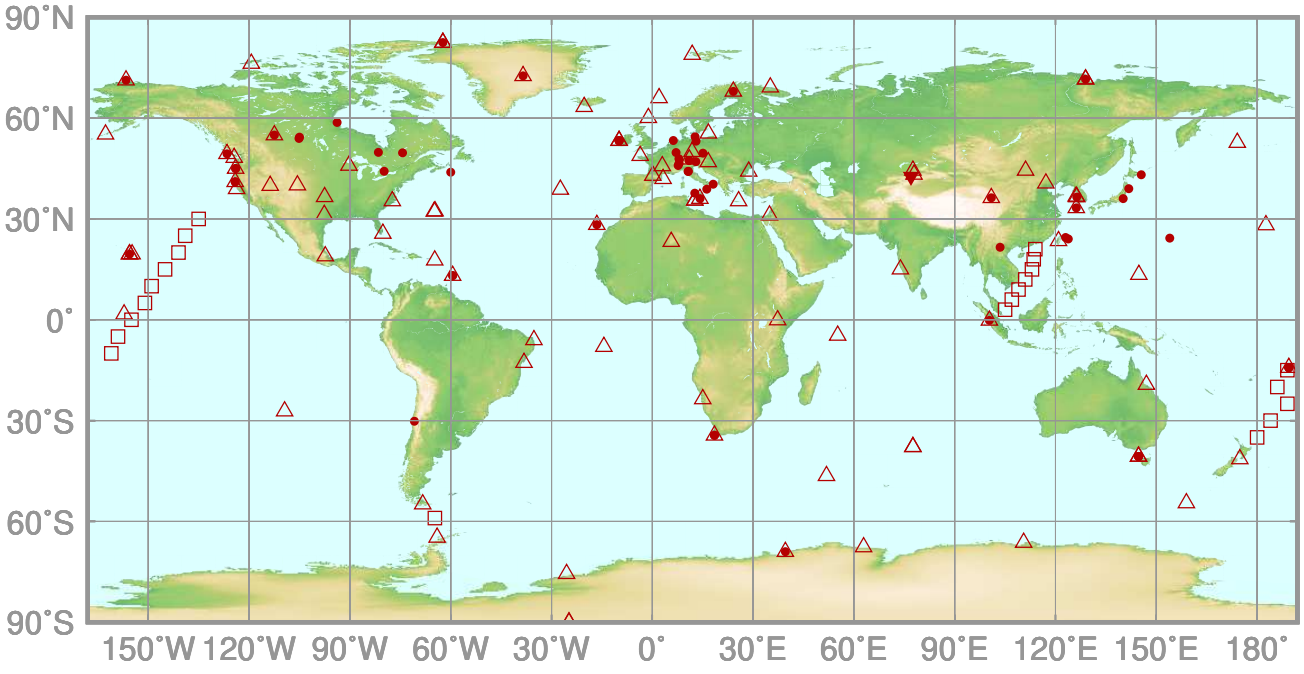

This map shows locations of the stations that have submitted data for monthly mean mole fractions.

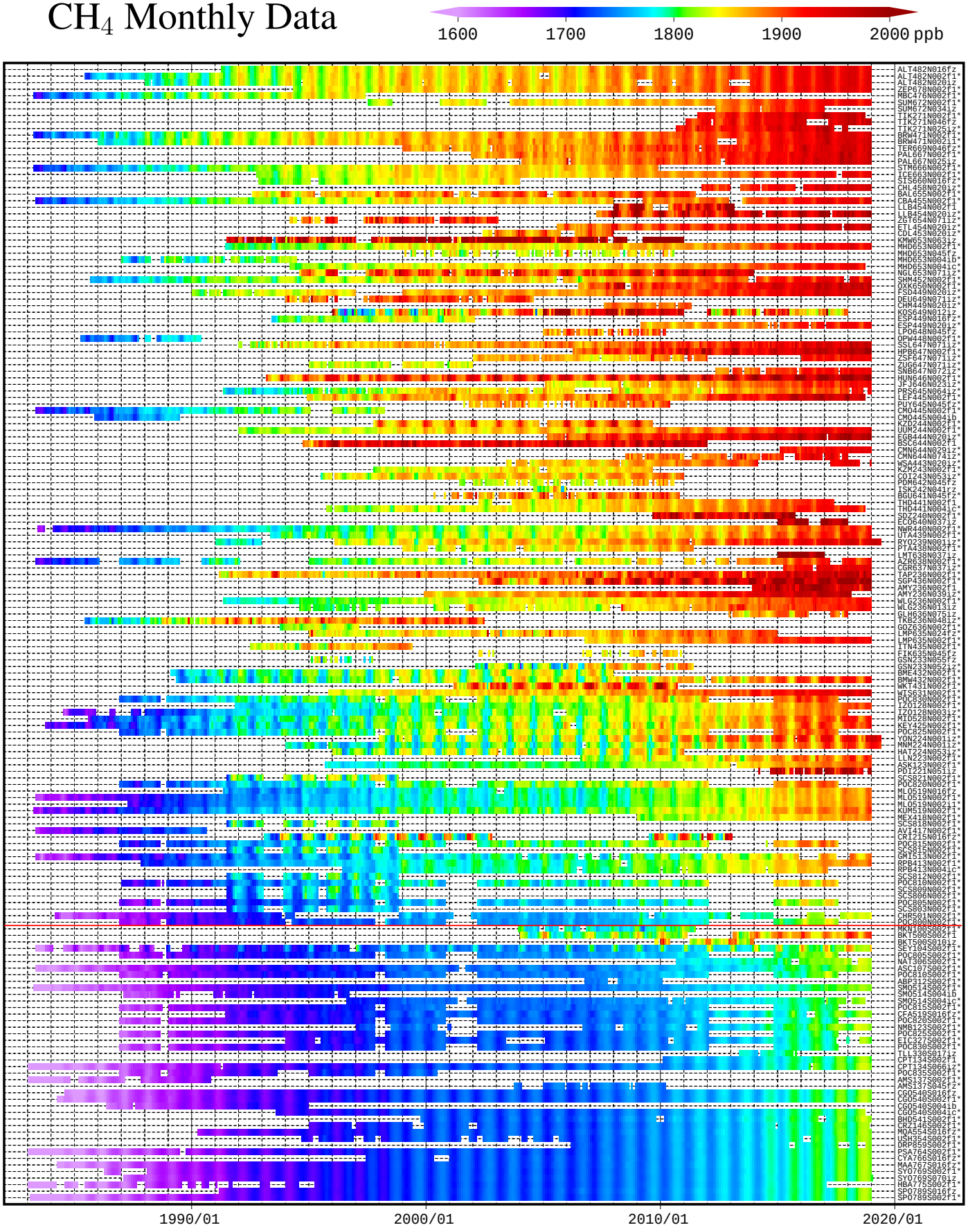

Plate 2.1 Monthly mean CH_4 mole fractions that have been reported to the WDCGG. The mole fractions are illustrated in different colors. The sites are listed in order from north to south. The red line indicates the equator. In cases where monthly means are not reported, the WDCGG calculates them from hourly or other mole fractions reported to the WDCGG by simple arithmetic mean. The data from the sites with an asterisk at the end of the station index were used for the analyses shown in Plate 2.2 (see Appendix A).

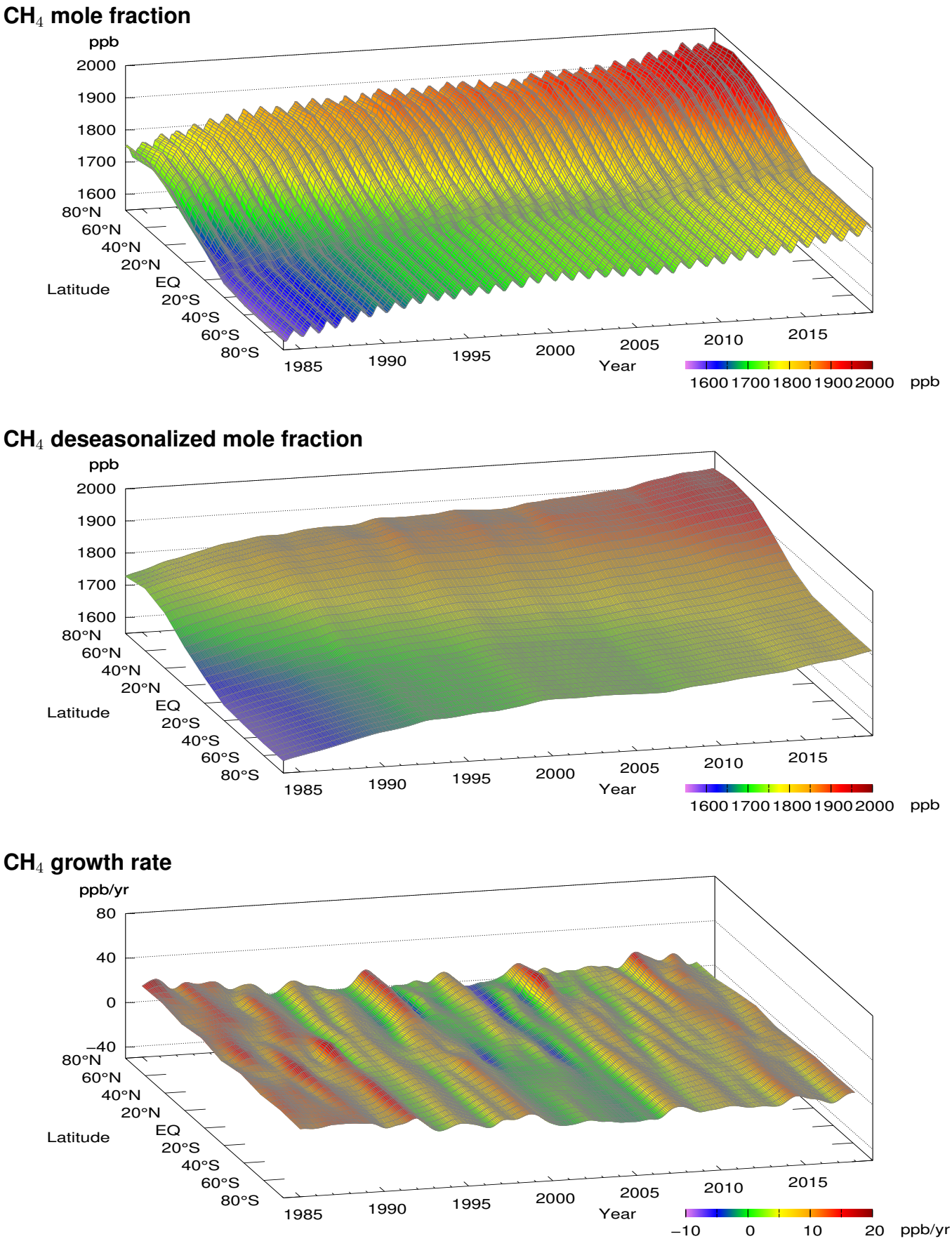

Plate 2.2 Variation of zonally averaged monthly mean CH_4 mole fractions (top), deseasonalized long-term trends (middle), and growth rates (bottom). The zonally averaged mole fractions were calculated for each 20° zone. The deseasonalized trends and growth rates were derived as described in Appendix A.

2. METHANE (CH_4)

Atmospheric mole fractions of methane (CH_4) – the second most significant anthropogenic greenhouse gas – have been increasing since the beginning of the industrial era (1750). The global mean mole fraction of CH_4 was 1,869±2 ppb in 2018, representing an increase of 10 ppb relative to the previous year and 259% of the pre-industrial level of 722 ppb. CH_4 is responsible for around 17% of radiative forcing (relative to the pre-industrial era) caused by long-lived greenhouse gases (WMO, 2019).

CH_4 has a variety of natural and anthropogenic sources. Natural ones are predominantly wetlands, with various other minor but significant sources including fresh water, wild animals, termites and geological sources. Emissions from ruminant livestock and rice paddies associated with agricultural activities are categorized as anthropogenic sources. Other sources are directly related to industrial activity, including gas and oil exploration, waste management and biomass burning. These anthropogenic sources produce large and comparable amounts of CH_4. In contrast to the variety of sources, sinks are predominantly attributed to the destruction of CH_4 via reaction with a hydroxyl (OH) radical, which is especially abundant over oceans at low latitudes since it forms from the exposure of water vapor to ultraviolet (UV) radiation.

Global mean mole fractions

The blue dots in Fig. 2.1 show global mean CH_4 monthly averaged mole fractions (top) and related growth rates (bottom) based on the WDCGG data analysis described in Appendix A. Clear seasonal cycle is observed, with higher values from boreal winter to spring and lower values in summer. The red line in the top panel shows the residual component after removal of seasonal cycles from globally averaged monthly mean mole fractions (referred to here as the long-term trend).

The seasonal cycle of CH_4 mole fractions is primarily driven by the destruction of CH_4 via reaction with OH radical. More such radicals are generated in summer due to enhanced UV radiation, resulting in increased CH_4 destruction. Biogenic sources such as wetlands also have individual characteristics of seasonal variability, contributing to variations in observed CH_4 mole fractions.

The overall profile of globally averaged CH_4 mole fractions shows a continuous increase throughout the

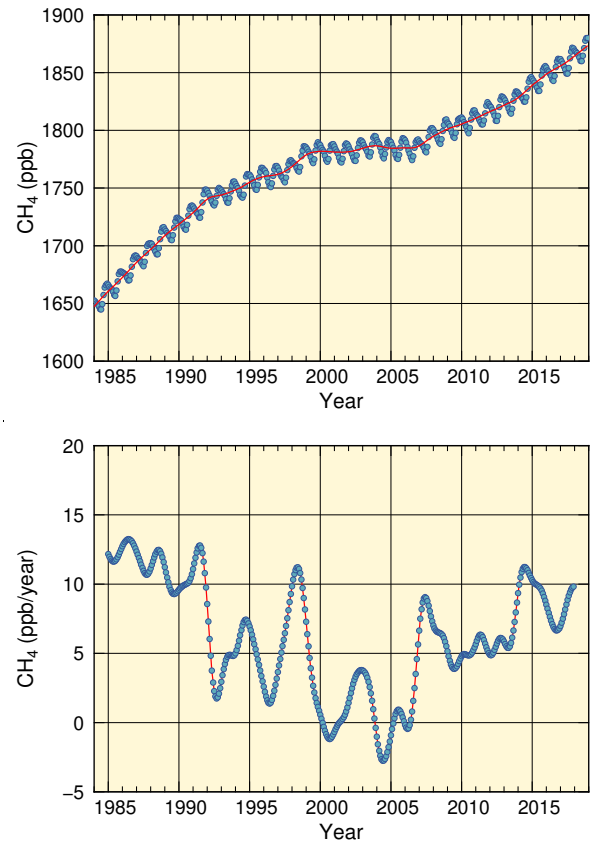

Fig. 2.1 Globally averaged monthly mean mole fraction of CH_4 from 1984 to 2018 and the deseasonalized long-term trend plotted as red line (top), and its growth rate (bottom).

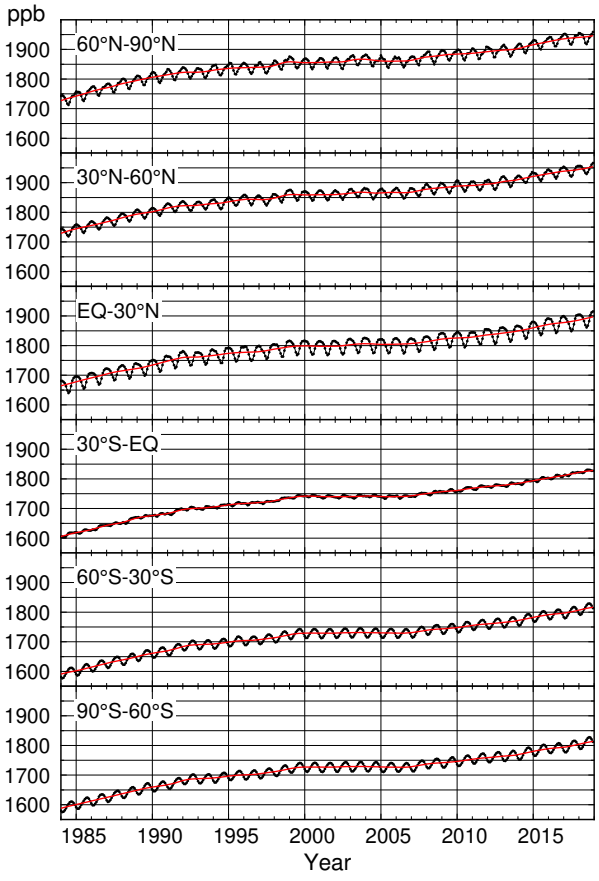

Fig. 2.2 Monthly mean mole fractions of CH_4 from 1984 to 2018 for each 30° latitudinal zone (black) and their deseasonalized long-term trends (red).

period for which observational data are available. Notably, the increase almost stagnated from 1999 to 2006. As shown in the bottom panel, the growth rate actually began to decrease in the late 1990s (in fact approaching zero during this period) for reasons that remain under discussion (IPCC (2013) and references noted therein). For example, analysis based on the inverse modelling demonstrated that atmospheric methane growth during the 1990s was caused by a decline in anthropogenic emissions (Bousquet *et al.*, 2006). These emissions started rising again in 1999 but the effect has been masked by a coincident decrease in wetland emissions. The situation changes in 2007 and mole fractions began increasing again. Recent studies, including work based on CH_4 isotopic composition observation, have suggested that increased CH_4 emissions from wetlands in the tropics and anthropogenic sources in the mid-latitudes of the Northern Hemisphere triggered the resumed increase in global mean mole fractions (WMO, 2019).

Latitudinal dependence of mole fractions

The black lines in Fig. 2.2 show CH_4 mole fractions averaged over six 30° latitudinal bands. Long-term trends are shown by the red lines in each panel and summarized in the top panel of Figure 2.3. The bottom panel of this figure shows growth rates of CH_4 for the six latitudinal bands, and Figure 2.4 shows average seasonal cycles of CH_4 mole fractions for each band.

As shown in the top panel of Figure 2.3, the difference in the six long-term trends is especially significant between 30 – 60°N and EQ – 30°N and between EQ – 30°N and 30°S – EQ, indicating that CH_4 mole fractions exhibit a large latitudinal gradient in the mid- and low latitudes of the Northern Hemisphere. This is largely attributable to high concentrations of major CH_4 sources in the Northern Hemisphere and to an abundance of OH radicals over oceanic regions extending southward.

The CH_4 growth rate exhibits similar but not identical characteristics in all latitudinal bands, as shown in the bottom panel of Figure 2.3. There are singular peaks and troughs, each of which has an individual complex origin, and collective explanation of two or more peaks is challenging. For example, the peaks observed in every band in 1998 are attributed to enhanced CH_4 emissions from tropical wetland areas in association with the major El Niño event observed the same year, and to forest/peat fires in Siberia and elsewhere (Dlugokencky *et al.*, 2001).

Figure 2.4 shows clear seasonal cycles of CH_4 mole fractions in both hemispheres, while those of CO_2 mole fractions are only pronounced in the Northern Hemisphere (Fig. 1.5). This difference is related to the differences in the processes behind the seasonal cycles of the two species. CH_4 sinks are mainly driven by the availability of OH radicals produced over oceans, which peak during summer in both hemispheres and at the same time. In contrast, CO_2 sinks in summer are mainly driven by terrestrial biosphere activity, which is limited in the ocean-rich Southern Hemisphere and has pronounced difference in the month of the maximum uptake in different latitudes. The cycles have a roughly opposite phase in each hemisphere because the seasons are opposite. The relatively low amplitude of seasonal cycles for CH_4 mole fractions in the low latitudes of the Southern Hemisphere indicates that the atmosphere in this region tends to be influenced by the northern hemisphere, and the cycles are partially offset. In the low latitudes of the Northern Hemisphere, mole fractions are significantly lower in summer because OH radicals are plentiful over ocean

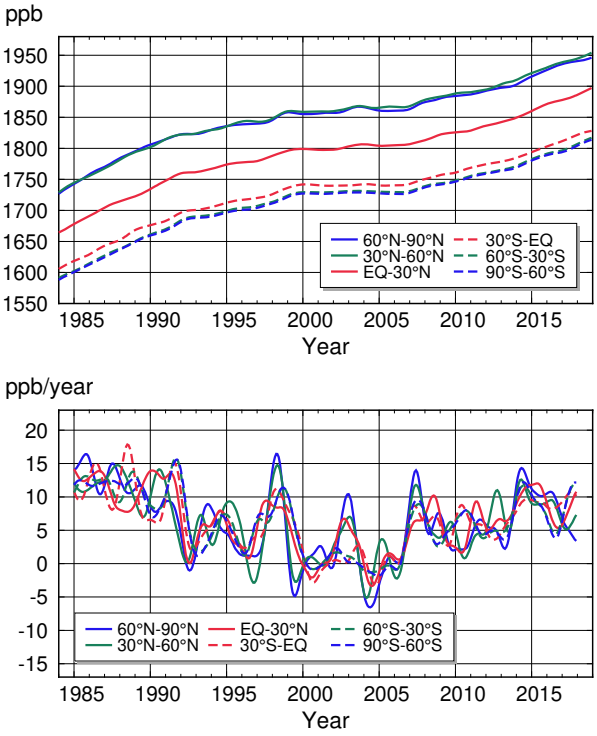

Fig. 2.3 Long-term trends of the CH_4 mole fractions for each 30° latitudinal zone (top) and their growth rates (bottom).

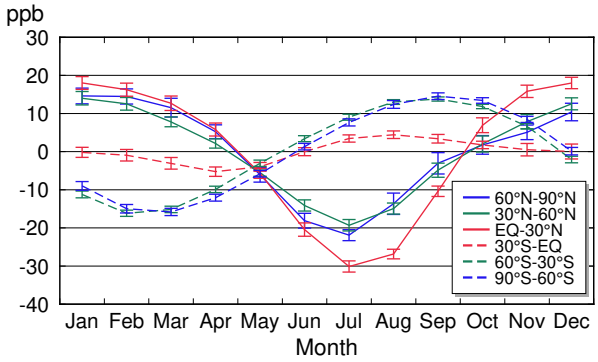

Fig. 2.4 Average seasonal cycles of CH_4 mole fractions for each 30° latitudinal zone obtained by subtracting long-term trends from the zonal mean time series. Vertical error bars represent the range of ±1σ calculated for each month (period 1984 to 2018).

areas due to enhanced UV radiation. As a whole, amplitudes for seasonal cycles of CH_4 mole fractions are larger in the Northern Hemisphere, and the global mean CH_4 mole fraction is therefore at its annual minimum in boreal summer (Fig. 2.1).

3.

NITROUS OXIDE

(N_2O)

● : CONTINUOUS STATION

△ : FLASK STATION

□ : FLASK MOBILE (SHIP)

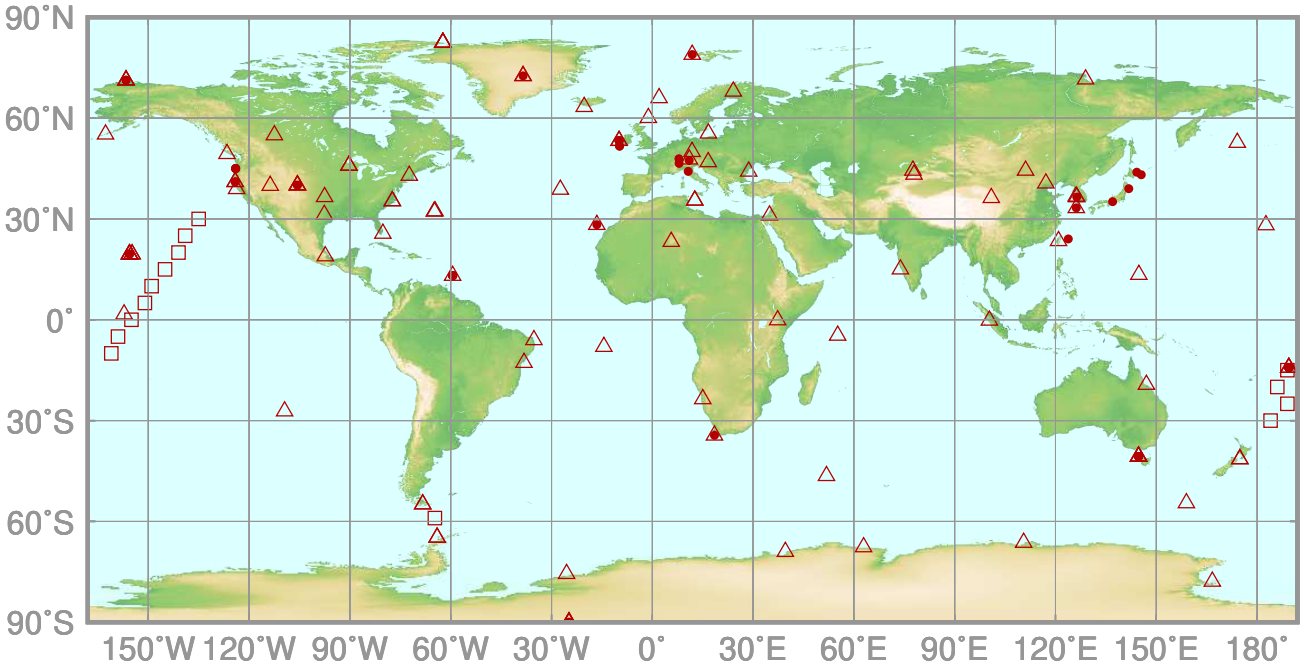

This map shows locations of the stations that have submitted data for monthly mean mole fractions.

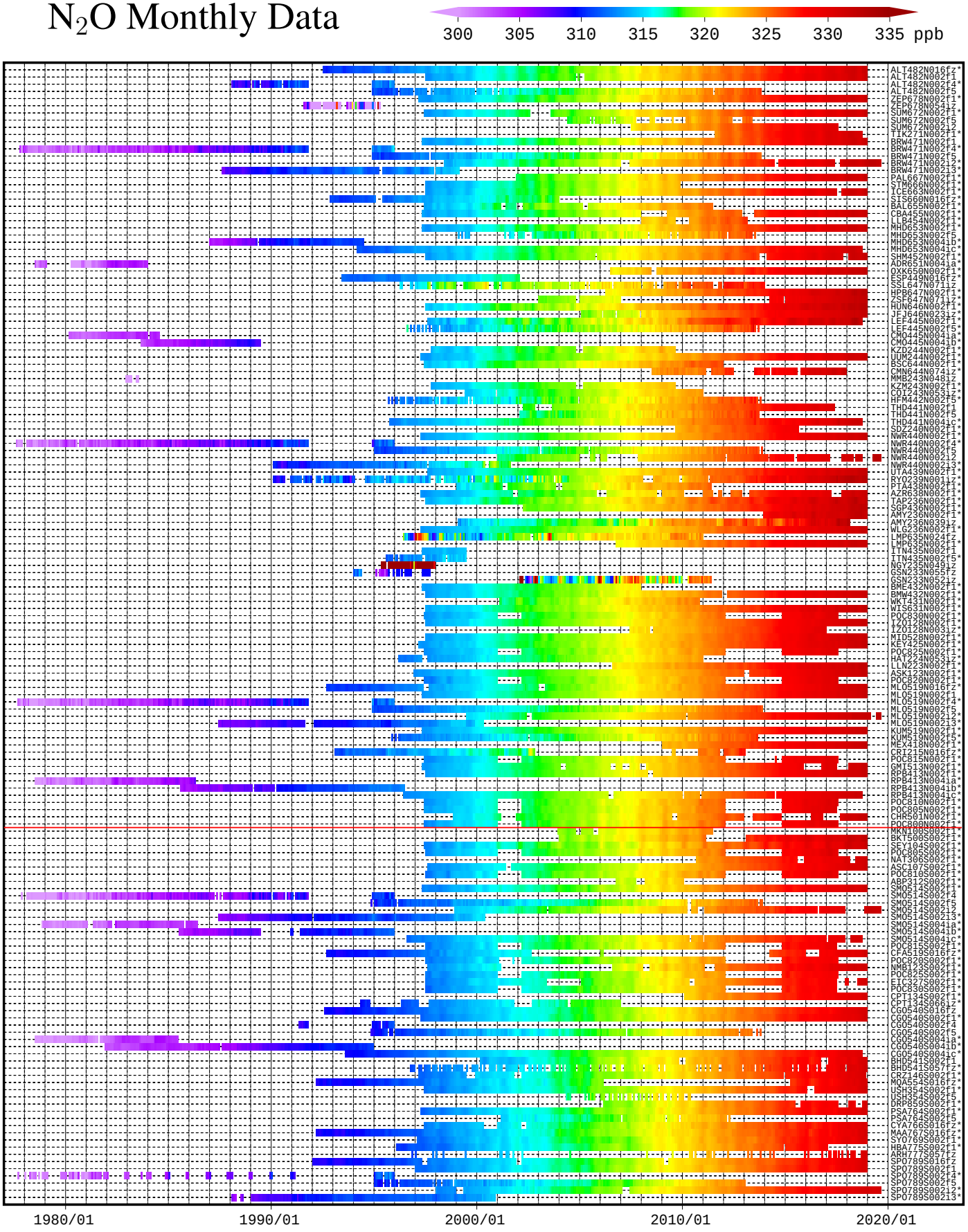

Plate 3.1 Monthly mean N_2O mole fractions that have been reported to the WDCGG. The mole fractions are illustrated in different colors. The sites are listed in order from north to south. The red line indicates the equator. The data from the sites with an asterisk at the end of the station index were used for the analyses shown in Plate 3.2 (see Appendix A).

N_2O mole fraction

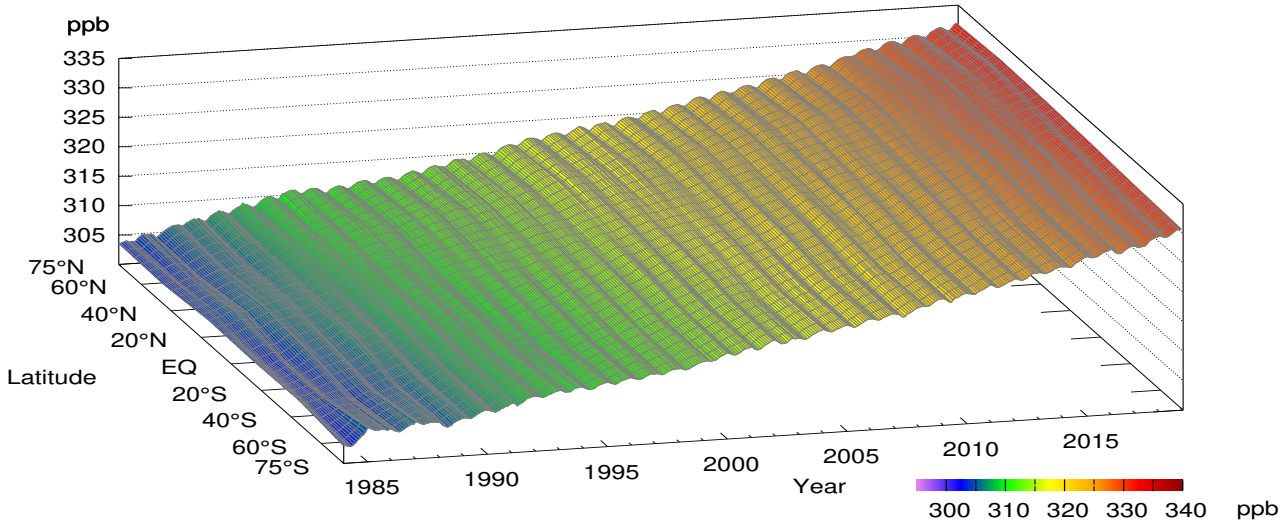

N_2O deseasonalized mole fraction

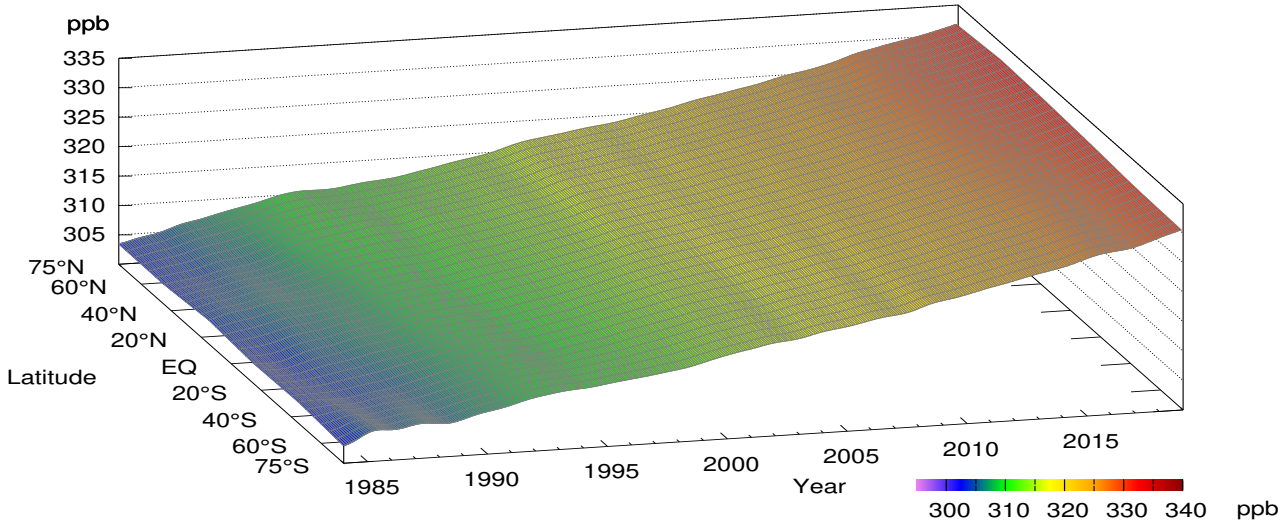

N_2O growth rate

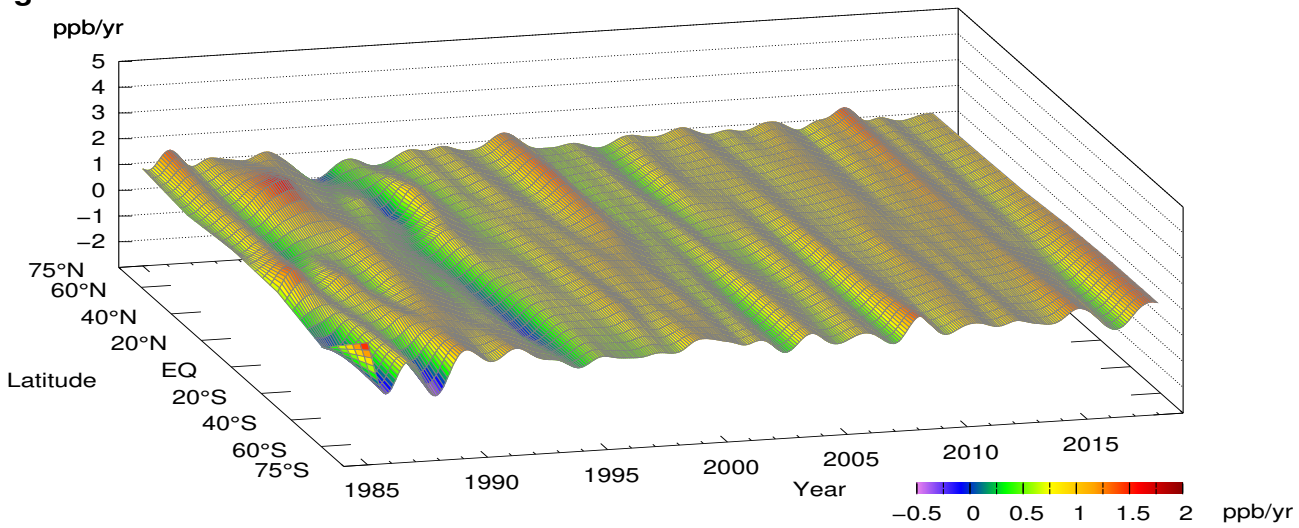

Plate 3.2 Variation of zonally averaged monthly mean N_2O mole fractions (top), deseasonalized long-term trends (middle), and growth rates (bottom). The zonally averaged mole fractions were calculated for each 30° zone. The deseasonalized trends and growth rates were derived as described in Appendix A.

3. NITROUS OXIDE (N_2O)

Atmospheric mole fractions of nitrous oxide (N_2O) – a significant factor in global warming – have been increasing since the beginning of the industrial era (1750). The global mean mole fraction in 2018 was 331.1±0.1 ppb, representing an increase of 1.2 ppb relative to the previous year and 123% of the pre-industrial level of 270 ppb. N_2O is responsible for approximately 6% of total radiative forcing (relative to the pre-industrial era) from long-lived greenhouse gases (WMO, 2019).

N_2O sources include microbial processes (nitrification and denitrification), oceans, nitrogen fertilizers generally used in agriculture and fossil fuel/biomass combustion. Global human-induced emissions, which are dominated by nitrogen additions to croplands, increased by 30% over the past four decades and are mainly responsible for the growth in the atmospheric burden (Tian *et al*., 2020). N_2O is relatively stable in the troposphere with a lifetime of around 121 years. Its mole fraction is relatively uniformly distributed in the troposphere and declines in the stratosphere, where it is destroyed via ultraviolet (UV) photo-decomposition.

Global and hemispheric average mole fractions

Figure 3.1 shows global mean N_2O mole fraction and related growth rates. Details of the analysis are provided in Appendix A. Unlike CO_2 and CH_4, N_2O mole fractions exhibit low seasonal variability. Nevertheless, the same procedure as that for removal of seasonal cycles for CO_2 and CH_4 is performed, and the residual is shown by the red line in the top panel. Values differ only minimally from those of the original N_2O mole fractions due to low seasonal variability. Figure 3.2 shows N_2O mole fractions averaged over the Northern Hemisphere (dark blue) and the Southern Hemisphere (light blue) in the top panel, with corresponding growth rates in the bottom panel.

Throughout the period for which observation data are available, N_2O mole fractions have steadily increased in both hemispheres, and therefore over the whole globe. Values tend to be higher in the Northern Hemisphere, mainly due to high concentrations of anthropogenic and microbial sources in continental areas.

The growth rate of N_2O is positive over the period as a whole, although significant inter-annual variations are

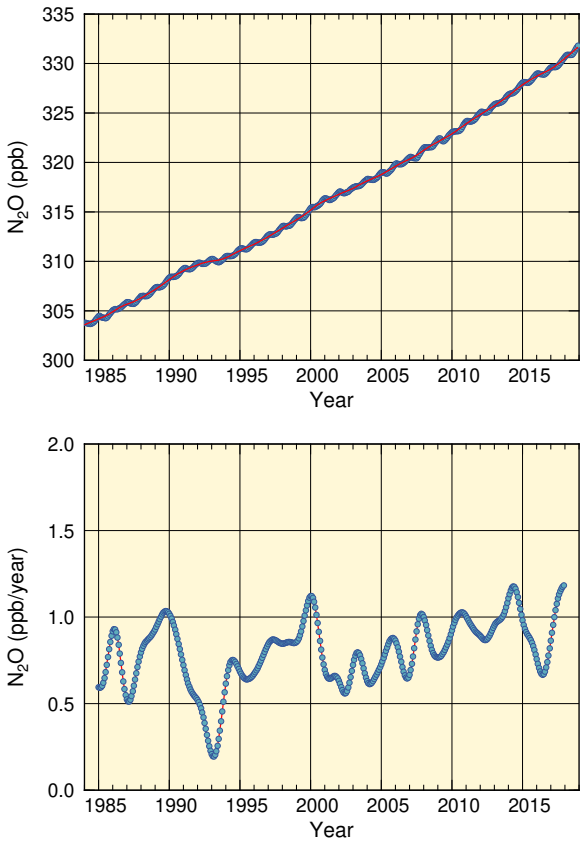

Fig. 3.1 Globally averaged monthly mean mole fraction of N_2O from 1984 to 2018 and the deseasonalized long-term trend shown as a red line (top), and its growth rate (bottom).

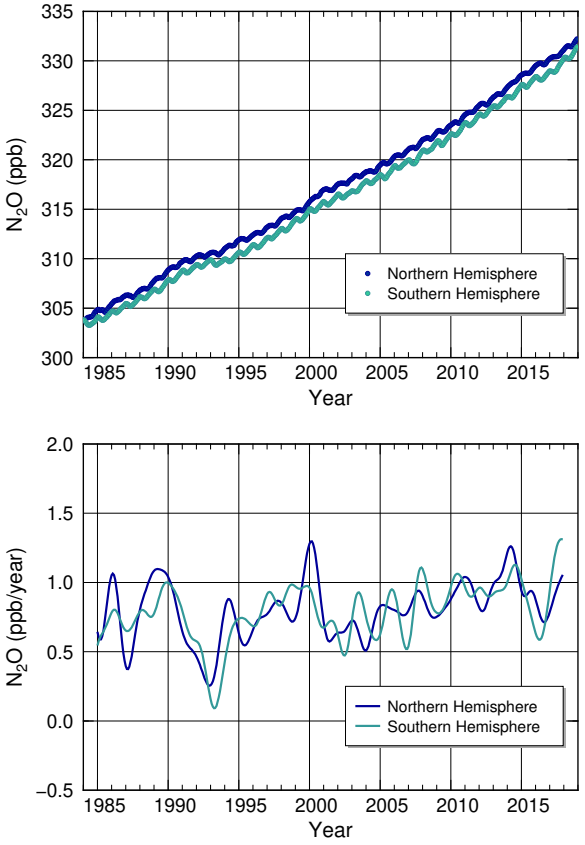

Fig. 3.2 Monthly mean mole fractions of N_2O from 1984 to 2018 (top) and their growth rates (bottom), averaged over the Northern and Southern Hemispheres.

observed. These are partially due to changes in the state of the stratosphere, where N_2O is destroyed, and the variability of microbial processes in soil and/or oceanic processes may also contribute (IPCC, 2013). However, quantitative verification of specific variability patterns is challenging due to the complexity of related processes and uncertainty over the intensities and locations of N_2O sources. Accordingly, further extension of the global monitoring network is needed.

4.

HALOCARBONS AND OTHER HALOGENATED SPECIES

● : CONTINUOUS STATION

△ : FLASK STATION

□ : FLASK MOBILE (SHIP)

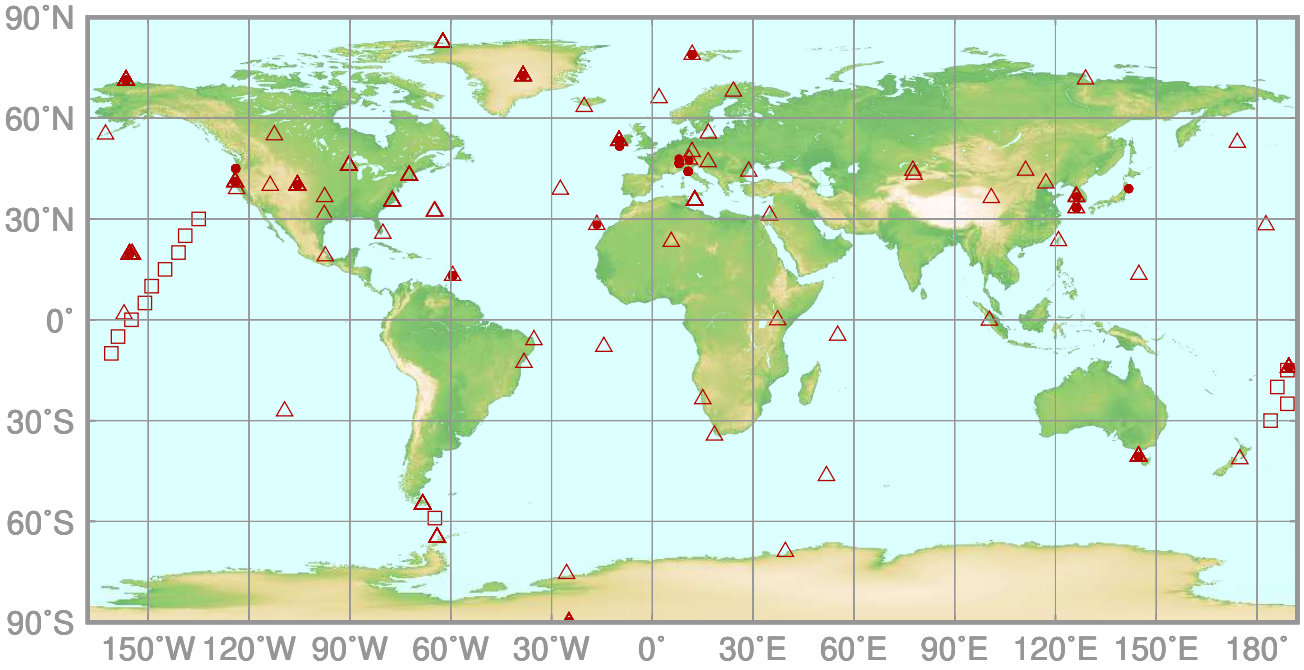

This map shows locations of the stations that have submitted data for monthly mean mole fractions.

(a) CFC-11 Monthly Data

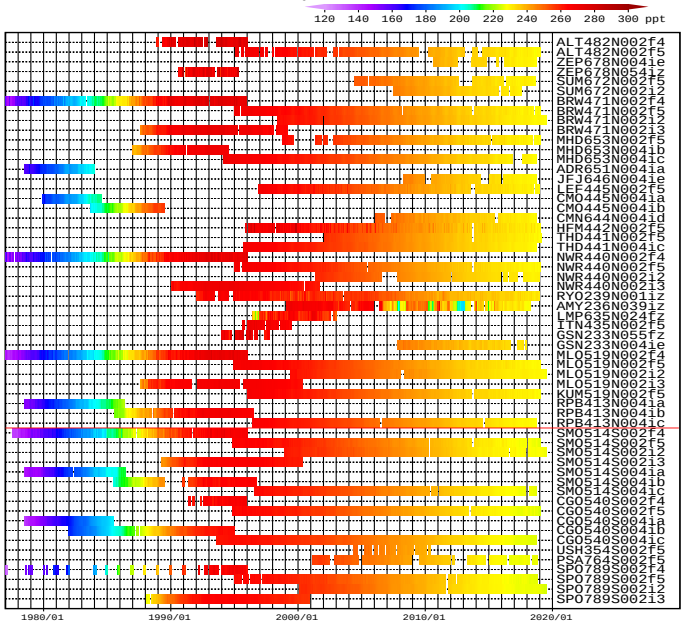

(b) CFC-12 Monthly Data

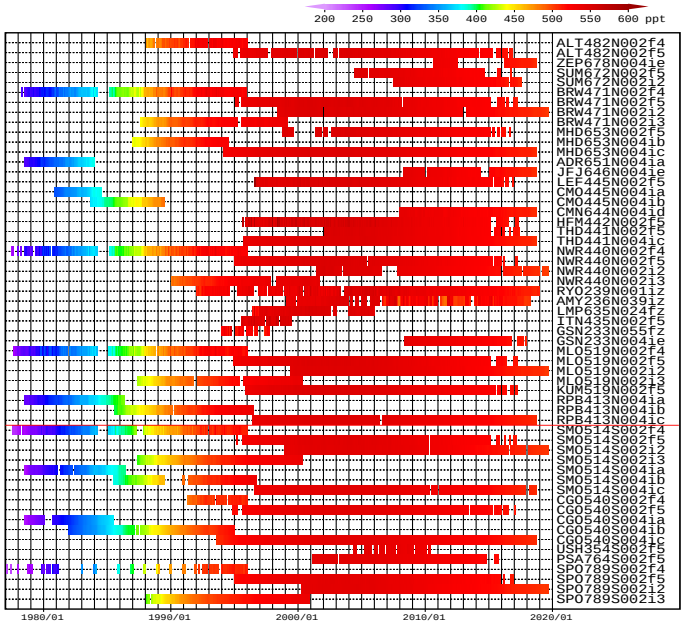

(c) CFC-113 Monthly Data

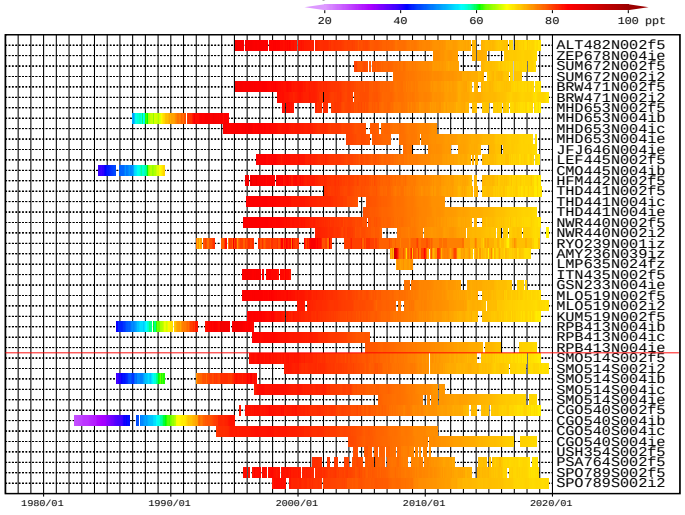

(d) CCl_4 Monthly Data

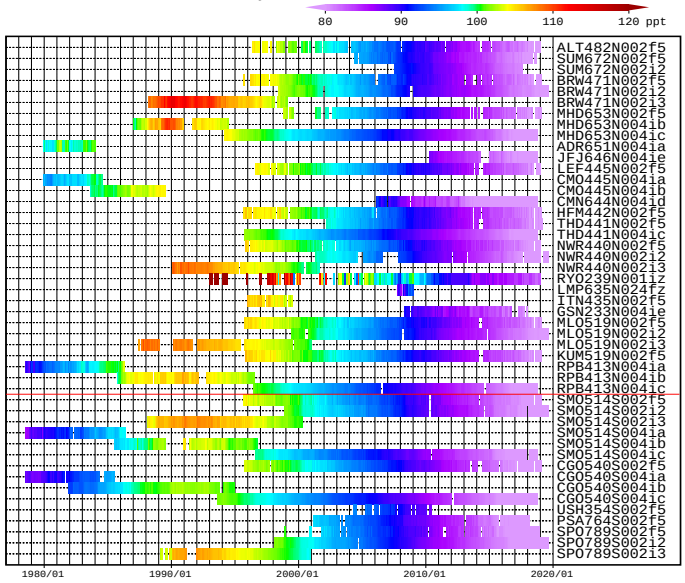

(e) CH_3CCl_3 Monthly Data

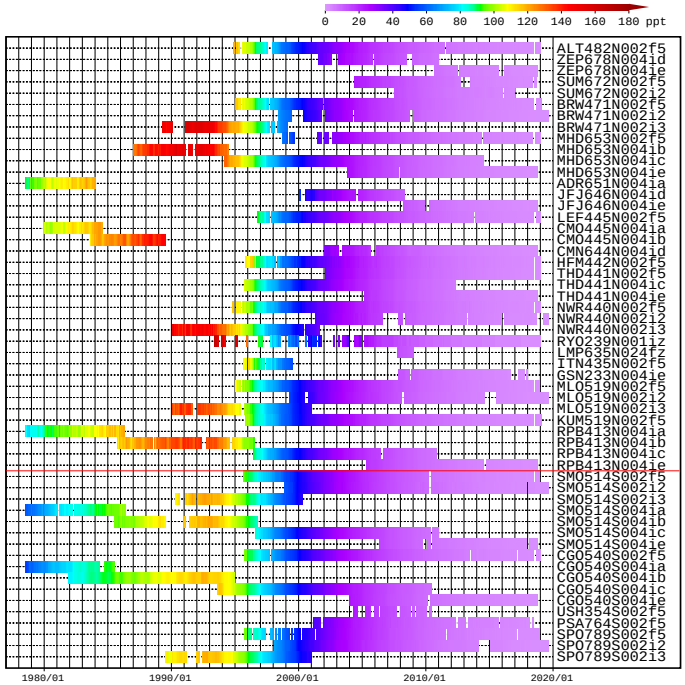

(f) Halon-1211 Monthly Data

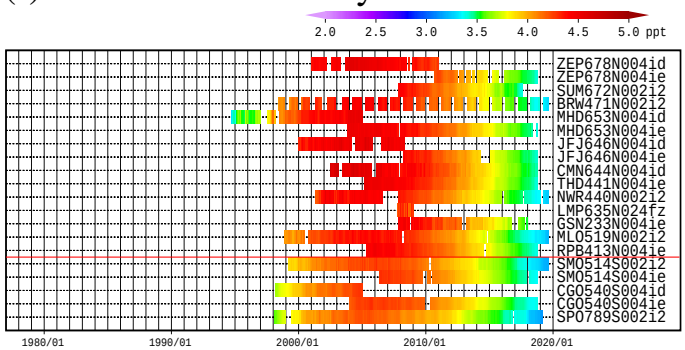

Plate 4.1 Monthly mean (a) CFC-11, (b) CFC-12, (c) CFC-113, (d) CCl_4, (e) CH_3CCl_3, (f) Halon-1211 mole fractions that have been reported to the WDCGG. The mole fractions are illustrated in different colors. The sites are listed in order from north to south. The red line indicates the equator.

(a) Halon-1301 Monthly Data

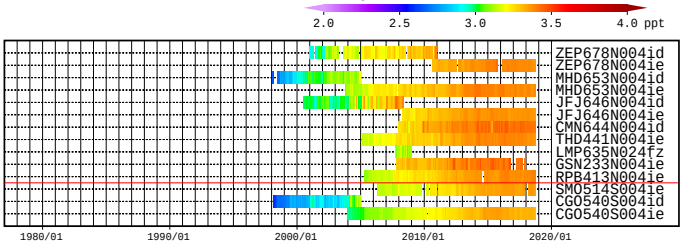

(b) HCFC-22 Monthly Data

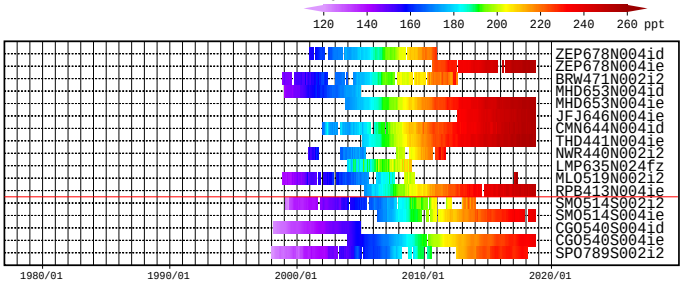

(c) HCFC-141b Monthly Data

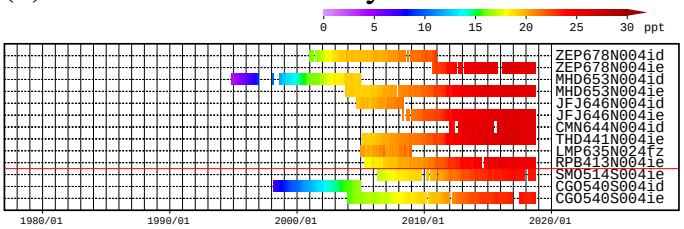

(d) HCFC-142b Monthly Data

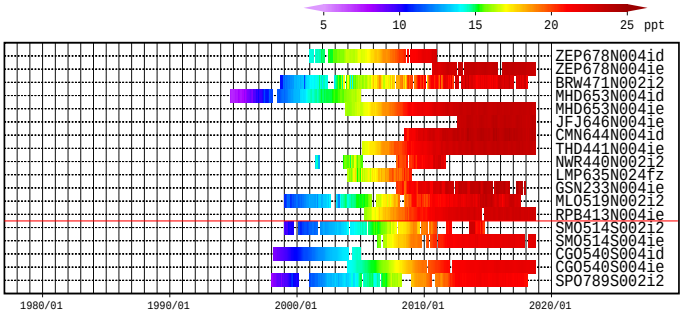

(e) HFC-134a Monthly Data

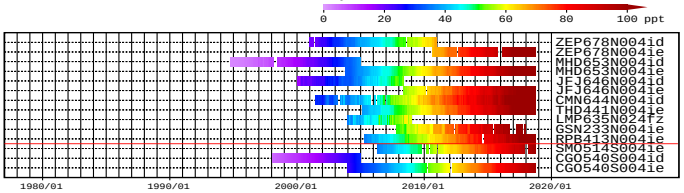

(f) HFC-152a Monthly Data

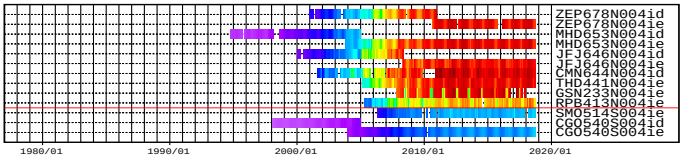

(g) CH_3Cl Monthly Data

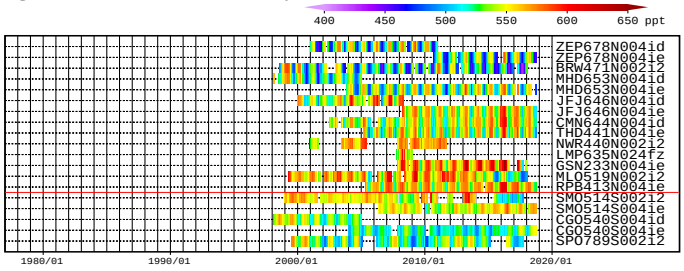

(h) SF_6 Monthly Data

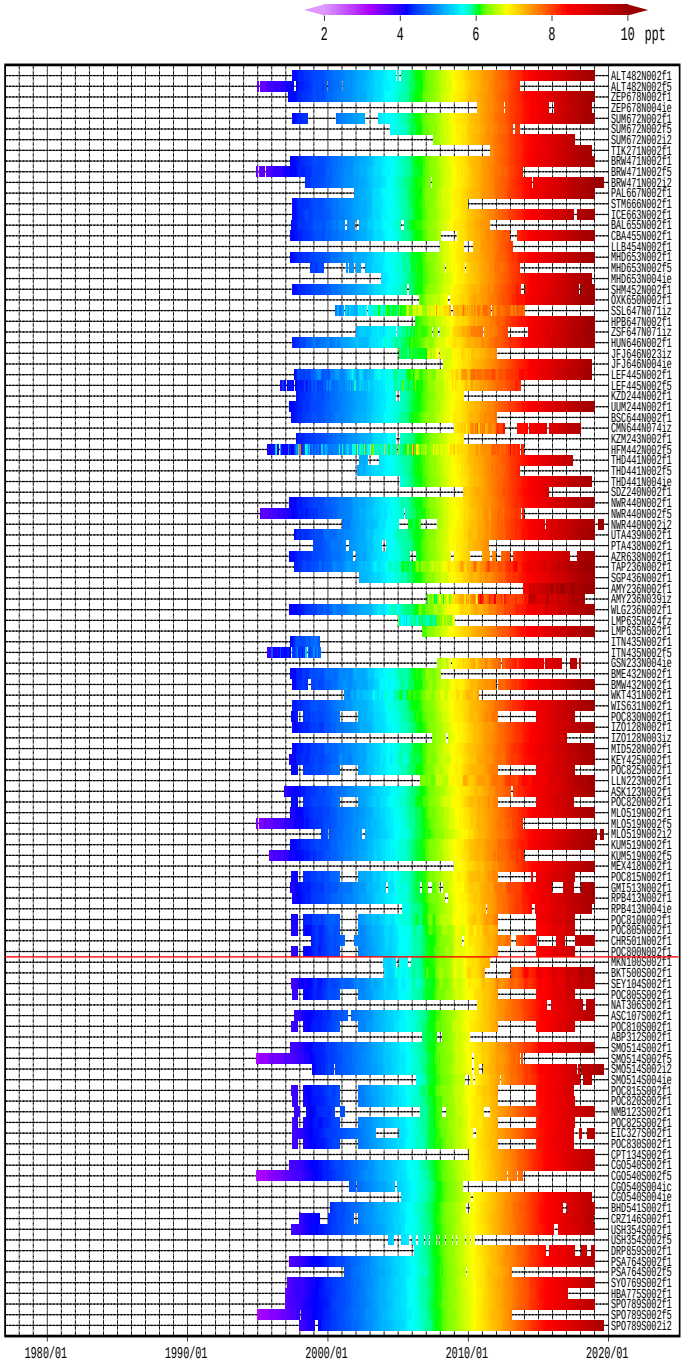

Plate 4.2 Monthly mean (a) Halon-1301, (b) HCFC-22, (c) HCFC-141b, (d) HCFC-142b, (e) HFC-134a, (f) HFC-152a, (g) CH_3Cl, (h) SF_6 mole fractions that have been reported to the WDCGG. The mole fractions are illustrated in different colors. The sites are listed in order from north to south. The red line indicates the equator.

4. HALOCARBONS AND OTHER HALOGENATED SPECIES

Halocarbons are generally carbon compounds containing halogens. Most are artificially generated and have much lower atmospheric mole fractions than major greenhouse gases, but contribute significantly to global warming. These gases together are responsible for around 11% of the total increase in radiative forcing since the pre-industrial era (1750) caused by long-lived greenhouse gases (WMO, 2019).

Major examples include chlorofluorocarbons (CFCs; carbon compounds containing both fluorine and chlorine), with CFC-11, CFC-12 and CFC-113 having particularly significant impacts on global warming. CFCs used to be mass-produced as refrigerants, propellants, detergents and other functional substances until their connection with stratospheric ozone depletion became evident. After CFC production and consumption were internationally prohibited under the Montreal Protocol in 1989, mole fractions of CFC-11, CFC-12 and CFC-113 decreased. Recently, however, a slowing of the decrease in CFC-11 mole fractions has been observed (see Figure 4.1, 4.2). This is considered to be associated with CFC-11 emissions from production in eastern Asia (Montzka *et al*., 2018).

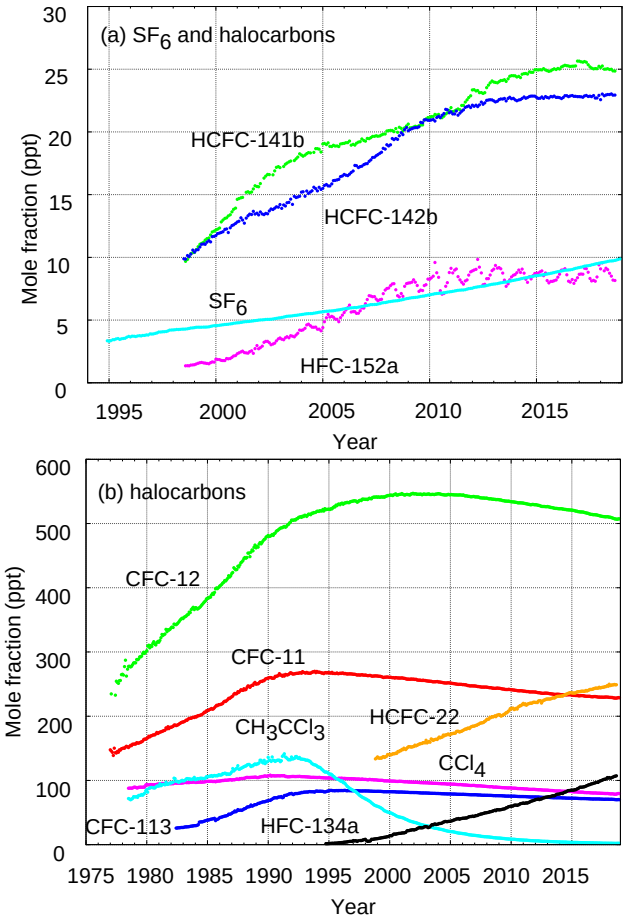

Fig. 4.1 Monthly mean mole fractions of SF_6 and the most important halocarbons: (a) SF_6 and lower mole fractions of halocarbons, and (b) higher halocarbon mole fractions. A number of stations are used for the analyses: SF_6 (85), CFC-11 (23), CFC-12 (25), CFC-113 (21), CCl_4 (22), CH_3CCl_3 (24), HCFC-141b (9), HCFC-142b (14), HCFC-22 (13), HFC-134a (10), HFC-152a (9).

Carbon tetrachloride (CCl_4), methyl chloroform (1,1,1-trichloroethane, CH_3CCl_3), halons and hydrochlorofluorocarbons (HCFCs) are also considered ozone-depleting substances, with related production and consumption regulated under the Montreal Protocol and associated amendments made in the 1990s. Halons are carbon compounds containing bromine, with Halon-1211 and Halon-1301 as typical species. HCFCs represent carbon compounds containing hydrogen, in addition to fluorine and chlorine, with HCFC-22, HCFC-141b and HCFC-142b as major examples. Mole fractions of CCl_4, CH_3CCl_3 and Halon-1211 are decreasing. Growth rates of Halon-1301, HCFC-141b and HCFC-142b have levelled off in recent years, and mole fractions of HCFC-22 are increasing more slowly than before (Figure 4.1, 4.2).

Hydrofluorocarbons (HFCs; carbon compounds containing hydrogen and fluorine but no chlorine) have no ozone depletion potential, and were developed as substitutes for CFCs and HCFCs. However, due to their significant greenhouse effects, they are regulated under the Kigali amendment to the Montreal Protocol adopted in 2016 (effective as of 2019). Typical species include HFC-134a and HFC-152a. Mole fractions of HFC-134a are increasing, while the growth rate of HFC-152a has levelled off in recent years (Figure 4.1, 4.2).

Unlike other halocarbons, methyl chloride (chloromethane, CH_3Cl) comes from natural sources. Mole fractions of CH_3Cl show no significant long-term trend, although clear seasonal cycles are observed (see Figure 4.2). CH_3Cl is not regulated under the Montreal Protocol, but its status is monitored at many observation stations.

Although not technically a halocarbon, sulfur hexafluoride (SF_6) is often discussed together with halocarbons and other halogenated gases. SF_6 has very significant greenhouse effects despite its low abundance, and is targeted for reduction by the Kyoto Protocol. Mole fractions of SF_6 show a continuous increase (see Figure 4.1, 4.2). SF_6 is a substance which originates only from anthropogenic sources used primarily in the electricity and electronics supply industries, e.g. the semiconductor industry, where it is used as an electronic insulator due to its inertness. Increasing demand for the electricity and power networks will continue leading to SF_6 increases in the atmosphere.

Figure 4.2 displays mole fractions of these 14 gas species, with circles representing monthly mean values at individual stations (rather than values averaged over different stations). Solid and open circles correspond to

stations in the Northern Hemisphere and Southern Hemisphere, respectively. Due to more intensive production of artificial halocarbons in the Northern Hemisphere, related mole fractions tend to be higher in this region, especially in their increasing phases.

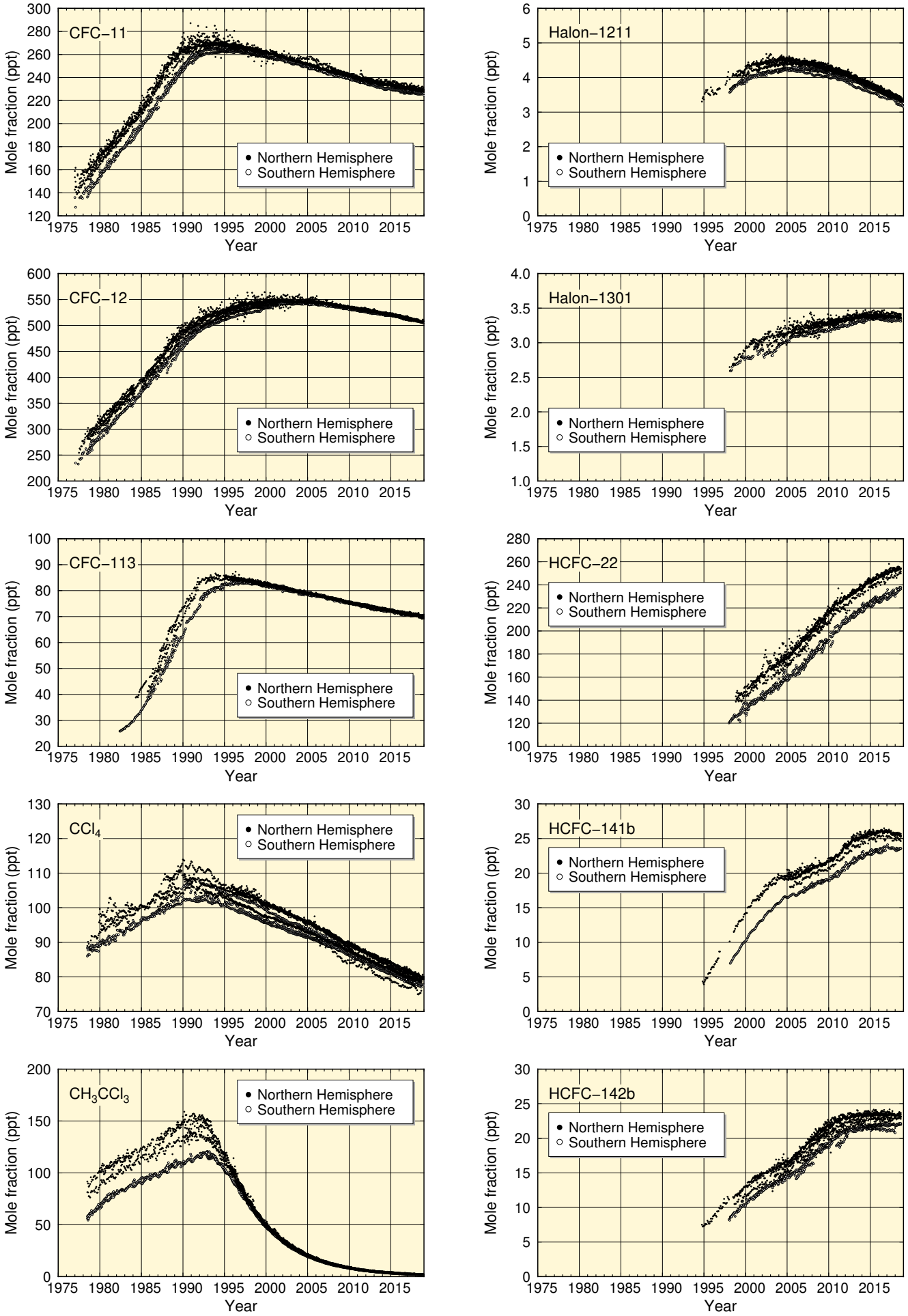

Fig. 4.2 Time series of the monthly mean mole fractions of halocarbons, other halogenated species and sulfur hexafluoride at individual stations. Solid circles show mole fractions in the Northern Hemisphere and open circles show those measured in the Southern Hemisphere.

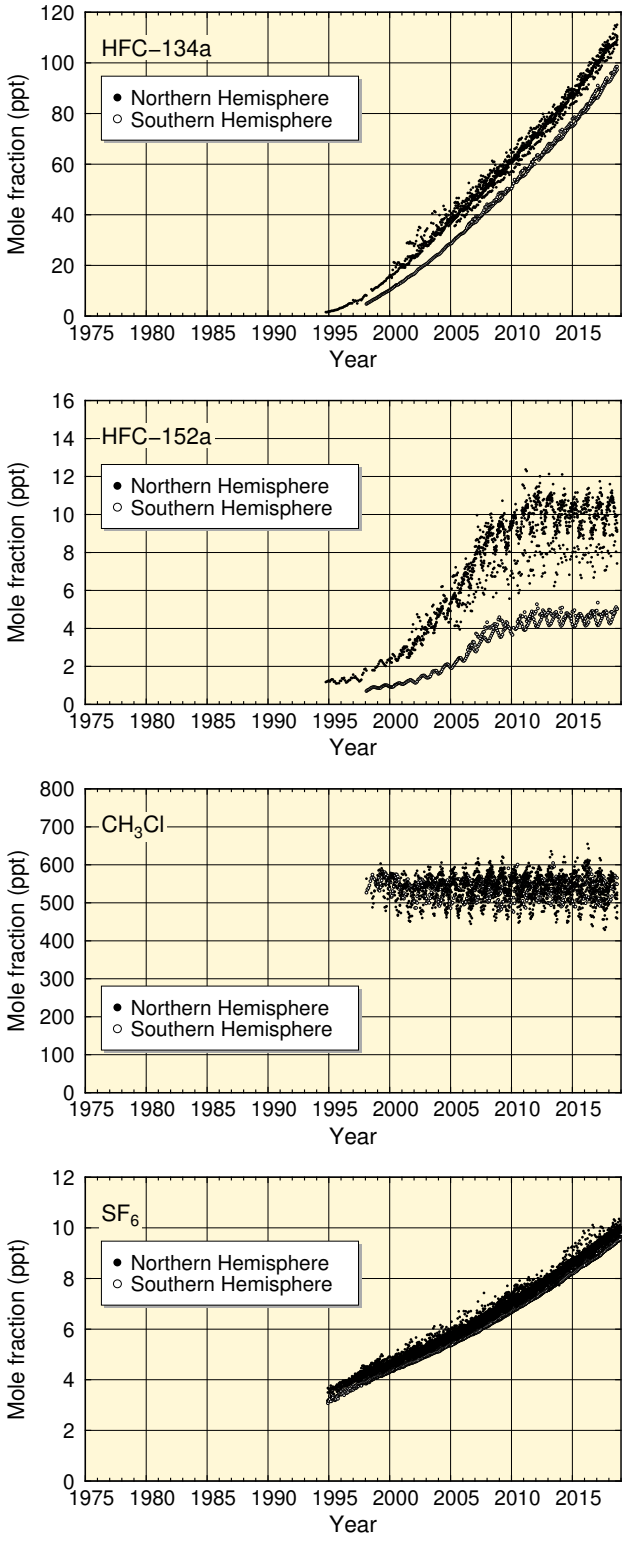

Fig. 4.2 (Continued)

5.

CARBON MONOXIDE

(CO)

● : CONTINUOUS STATION

△ : FLASK STATION

□ : FLASK MOBILE (SHIP)

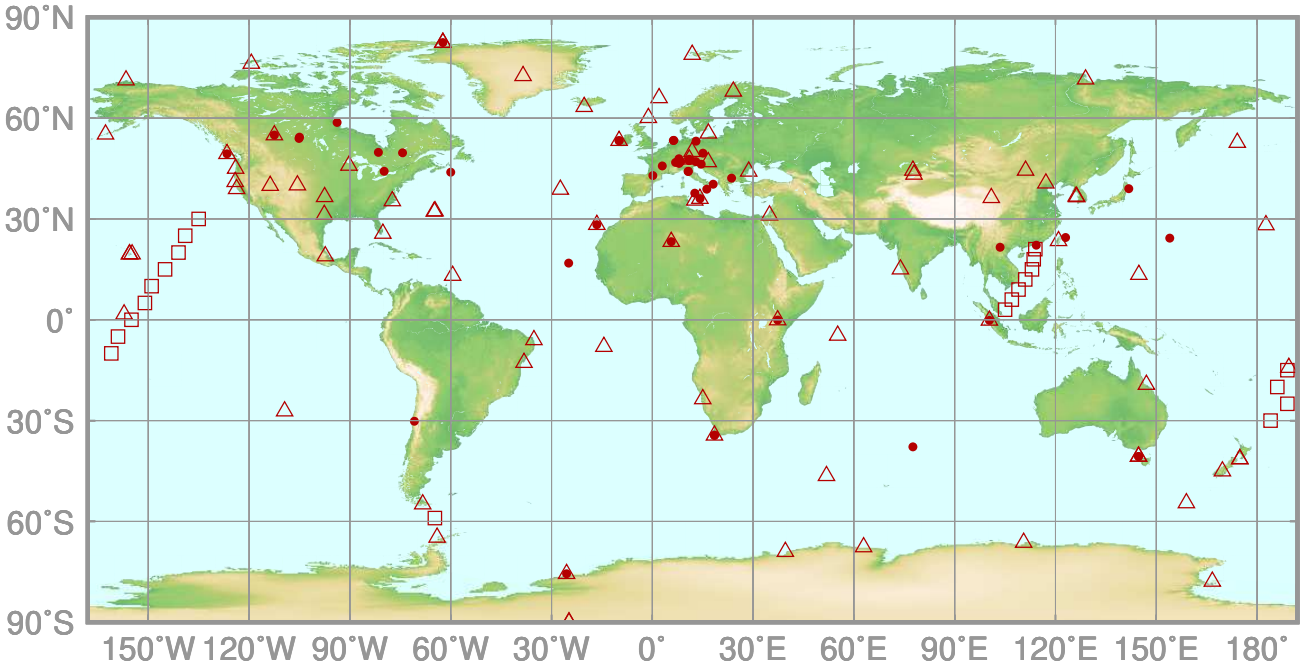

This map shows locations of the stations that have submitted data for monthly mean mole fractions.

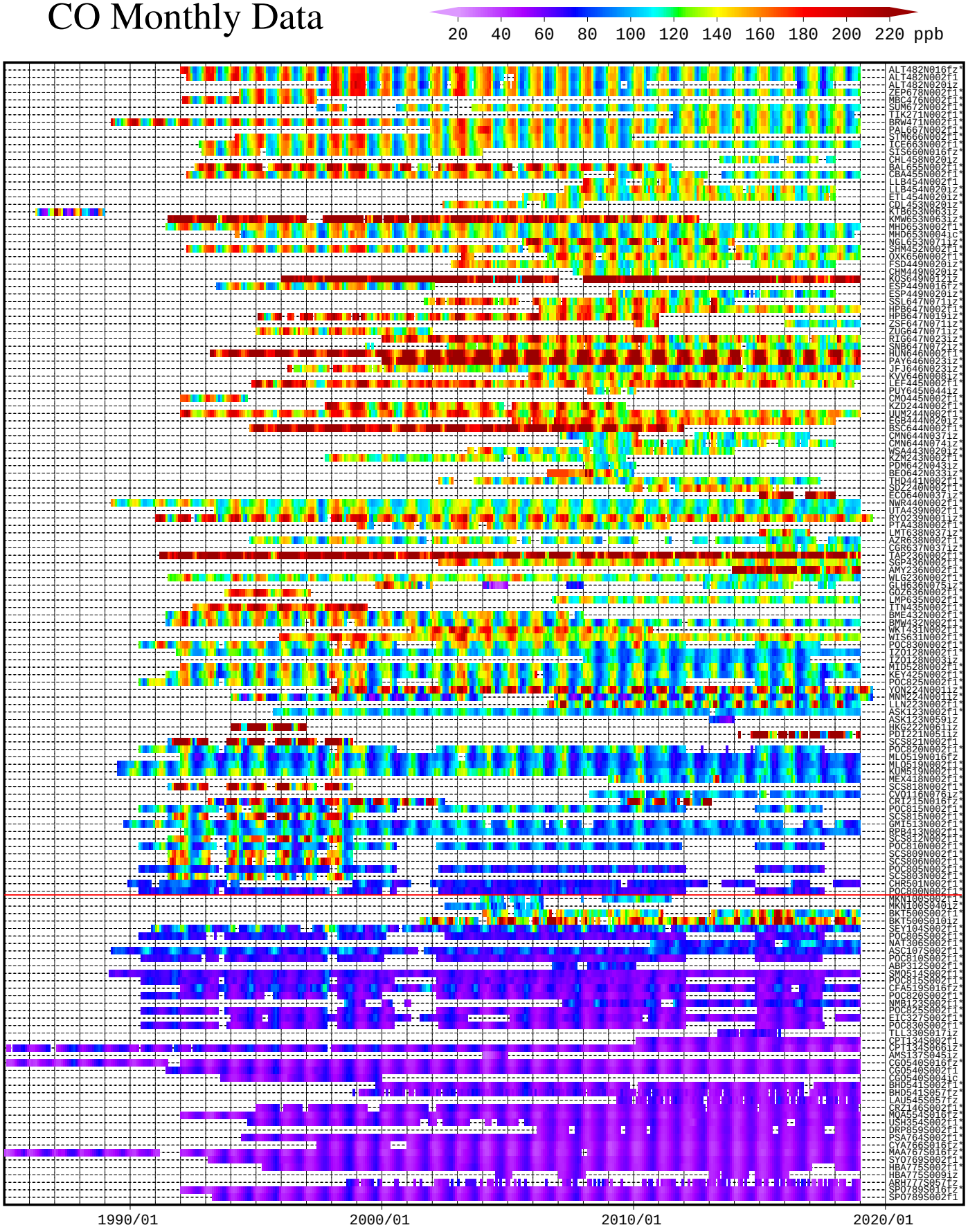

Plate 5.1 Monthly mean CO mole fractions that have been reported to the WDCGG. The mole fractions are illustrated in different colors. The sites are listed in order from north to south. The red line indicates the equator. The data from the sites with an asterisk at the end of the station index were used for the analyses shown in Plate 5.2 (see Appendix A).

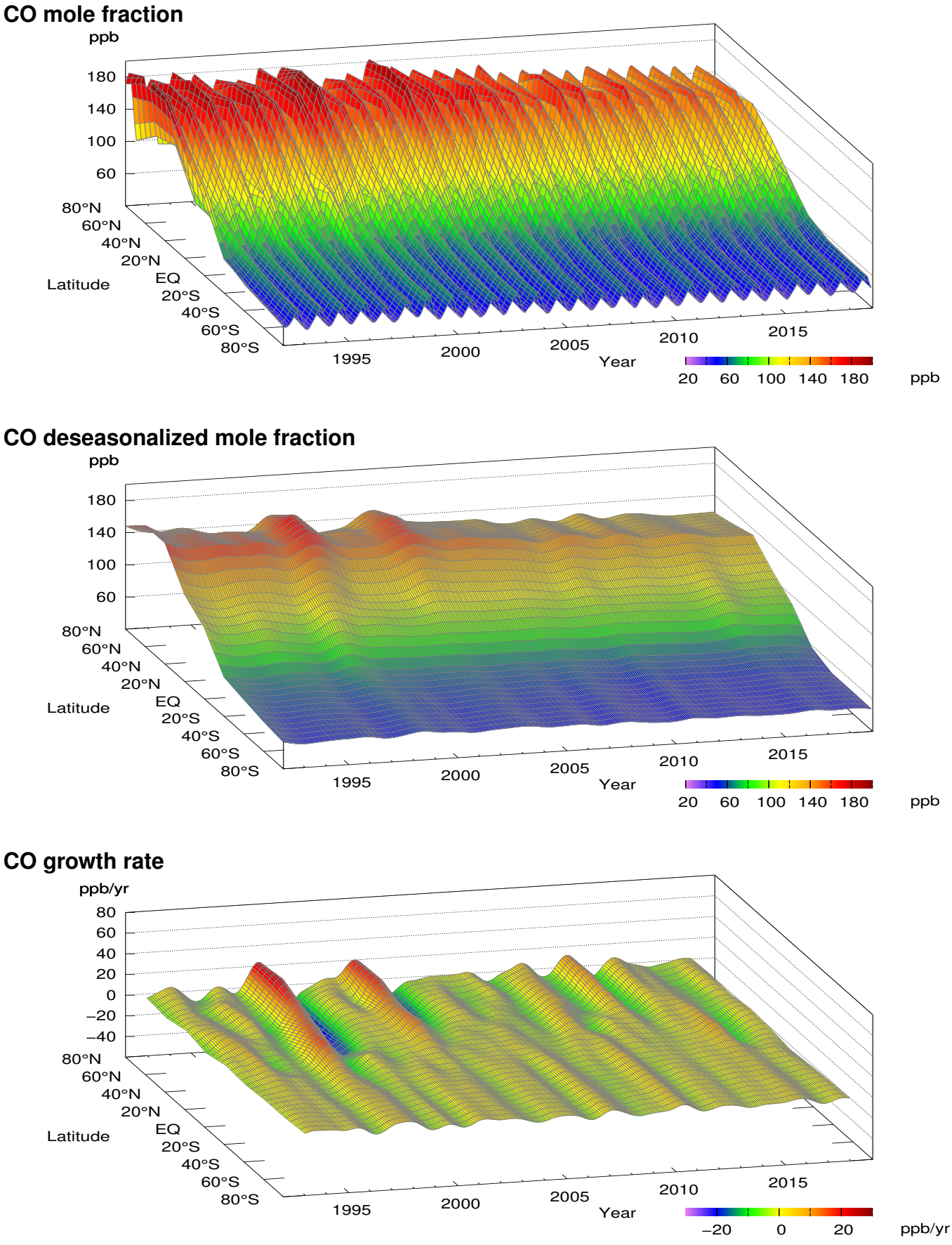

Plate 5.2 Variation of zonally averaged monthly mean CO mole fractions (top), deseasonalized long-term trends (middle), and growth rates (bottom). The zonally averaged mole fractions were calculated for each 20° zone. The deseasonalized trends and growth rates were derived as described in Appendix A.

5. CARBON MONOXIDE (CO)

Carbon monoxide (CO) is not categorized as a greenhouse gas because it absorbs hardly any infrared radiation from the earth. However, it influences major greenhouse gases, particularly through reaction with hydroxyl (OH) radical, and is therefore often addressed in the context of global warming. CO is also part of the global carbon cycle.

In contrast to the situation with major greenhouse gases, CO calibration scales cannot be easily interlinked (see Appendix B). In this research, analysis performed irrespective of scale differences showed a global mean CO mole fraction of 91±2 ppb for 2018. Similarly, the analysis results presented in this chapter are based on observations performed on different scales.

CO is emitted into the atmosphere from fossil fuel/biomass combustion among other sources, and is destroyed predominantly via reaction with OH radicals. Due to its chemical reactivity, CO is characterized by a relatively short lifetime (in the range of tens of days) and large spatial variations. Ice core measurements performed by Haan and Raynaud (1998) revealed that the CO mole fractions of approximately 90 ppb observed in Greenland around 1750 had increased to approximately 110 ppb by 1950, indicating an impact from human activity. CO mole fractions have shown a gradual decline since around the beginning of the 21st century, particularly in the Northern Hemisphere (IPCC, 2013).

Global mean mole fractions

The blue dots in Fig. 5.1 show global mean CO mole fractions (top) and related growth rates (bottom) based on the analysis described in Appendix A. Clear seasonal variability is observed, and the long-term trend was determined after subtraction of the seasonal component (shown by the red line in the top panel of Fig. 5.1). The global mean CO mole fraction exhibits a gradual decrease, with the growth rate oscillating around zero. Mole fractions exhibit clear seasonal cycles, being lower in boreal summer and higher in winter. This is mainly because OH radicals, which react with and destroy CO, become more abundant in summer due to enhanced ultraviolet (UV) radiation. Seasonally varying sources such as biomass combustion, domestic combustion and traffic emissions also contribute to these cycles.

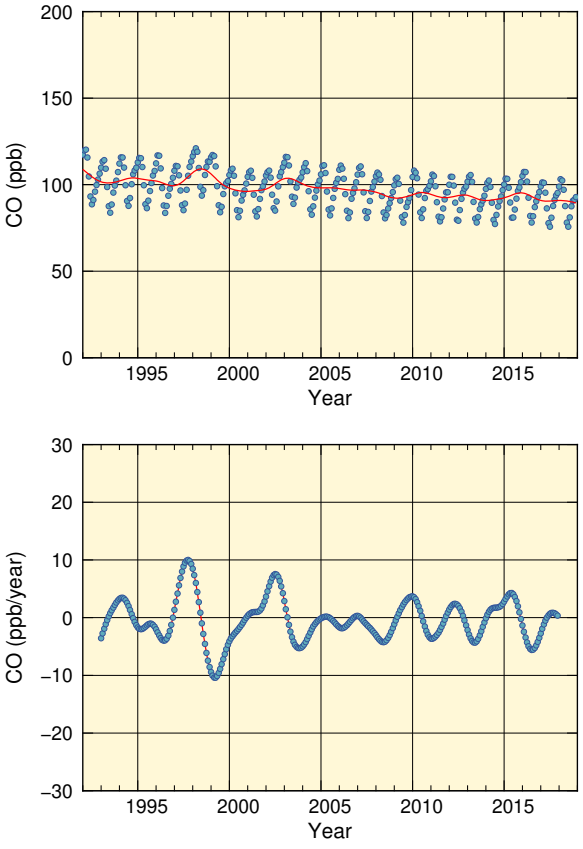

Fig. 5.1 Globally averaged monthly mean mole fraction of CO from 1992 to 2018 and the deseasonalized long-term trend in red line (top), and its growth rate (bottom).

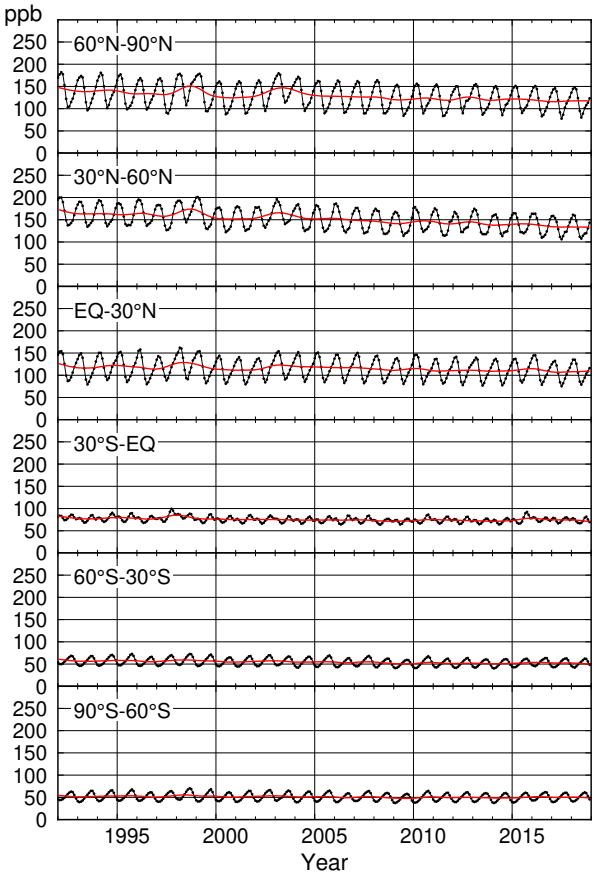

Fig. 5.2 Monthly mean mole fractions of CO from 1992 to 2018 for each 30° latitudinal zone (black) and their deseasonalized long-term trends (red).

Latitudinal dependence of mole fractions

The black lines in Fig. 5.2 show CO mole fractions averaged over six 30° latitudinal bands, and the red lines show corresponding long-term trends. These trends are collectively shown in the top panel of Figure 5.3, and the corresponding growth rates are shown in the bottom panel. Average seasonal cycles of CO mole fractions for every latitudinal band are shown in Figure 5.4.

As shown in Figure 5.3, northern regions tend to have higher mole fractions, indicating the presence of more CO sources such as fossil fuel/biomass combustion. CO mole fractions in the Northern Hemisphere have shown slight declines throughout the period for which global averaging is feasible, and have remained almost constant in the Southern Hemisphere. CO growth rates also exhibit significant spatial and temporal variability, and tend to be readily influenced by local events with limited time durations. By way of example, the large growth rate peak of 1997/1998 observed in the Northern Hemisphere and elsewhere may be considered attributable to forest fires in Siberia and tropical areas (Novelli *et al.*, 2003).

The amplitude of seasonal cycles for CO mole fractions is larger in northern bands than in southern bands, as shown in Figure 5.4. In the Northern Hemisphere, CO emitted from fossil fuel combustion accumulates in the mid- and high latitudes during winter and early spring under low OH radical conditions. In addition, CO emissions from biomass combustion in the low latitudes peak in early spring. In summer, most of the CO accumulated during winter is destroyed by OH radicals. In the Southern Hemisphere, seasonal cycles of CO mole fractions are driven by emissions from biomass burning in the tropics and removal via reaction with OH radicals, resulting in a smaller seasonal-cycle amplitude (Novelli *et al.*, 1998). The phase of seasonal cycles for CO mole fractions in the two hemispheres is opposed due to the reversed seasons. Seasonal variability in the low latitudes of the Southern Hemisphere is slightly more complex, probably under the influence of atmospheric conditions in the Northern Hemisphere.

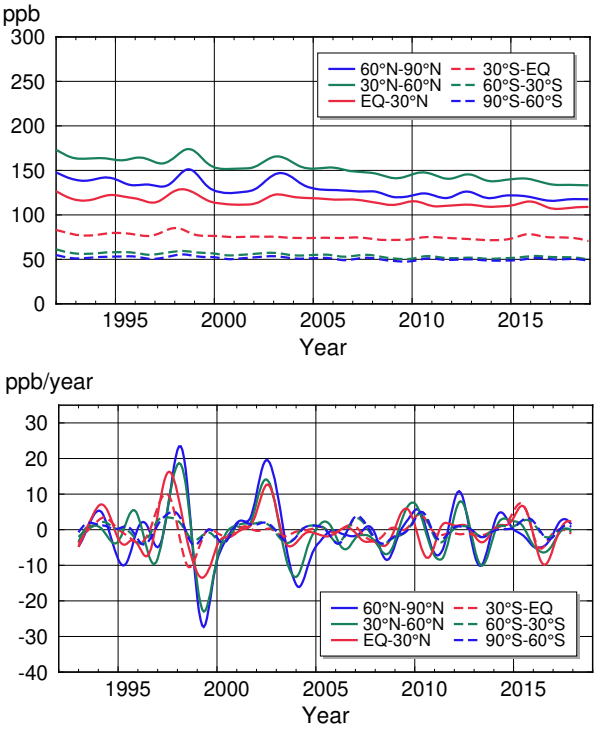

Fig. 5.3 Deseasonalized long-term trends of CO for each 30° latitudinal zone (top) and their growth rates (bottom).

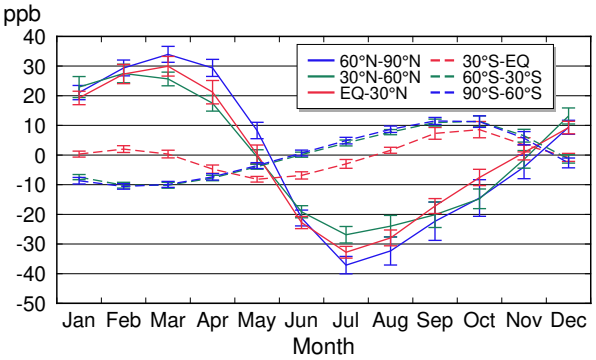

Fig. 5.4 Average seasonal cycles of CO mole fractions for each 30° latitudinal zone obtained by subtracting long-term trends from the zonal mean time series. Error bars represent the range of ±1σ calculated for each month (period 1992 to 2018).

APPENDICES

APPENDIX A ANALYSIS

This appendix summarizes the method used to calculate global mean mole fractions and related quantities of CO_2, CH_4, N_2O and CO as described by WMO (2009).

The analysis is applied to monthly mean mole fraction data reported to WDCGG by fixed stations and ships with fixed observation points. Where no monthly data are reported, values are calculated from daily or hourly valid data based on a simple arithmetic mean with the consent of data contributors. Data from mobile platforms such as ships without fixed observation points and aircraft are not used in this analysis, but are considered in other applications. Where data are reported for several different altitudes, those for the highest level are used due to their expected larger footprint.

For halocarbons, monthly mean mole fractions from observation at individual stations are presented. Scale differences have not been taken into account in this analysis.

The mole fraction is defined as the number of molecules of a target gas species divided by the number of all molecules of dry air. Values are expressed as parts per million (ppm), parts per billion (ppb) or parts per trillion (ppt), corresponding to the SI units of μmol/mol, nmol/mol and pmol/mol, respectively.

(1) Site selection

All observation data are objectively selected for global analysis as described here.

Data with a standard scale traceable to the WMO Mole Fraction Scale (or a compatible standard for conversion) are first selected. CO data are an exception due to the scarcity of standard scales for which accurate conversion to the WMO Scale is possible.

For individual sites, annual mean mole fractions relative to those of the South Pole (averaged over the years for which data are available) are plotted to show latitudinal distribution and fitted to the LOESS model curve (Cleveland and Devlin, 1988). Outlier sites beyond the 3 sigma (residual standard deviation) of the fitted curve are excluded from further analysis, and the process is iterated until exclusion terminates. Exclusion is not applied to N_2O due to the scarcity of annual mean data from the 1980s.

The numbers of sites that fit for global analysis (before and after this selection procedure) are shown in Table A1.

(2) Extension of observation data to cover the entire analysis period

Time-series data from some sites may contain gaps or fail to cover the entire analysis period. To ensure the homogeneity of globally averaged values over analysis periods exceeding 30 years, shortfalls in data coverage are compensated for using interpolation and extrapolation as described below.

Gaps in time-series representations are first interpolated for each site. The longest period among continuous monthly mean mole fraction data is identified, and the seasonal cycle and long-term trend are determined as detailed in WMO (2009). In short, a time series of mole fractions is approximated based on the sum of a Fourier series up to the third harmonic of the annual cycle and a non-periodic component determined via a Lanczos filter (Duchon, 1979) with a cut-off frequency of 0.48 cycles per year; the former is a seasonal cycle, and the latter is a long-term trend. Mole fractions in gaps are then interpolated with a line connecting each end of the deseasonalized monthly values and superimposed with the seasonal cycle.

After interpolation, the data are extrapolated via a number of statistical procedures. First, a time series of mole fraction growth rates is calculated for each observation site by differentiating the long-term trend as determined from mole fractions with gaps interpolated as above. Next, for each of six 30° latitudinal bands (60 – 90°N, 30°S – EQ, etc.), an average time series of growth rates is calculated as an arithmetic mean over sites located within the band. For individual sites, the long-term trend is then extended to cover the entire analysis period based on growth rates for the latitudinal band where the site is located, and is finally superimposed with the seasonal cycle for the site determined after interpolation.

Table A1. Numbers of sites before/after the selection procedure outlined in Section (1) for CO_2, CH_4, N_2O and CO

	CO_2	CH_4	N_2O	CO
Pre-selection [(a)]	165	140	101	134
Post-selection [(b)]	129	127	96	122

(a) Figures are derived from the number of the first seven characters of the Filename Code (e.g., RYO239N) in Plate 1.1, 2.1, 3.1 and 5.1 (or Table B3 to B6), excluding duplicates.
(b) As per (a), but with Filename Codes marked with asterisks.

(3) Calculation of global and hemispheric mean mole fractions

With the extension procedure described above, all sites selected as described in Section (1) have a time series of mole fractions covering the entire analysis period with no data gaps. From these data, latitudinal mean mole fractions are calculated for the six bands, and global and hemispheric mean mole fractions are then determined by averaging the mole fractions of six and three latitudinal bands, respectively, with weighting for surface area. The seasonal cycle, long-term trend and growth rate are then determined for every averaged time series. As long-term trend calculation is less precise at either end of mole fraction time-series representations (see WMO 2009 for details), growth rates originating from the related derivative function are characterized by larger uncertainty. Accordingly, growth rates for a year each from either end of the analysis period are not shown in the figures here.

(4) Uncertainty estimation

In this analysis, uncertainty in global mean mole fractions (at a 68% confidence level) is calculated using bootstrap analysis as described in Conway *et al*. (1994). From the dataset of mole fractions obtained after the site selection and data extension procedure described above, n sites are randomly selected, with duplication of the same sites allowed on condition that at least one site is selected from each of the six latitudinal bands, and a global mean mole fraction is calculated using the data from the n sites. The procedure is repeated m times to determine m different global mean mole fractions. Uncertainty is defined as the standard deviation of these mole fractions. In this analysis, the number of sites selected as described in Section (1) and 200 are chosen as n and m, respectively, for maximum stability in the standard deviation thus determined.

APPENDIX B CALIBRATION AND STANDARD SCALES

1. Calibration System in the GAW Programme

Under the Global Atmosphere Watch (GAW) Programme, the Central Calibration Laboratories (CCLs) are assigned to host a Primary (Reference) Standard/scale, while the World Calibration Centres (WCCs) and Regional Calibration Centres (RCC) are responsible for the scale propagation to the stations via distribution of calibration standards for certain compounds, conducting instrument calibrations, comparison campaigns, station audits and providing training to the station personnel. A Reference Standard/scale is designated for each variable to be used for all GAW measurements of that variable. Table B1 lists the organizations that serve as WCCs and CCLs for GAW (WMO, 2017). For CFCs, no central facilities or quality control systems have so far been established within the GAW Programme.

Table B1. Overview of the GAW Central Calibration Laboratories (GAW-CCL, Reference Standard) and World Calibration Centres for greenhouse and other related gases. The World Calibration Centres have assumed global responsibilities, except where indicated (Am, Americas; E/A, Europe and Africa; A/O, Asia and the South-West Pacific)

Compounds	Central Calibration Laboratory (Host of Primary Standard)	World Calibration Centre
Carbon Dioxide (CO_2)	NOAA/ESRL	NOAA/ESRL (Round Robin) Empa (audits)
Carbon Dioxide (CO_2) isotopes	MPI-BGC	
Methane (CH_4)	NOAA/ESRL	Empa (Am, E/A) JMA (A/O)
Nitrous Oxide (N_2O)	NOAA/ESRL	KIT/IMK-IFU
Chlorofluorocarbons (CFCs)		
Sulfur Hexafluoride (SF_6)	NOAA/ESRL	KMA
Molecular Hydrogen (H_2)	MPI-BGC	
Carbon Monoxide (CO)	NOAA/ESRL	Empa

2. Carbon Dioxide (CO_2)

In 1995, the National Oceanic and Atmospheric Administration's Earth System Research Laboratory (NOAA/ESRL; formerly the Climate Monitoring and Diagnostics Laboratory, or CMDL) in Boulder, Colorado, USA, took over a CLL role from the Scripps Institution of Oceanography (SIO) in San Diego, California, USA, and has since been responsible for maintenance of the GAW Primary Standard for CO_2. In this role, the laboratory maintains a high-precision manometric system for absolute calibration of CO_2 as reference for GAW monitoring worldwide (Zhao *et al.*, 1997), as well as carrying out round-robin operation in WCC functions. The standards of GAW monitoring laboratories should advisably be calibrated at least every three years at the CCL (WMO, 2020).

Under the WMO system, there have been several calibration scales for CO_2, including the SIO-based X74, X85, X87, X93 and X2002 scales and the NOAA/ESRL-based WMO Mole Fraction Scale, partially based on previous SIO scales. The CCL adopted the WMO X2005 scale, reflecting historical manometric calibrations of its set of cylinders and possible minor differences between SIO and NOAA/ESRL calibrations. The most current WMO Mole Fraction Scale is the WMO X2007 version.

To assess differences in standard scales among monitoring laboratories, NOAA/ESRL organizes intercomparisons and round-robin experiments endorsed by WMO every three years or so. Numerous laboratories contributed to the experiments organized in 1991 – 1992, 1995 – 1997, 1999 – 2000, 2002 – 2006, 2009 – 2012 and 2014 – 2015. Table B2 shows the results of the experiments performed in 2014 – 2015, in which mole fractions determined by various laboratories were compared with those determined by NOAA/ESRL (http://www.esrl.noaa.gov/gmd/ccgg/wmorr/wmorr_results.php).

Table B3 lists organizations and sites contributing to the present issue of the Data Summary with standard scales of reported data and histories of contribution to WMO intercomparison experiments.

Table B2. Round Robin results for the mole fraction of carbon dioxide. Differences between the mole fractions measured by various laboratories and the mole fractions measured by NOAA (Laboratory minus NOAA, ppm).

Laboratory	Measurement Date	Mole Fraction Difference (ppm)	
		Low 375-380 ppm	High 400-415 ppm
NCAR	Mar-14 & Jun-15	–0.01 ~ 0.02	–0.05
NOAA-CSD	Apr-14	0.06	0.03
NEON	May-14	0.01	0.02
NIST	Jul-14	–0.37	–0.49
Harvard University	Jul & Dec-14	0.05	0.01
PSU	Aug-14	0.03	-0.02
CALTECH	Sep-14	-0.02	-0.04
BLG	Oct-14	0.06	-0.09
AMERIFLUX	Nov-14	-0.01	-0.02
ECCC	Dec-14	0.09	0.06
HMS	Jun-15	0.03	0.02
AEMET	Aug-15	-0.01	-0.01
CSIRO	May-14	0.04	0.00
NIWA	Jun-14	0.08	-0.08
SAWS	Aug-14	0.16	0.14
CMA	Oct-14	0.02	-0.02
KMA	Jan-15	0.03	0.04
MGO	Aug-15	0.00	-0.03
LSCE	May-14	-0.05	-0.00
WCC-Empa	Jun-14	-0.10	-0.06
Empa	Jul-14	-0.07	-0.06
FMI	Sep-14 & Jul-15	0.01	-0.10
RUG	Dec-14	0.03	0.06
ECN	Jan-15	0.31	0.51
UEA	Mar-15	-0.31	-0.25
RHUL	Apr-15	-0.10	-0.02
UHEI-IUP	Jun-14	-0.03	-0.06
UBAG-SCHAU	Jul-14	0.05	-0.04
UBAG/ZUG	Sep-14	0.03	0.02
MPI-BGC	Nov-14	-0.01	-0.02
RSE	Jan-15	0.07	-0.08
IAFMC	Feb-15	-1.63	-1.62
ENEA	May-15	-0.01	-0.05
ICOS	Jul-15	-0.01	-0.03
JMA	Oct-13	-0.04	-0.04
MRI	Nov-13	-0.15	-0.14
AIST	Jan-14	0.13	0.18
NIES	Jan-14	-0.09	-0.04
TU	Feb-14	0.16	0.25

Table B3. Status of standard scales and calibration/intercomparison for CO_2.

Organi-zation	WDCGG Filename	Filename Code in Plate 1.1	Calib-ration Scale	WMO Inter-comparison
AEMET	co2_izo_surface-insitu_3_9999-9999_monthly.txt	IZO128N003iz*	WMO	91/92, 96/97, 99/00, 09/12, 14/15
AICH	co2_mkw_surface-insitu_5_9999-9999_monthly.txt	MKW234N005iz	WMO	
AIST	co2_tky_tower-insitu_6_6028-9999_monthly.txt	TKY236N006it		96/97, 99/00, 02/06, 09/12, 14/15
BMKG	co2_bkt_surface-insitu_10_9999-9999_monthly.txt	BKT500S010iz	WMO	
CMA	co2_wlg_surface-insitu_13_9999-9999_monthly.txt	WLG236N013iz*	WMO	96/97, 99/00, 02/06, 09/12, 14/15
CSIRO	co2_alt_surface-flask_16_9999-9999_monthly.txt co2_cfa_surface-flask_16_9999-9999_monthly.txt co2_cgo_surface-flask_16_9999-9999_monthly.txt co2_cgo_surface-insitu_16_9997-9999_monthly.txt co2_cgo_surface-insitu_16_9998-9999_monthly.txt co2_cgo_surface-insitu_16_9999-9999_monthly.txt co2_cri_surface-flask_16_9999-9999_monthly.txt co2_cya_surface-flask_16_9999-9999_monthly.txt co2_esp_surface-flask_16_9999-9999_monthly.txt co2_maa_surface-flask_16_9999-9999_monthly.txt co2_mlo_surface-flask_16_9999-9999_monthly.txt co2_mqa_surface-flask_16_9999-9999_monthly.txt co2_sis_surface-flask_16_9999-9999_monthly.txt co2_spo_surface-flask_16_9999-9999_monthly.txt	ALT482N016fz CFA519S016fz* CGO540S016fz CGO540S016ix* CGO540S016iy CGO540S016iz CRI215N016fz* CYA766S016fz* ESP449N016fz* MAA767S016fz* MLO519N016fz MQA554S016fz* SIS660N016fz* SPO789S016fz	WMO	91/92, 96/97, 99/00, 02/06, 09/12, 14/15
DMC	co2_tll_surface-insitu_17_9999-9999_monthly.txt	TLL330S017iz	WMO	
ECCC	co2_alt_surface-insitu_20_9999-9999_monthly.txt co2_cdl_surface-insitu_20_9999-9999_monthly.txt co2_chl_surface-insitu_20_9999-9999_monthly.txt co2_chm_surface-insitu_20_9999-9999_monthly.txt co2_egb_surface-insitu_20_9999-9999_monthly.txt co2_esp_surface-insitu_20_9999-9999_monthly.txt co2_etl_surface-insitu_20_9999-9999_monthly.txt co2_fsd_surface-insitu_20_9999-9999_monthly.txt co2_llb_surface-insitu_20_9999-9999_monthly.txt co2_wsa_surface-insitu_20_9999-9999_monthly.txt	ALT482N020iz CDL453N020iz* CHL458N020iz* CHM449N020iz* EGB444N020iz* ESP449N020iz* ETL454N020iz* FSD449N020iz* LLB454N020iz* WSA443N020iz*	WMO	91/92, 96/97, 99/00, 02/06, 09/12, 14/15
EMA	co2_cai_surface-insitu_22_9999-9999_monthly.txt co2_frf_surface-insitu_22_9999-9999_monthly.txt	CAI130N022iz FRF127N022iz		
Empa	co2_jfj_surface-insitu_23_9999-9999_monthly.txt	JFJ646N023iz*	WMO	09/12, 14/15
ENEA	co2_lmp_surface-flask_24_9999-9999_monthly.txt	LMP635N024fz*	WMO	91/92, 96/97, 99/00, 02/06, 09/12, 14/15
FMI	co2_pal_surface-insitu_25_9999-9999_monthly.txt	PAL667N025iz*	WMO	02/06, 09/12 14/15
GERC	co2_gsn_surface-insitu_52_9999-9999_monthly.txt	GSN233N052iz	WMO	
HKO	co2_hkg_surface-insitu_27_9999-9999_monthly.txt	HKG222N027iz*	WMO	
	co2_hko_surface-insitu_27_9999-9999_monthly.txt	HKO222N027iz	WMO NIST	
HMS	co2_hun_tower-insitu_28_6116-9999_monthly.txt co2_kps_surface-insitu_28_9999-9999_monthly.txt	HUN646N028it KPS646N028iz*	WMO	91/92, 96/97, 99/00, 02/06, 09/12, 14/15

IAA	co2_jbn_surface-insitu_18_9999-9999_monthly.txt	JBN762S018iz*	WMO	
IAFMS	co2_cmn_surface-insitu_29_9999-9999_monthly.txt	CMN644N029iz*	WMO	91/92, 96/97, 02/06, 14/15
IGP	co2_hua_surface-insitu_30_9999-9999_monthly.txt	HUA312S030iz	WMO	
IMKIFU	co2_wnk_surface-insitu_31_9999-9999_monthly.txt co2_zug_surface-insitu_31_9999-9999_monthly.txt	WNK647N031iz ZUG647N031iz	WMO	99/00
INMH	co2_fdt_surface-insitu_58_9999-9999_monthly.txt	FDT645N058iz		
INRNE	co2_beo_surface-insitu_33_9999-9999_monthly.txt	BEO642N033iz	WMO	
IOEP	co2_dig_surface-insitu_35_9999-9999_monthly.txt	DIG654N035iz		
ISAC	co2_cgr_surface-insitu_37_9999-9999_monthly.txt co2_lmt_surface-insitu_37_9999-9999_monthly.txt	CGR637N037iz* LMT638N037iz	WMO	
	co2_eco_surface-insitu_37_9999-9999_monthly.txt	ECO640N037iz		
ITM	co2_zep_surface-insitu_38_9999-9999_monthly.txt	ZEP678N038iz	WMO	96/97, 99/00, 09/12
JMA	co2_mnm_surface-insitu_1_9999-9999_monthly.txt co2_ryo_surface-insitu_1_9999-9999_monthly.txt co2_yon_surface-insitu_1_9999-9999_monthly.txt	MNM224N001iz* RYO239N001iz* YON224N001iz*	WMO	91/92, 96/97, 99/00, 02/06, 09/12, 14/15
KMA	co2_amy_surface-insitu_39_9999-9999_monthly.txt co2_jgs_surface-insitu_39_9999-9999_monthly.txt	AMY236N039iz* JGS233N039iz	WMO	02/06, 09/12 14/15
	co2_ksg_surface-insitu_39_9999-9999_monthly.txt	KSG762S039iz	KRISS	
KSNU	co2_isk_surface-remote_41_9999-9999_monthly.txt	ISK242N041rz		
KUP	co2_jfj_surface-insitu_42_9999-9999_monthly.txt	JFJ646N042iz*	WMO	09/12
LSCE	co2_ams_surface-insitu_45_9998-9999_monthly.txt co2_bgu_surface-flask_45_9999-9999_monthly.txt co2_lpo_surface-flask_45_9999-9999_monthly.txt co2_mhd_surface-insitu_45_9999-9999_monthly.txt co2_pdm_surface-flask_45_9999-9999_monthly.txt co2_puy_surface-insitu_45_9999-9999_monthly.txt	AMS137S045iy* BGU641N045fz* LPO648N045fz MHD653N045iz PDM642N045fz* PUY645N045iz*	WMO	91/92, 96/97, 99/00, 02/06, 09/12, 14/15
	co2_fik_surface-flask_45_9999-9999_monthly.txt	FIK635N045fz		
METRI	co2_gsn_surface-flask_55_9999-9999_monthly.txt	GSN233N055fz*	WMO	96/97
MGO	co2_ber_surface-flask_46_9999-9999_monthly.txt co2_kot_surface-flask_46_9999-9999_monthly.txt co2_kyz_surface-flask_46_9999-9999_monthly.txt co2_stc_surface-flask_46_9999-9999_monthly.txt co2_ter_surface-flask_46_9999-9999_monthly.txt co2_tik_surface-flask_46_9999-9999_monthly.txt	BER255N046fz* KOT276N046fz* KYZ240N046fz* STC654N046fz* TER669N046fz* TIK271N046fz*	WMO	14/15
MMD	co2_dmv_surface-insitu_47_9999-9999_monthly.txt	DMV504N047iz	WMO	
MRI	co2_tkb_tower-insitu_48_6201-9999_monthly.txt	TKB236N048it	MRI-87	91/92, 96/97, 99/00, 02/06, 09/12, 14/15
NIES	co2_coi_surface-insitu_53_9999-9999_monthly.txt co2_hat_surface-insitu_53_9999-9999_monthly.txt	COI243N053iz* HAT224N053iz*	NIES 95**	96/97, 99/00, 02/06, 09/12, 14/15
NIWA	co2_bhd_surface-insitu_57_9999-9999_monthly.txt	BHD541S057iz*	WMO	91/92, 96/97, 99/00, 02/06, 09/12, 14/15
NOAA	co2_abp_surface-flask_2_3001-9999_monthly.txt co2_alt_surface-flask_2_3001-9999_monthly.txt co2_ams_surface-flask_2_3001-9999_monthly.txt co2_amy_surface-flask_2_3001-9999_monthly.txt co2_asc_surface-flask_2_3001-9999_monthly.txt co2_ask_surface-flask_2_3001-9999_monthly.txt	ABP312S002f1* ALT482N002f1* AMS137S002f1 AMY236N002f1 ASC107S002f1* ASK123N002f1*	WMO	91/92, 96/97, 99/00, 02/06, 09/12, 14/15

	co2_avi_surface-flask_2_3001-9999_monthly.txt	AVI417N002f1*		
	co2_azr_surface-flask_2_3001-9999_monthly.txt	AZR638N002f1*		
	co2_bal_surface-flask_2_3001-9999_monthly.txt	BAL655N002f1*		
	co2_bhd_surface-flask_2_3001-9999_monthly.txt	BHD541S002f1		
	co2_bkt_surface-flask_2_3001-9999_monthly.txt	BKT500S002f1		
	co2_bme_surface-flask_2_3001-9999_monthly.txt	BME432N002f1*		
	co2_bmw_surface-flask_2_3001-9999_monthly.txt	BMW432N002f1*		
	co2_brw_surface-flask_2_3001-9999_monthly.txt	BRW471N002f1		
	co2_brw_surface-insitu_2_3001-9999_monthly.txt	BRW471N002i1*		
	co2_bsc_surface-flask_2_3001-9999_monthly.txt	BSC644N002f1		
	co2_cba_surface-flask_2_3001-9999_monthly.txt	CBA455N002f1*		
	co2_cgo_surface-flask_2_3001-9999_monthly.txt	CGO540S002f1*		
	co2_chr_surface-flask_2_3001-9999_monthly.txt	CHR501N002f1*		
	co2_cmo_surface-flask_2_3001-9999_monthly.txt	CMO445N002f1*		
	co2_cpt_surface-flask_2_3001-9999_monthly.txt	CPT134S002f1		
	co2_crz_surface-flask_2_3001-9999_monthly.txt	CRZ146S002f1*		
	co2_drp_ship-flask_2_3001-9999_monthly.txt	DRP859S002f1*		
	co2_eic_surface-flask_2_3001-9999_monthly.txt	EIC327S002f1*		
	co2_gmi_surface-flask_2_3001-9999_monthly.txt	GMI513N002f1*		
	co2_goz_surface-flask_2_3001-9999_monthly.txt	GOZ636N002f1*		
	co2_hba_surface-flask_2_3001-9999_monthly.txt	HBA775S002f1*		
	co2_hpb_surface-flask_2_3001-9999_monthly.txt	HPB647N002f1*		
	co2_hun_surface-flask_2_3001-9999_monthly.txt	HUN646N002f1*		
	co2_ice_surface-flask_2_3001-9999_monthly.txt	ICE663N002f1*		
	co2_izo_surface-flask_2_3001-9999_monthly.txt	IZO128N002f1		
	co2_key_surface-flask_2_3001-9999_monthly.txt	KEY425N002f1*		
	co2_kum_surface-flask_2_3001-9999_monthly.txt	KUM519N002f1*		
	co2_kzd_surface-flask_2_3001-9999_monthly.txt	KZD244N002f1*		
	co2_kzm_surface-flask_2_3001-9999_monthly.txt	KZM243N002f1*		
	co2_lef_surface-flask_2_3001-9999_monthly.txt	LEF445N002f1*		
	co2_llb_surface-flask_2_3001-9999_monthly.txt	LLB454N002f1		
	co2_lln_surface-flask_2_3001-9999_monthly.txt	LLN223N002f1*		
	co2_lmp_surface-flask_2_3001-9999_monthly.txt	LMP635N002f1*		
	co2_mbc_surface-flask_2_3001-9999_monthly.txt	MBC476N002f1*		
	co2_mex_surface-flask_2_3001-9999_monthly.txt	MEX418N002f1*		
	co2_mhd_surface-flask_2_3001-9999_monthly.txt	MHD653N002f1*		
	co2_mid_surface-flask_2_3001-9999_monthly.txt	MID528N002f1*		
	co2_mkn_surface-flask_2_3001-9999_monthly.txt	MKN100S002f1*		
	co2_mlo_surface-flask_2_3001-9999_monthly.txt	MLO519N002f1		
	co2_mlo_surface-insitu_2_3001-9999_monthly.txt	MLO519N002i1*		
	co2_nat_surface-flask_2_3001-9999_monthly.txt	NAT306S002f1*		
	co2_nmb_surface-flask_2_3001-9999_monthly.txt	NMB123S002f1*		
	co2_nwr_surface-flask_2_3001-9999_monthly.txt	NWR440N002f1*		
	co2_opw_surface-flask_2_3001-9999_monthly.txt	OPW448N002f1*		
	co2_oxk_surface-flask_2_3001-9999_monthly.txt	OXK650N002f1*		
	co2_pal_surface-flask_2_3001-9999_monthly.txt	PAL667N002f1		
	co2_poc_ship-flask_2_3001-3001_monthly.txt	POC800N002f1*		
	co2_poc_ship-flask_2_3001-3002_monthly.txt	POC805N002f1*		
	co2_poc_ship-flask_2_3001-3003_monthly.txt	POC810N002f1*		
	co2_poc_ship-flask_2_3001-3004_monthly.txt	POC815N002f1*		
	co2_poc_ship-flask_2_3001-3005_monthly.txt	POC820N002f1*		
	co2_poc_ship-flask_2_3001-3006_monthly.txt	POC825N002f1*		
	co2_poc_ship-flask_2_3001-3007_monthly.txt	POC830N002f1*		
	co2_poc_ship-flask_2_3001-3012_monthly.txt	POC805S002f1*		
	co2_poc_ship-flask_2_3001-3013_monthly.txt	POC810S002f1*		
	co2_poc_ship-flask_2_3001-3014_monthly.txt	POC815S002f1*		

	co2_poc_ship-flask_2_3001-3015_monthly.txt co2_poc_ship-flask_2_3001-3016_monthly.txt co2_poc_ship-flask_2_3001-3017_monthly.txt co2_poc_ship-flask_2_3001-3018_monthly.txt co2_psa_surface-flask_2_3001-9999_monthly.txt co2_pta_surface-flask_2_3001-9999_monthly.txt co2_rpb_surface-flask_2_3001-9999_monthly.txt co2_scs_ship-flask_2_3001-3101_monthly.txt co2_scs_ship-flask_2_3001-3102_monthly.txt co2_scs_ship-flask_2_3001-3103_monthly.txt co2_scs_ship-flask_2_3001-3104_monthly.txt co2_scs_ship-flask_2_3001-3105_monthly.txt co2_scs_ship-flask_2_3001-3106_monthly.txt co2_scs_ship-flask_2_3001-3107_monthly.txt co2_sdz_surface-flask_2_3001-9999_monthly.txt co2_sey_surface-flask_2_3001-9999_monthly.txt co2_sgp_surface-flask_2_3001-9999_monthly.txt co2_shm_surface-flask_2_3001-9999_monthly.txt co2_smo_surface-flask_2_3001-9999_monthly.txt co2_smo_surface-insitu_2_3001-9999_monthly.txt co2_spo_surface-flask_2_3001-9999_monthly.txt co2_spo_surface-insitu_2_3001-9999_monthly.txt co2_stc_surface-flask_2_3001-9999_monthly.txt co2_stm_surface-flask_2_3001-9999_monthly.txt co2_sum_surface-flask_2_3001-9999_monthly.txt co2_syo_surface-flask_2_3001-9999_monthly.txt co2_tap_surface-flask_2_3001-9999_monthly.txt co2_thd_surface-flask_2_3001-9999_monthly.txt co2_tik_surface-flask_2_3001-9999_monthly.txt co2_ush_surface-flask_2_3001-9999_monthly.txt co2_uta_surface-flask_2_3001-9999_monthly.txt co2_uum_surface-flask_2_3001-9999_monthly.txt co2_wis_surface-flask_2_3001-9999_monthly.txt co2_wlg_surface-flask_2_3001-9999_monthly.txt co2_zep_surface-flask_2_3001-9999_monthly.txt	POC820S002f1* POC825S002f1* POC830S002f1* POC835S002f1* PSA764S002f1* PTA438N002f1* RPB413N002f1* SCS803N002f1* SCS806N002f1* SCS809N002f1* SCS812N002f1* SCS815N002f1* SCS818N002f1* SCS821N002f1* SDZ240N002f1 SEY104S002f1* SGP436N002f1* SHM452N002f1* SMO514S002f1 SMO514S002i1* SPO789S002f1 SPO789S002i1* STC654N002f1 STM666N002f1* SUM672N002f1* SYO769S002f1* TAP236N002f1 THD441N002f1* TIK271N002f1 USH354S002f1* UTA439N002f1* UUM244N002f1* WIS631N002f1* WLG236N002f1* ZEP678N002f1*		
OSAKAU	co2_sui_surface-insitu_60_9999-9999_monthly.txt	SUI234N060iz		
RIVM	co2_kmw_surface-insitu_63_9999-9999_monthly.txt	KMW653N063iz	NIST	
RSE	co2_prs_surface-insitu_64_9999-9999_monthly.txt	PRS645N064iz*	WMO	99/00, 02/06 14/15
SAIPF	co2_ddr_surface-insitu_65_9999-9999_monthly.txt co2_kis_surface-insitu_65_9999-9999_monthly.txt co2_urw_surface-insitu_65_9999-9999_monthly.txt	DDR236N065iz* KIS236N065iz URW235N065iz	WMO	
SAWS	co2_cpt_surface-insitu_66_9999-1001_monthly.txt	CPT134S066iz*	WMO	99/00, 02/06, 09/12, 14/15
SHIZU	co2_hmm_surface-insitu_67_9999-9999_monthly.txt	HMM234N067iz		
TU	co2_syo_surface-insitu_70_9999-9999_monthly.txt	SYO769S070iz	Tohoku Univ. 2010	91/92, 96/97, 99/00, 02/06, 09/12
UBAA	co2_snb_surface-insitu_72_9999-9999_monthly.txt	SNB647N072iz*	WMO	
UBAG	co2_brt_surface-insitu_71_9999-9999_monthly.txt co2_deu_surface-insitu_71_9999-9999_monthly.txt co2_ngl_surface-insitu_71_9999-9999_monthly.txt co2_ssl_surface-insitu_71_9998-9999_monthly.txt co2_ssl_surface-insitu_71_9999-9999_monthly.txt co2_wal_surface-insitu_71_9999-9999_monthly.txt	BRT648N071iz* DEU649N071iz NGL653N071iz SSL647N071iy SSL647N071iz* WAL652N071iz	WMO	91/92, 96/97, 99/00, 02/06, 09/12, 14/15

	co2_wes_surface-insitu_71_9999-9999_monthly.txt co2_zgt_surface-insitu_71_9999-9999_monthly.txt co2_zsf_surface-insitu_71_9999-9999_monthly.txt co2_zug_surface-insitu_71_9999-9999_monthly.txt	WES654N071iz ZGT654N071iz ZSF647N071iz* ZUG647N071iz*		
UMLT	co2_glh_surface-insitu_75_9999-9999_monthly.txt	GLH636N075iz		
VNMHA	co2_pdi_surface-insitu_51_9999-9999_monthly.txt	PDI221N051iz	WMO	

* Stations marked with an asterisk are used for the calculation of global mean mole fractions and related quantities. The site selection procedure is described in Appendix A.
** NIES 95 CO_2 scale is 0.10 to 0.14 ppm lower than that of WMO in the range 355 to 385 ppm.
(Machida *et al*., WMO/GAW Report No. 186, 26-29, 2009.)

3. Methane (CH_4)

The GAW Programme has a CCL for CH_4 at NOAA/ESRL (Dlugokencky *et al.*, 2005; WMO, 2017). Two WCCs for CH_4 are also run by the Swiss Federal Laboratory for Materials Testing and Research (Empa; Dübendorf, Switzerland) and the Japan Meteorological Agency (JMA; Tokyo, Japan) (WMO, 2017).

The current WMO Mole Fraction Scale is X2004A, which consists of 16 existing standards covering the range of the previous WMO X2004 scale and 6 new standards to expand the range of the scale. Table B4 summarizes the CH_4 standard scales used by stations contributing to the WDCGG and lists provisional multiplying conversion factors applied for analysis in the Data Summary. In this issue, the factor for conversion between the X2004A and X2004 scales is taken as 1 because the difference between them is minor.

Mole fractions on the WMO X2004 scale are 1.0124 times higher than those on the NOAA 1983 scale (Dlugokencky *et al.*, 2005). Values on the NOAA 1983 scale are up to around 1.5% lower than those of the Tohoku University gravimetric scale (Aoki *et al.*, 1992; Dlugokencky *et al.*, 1994) and 1.0151 times lower than those on the scale of the Atmospheric Environment Service (AES, now known as Environment and Climate Change Canada (ECCC)) (Worthy *et al.*, 1998). The conversion factor 1.0124 / 1.0151 = 0.9973 is adopted for comparison of the ECCC scale with the WMO X2004 scale. The Tohoku University scale can be converted to the WMO X2004A scale by multiplying by 1.0001 (Prinn *et al.*, 2018).

Table B4. Status of the standard scales of CH_4 with conversion factors.

Organi-zation	WDCGG Filename	Filename Code in Plate 2.1	Calibration Scale	Conv-ersion Factor
AEMET	ch4_izo_surface-insitu_3_9999-9999_monthly.txt	IZO128N003iz*	WMO X2004A	1
AGAGE	ch4_cgo_surface-insitu_4_2011-2016_monthly.txt ch4_cgo_surface-insitu_4_2021-2021_monthly.txt ch4_cmo_surface-insitu_4_2011-2016_monthly.txt ch4_mhd_surface-insitu_4_2011-2016_monthly.txt ch4_mhd_surface-insitu_4_2021-2021_monthly.txt ch4_rpb_surface-insitu_4_2021-2021_monthly.txt ch4_smo_surface-insitu_4_2011-2016_monthly.txt ch4_smo_surface-insitu_4_2021-2021_monthly.txt ch4_thd_surface-insitu_4_2021-2021_monthly.txt	CGO540S004ib CGO540S004ic* CMO445N004ib MHD653N004ib* MHD653N004ic* RPB413N004ic* SMO514S004ib SMO514S004ic* THD441N004ic*	Tohoku Univ.	1.0001
BMKG	ch4_bkt_surface-insitu_10_9999-9999_monthly.txt	BKT500S010iz	WMO X2004	1
CHMI	ch4_kos_surface-insitu_12_9999-9999_monthly.txt	KOS649N012iz		
CMA	ch4_wlg_surface-insitu_13_9999-9999_monthly.txt	WLG236N013iz	WMO X2004	1
CSIRO	ch4_alt_surface-flask_16_9999-9999_monthly.txt ch4_cfa_surface-flask_16_9999-9999_monthly.txt ch4_cgo_surface-flask_16_9999-9999_monthly.txt ch4_cri_surface-flask_16_9999-9999_monthly.txt ch4_cya_surface-flask_16_9999-9999_monthly.txt ch4_esp_surface-flask_16_9999-9999_monthly.txt ch4_maa_surface-flask_16_9999-9999_monthly.txt ch4_mlo_surface-flask_16_9999-9999_monthly.txt ch4_mqa_surface-flask_16_9999-9999_monthly.txt ch4_sis_surface-flask_16_9999-9999_monthly.txt	ALT482N016fz CFA519S016fz* CGO540S016fz CRI215N016fz* CYA766S016fz* ESP449N016fz* MAA767S016fz* MLO519N016fz MQA554S016fz* SIS660N016fz*	WMO X2004A	1

	ch4_spo_surface-flask_16_9999-9999_monthly.txt	SPO789S016fz		
DMC	ch4_tll_surface-insitu_17_9999-9999_monthly.txt	TLL330S017iz	WMO X2004	1
ECCC	ch4_alt_surface-insitu_20_9999-9999_monthly.txt ch4_cdl_surface-insitu_20_9999-9999_monthly.txt ch4_chl_surface-insitu_20_9999-9999_monthly.txt ch4_chm_surface-insitu_20_9999-9999_monthly.txt ch4_egb_surface-insitu_20_9999-9999_monthly.txt ch4_esp_surface-insitu_20_9999-9999_monthly.txt ch4_etl_surface-insitu_20_9999-9999_monthly.txt ch4_fsd_surface-insitu_20_9999-9999_monthly.txt ch4_llb_surface-insitu_20_9999-9999_monthly.txt ch4_wsa_surface-insitu_20_9999-9999_monthly.txt	ALT482N020iz CDL453N020iz* CHL458N020iz* CHM449N020iz* EGB444N020iz* ESP449N020iz* ETL454N020iz* FSD449N020iz* LLB454N020iz* WSA443N020iz*	WMO X2004A	1
Empa	ch4_jfj_surface-insitu_23_9999-9999_monthly.txt	JFJ646N023iz*	WMO X2004A	1
ENEA	ch4_lmp_surface-flask_24_9999-9999_monthly.txt	LMP635N024fz*	WMO X2004	1
FMI	ch4_pal_surface-insitu_25_9999-9999_monthly.txt ch4_tik_surface-insitu_25_9999-9999_monthly.txt	PAL667N025iz TIK271N025iz*	WMO X2004A	1
GERC	ch4_gsn_surface-insitu_52_9999-9999_monthly.txt	GSN233N052iz*	WMO X2004	1
IAFMS	ch4_cmn_surface-insitu_29_9999-9999_monthly.txt	CMN644N029iz*	WMO X2004	1
INSTAAR	ch4_sum_surface-insitu_34_9999-9999_monthly.txt	SUM672N034iz		
ISAC	ch4_cgr_surface-insitu_37_9999-9999_monthly.txt ch4_lmt_surface-insitu_37_9999-9999_monthly.txt	CGR637N037iz* LMT638N037iz	WMO X2004A	1
	ch4_eco_surface-insitu_37_9999-9999_monthly.txt	ECO640N037iz		
JMA	ch4_mnm_surface-insitu_1_9999-9999_monthly.txt ch4_ryo_surface-insitu_1_9999-9999_monthly.txt ch4_yon_surface-insitu_1_9999-9999_monthly.txt	MNM224N001iz* RYO239N001iz* YON224N001iz*	WMO X2004A	1
KMA	ch4_amy_surface-insitu_39_9999-9999_monthly.txt	AMY236N039iz*	WMO X2004 WMO X2004A KRISS	1 1
KSNU	ch4_isk_surface-remote_41_9999-9999_monthly.txt	ISK242N041rz		
LSCE	ch4_ams_surface-flask_45_9999-9999_monthly.txt ch4_bgu_surface-flask_45_9999-9999_monthly.txt ch4_lpo_surface-flask_45_9999-9999_monthly.txt ch4_pdm_surface-flask_45_9999-9999_monthly.txt ch4_puy_surface-flask_45_9999-9999_monthly.txt	AMS137S045fz* BGU641N045fz* LPO648N045fz PDM642N045fz PUY645N045fz*	NOAA 1983	1.0124
	ch4_fik_surface-flask_45_9999-9999_monthly.txt ch4_mhd_surface-flask_45_9999-9999_monthly.txt	FIK635N045fz MHD653N045fz		
METRI	ch4_gsn_surface-flask_55_9999-9999_monthly.txt	GSN233N055fz	SIO-97	
MGO	ch4_ter_surface-flask_46_9999-9999_monthly.txt ch4_tik_surface-flask_46_9999-9999_monthly.txt	TER669N046fz* TIK271N046fz	WMO X2004A	1
MRI	ch4_tkb_surface-insitu_48_9999-9999_monthly.txt	TKB236N048iz*	MRI	0.9973
NIES	ch4_coi_surface-insitu_53_9999-9999_monthly.txt ch4_hat_surface-insitu_53_9999-9999_monthly.txt	COI243N053iz* HAT224N053iz*	NIES	0.9973
NOAA	ch4_abp_surface-flask_2_3001-9999_monthly.txt ch4_alt_surface-flask_2_3001-9999_monthly.txt ch4_ams_surface-flask_2_3001-9999_monthly.txt ch4_amy_surface-flask_2_3001-9999_monthly.txt ch4_asc_surface-flask_2_3001-9999_monthly.txt ch4_ask_surface-flask_2_3001-9999_monthly.txt ch4_avi_surface-flask_2_3001-9999_monthly.txt ch4_azr_surface-flask_2_3001-9999_monthly.txt ch4_bal_surface-flask_2_3001-9999_monthly.txt	ABP312S002f1* ALT482N002f1* AMS137S002f1* AMY236N002f1 ASC107S002f1* ASK123N002f1* AVI417N002f1* AZR638N002f1* BAL655N002f1*	WMO X2004A	1

	ch4_bhd_surface-flask_2_3001-9999_monthly.txt	BHD541S002f1*		
	ch4_bkt_surface-flask_2_3001-9999_monthly.txt	BKT500S002f1		
	ch4_bme_surface-flask_2_3001-9999_monthly.txt	BME432N002f1*		
	ch4_bmw_surface-flask_2_3001-9999_monthly.txt	BMW432N002f1*		
	ch4_brw_surface-flask_2_3001-9999_monthly.txt	BRW471N002f1*		
	ch4_brw_surface-insitu_2_3001-9999_monthly.txt	BRW471N002i1*		
	ch4_bsc_surface-flask_2_3001-9999_monthly.txt	BSC644N002f1		
	ch4_cba_surface-flask_2_3001-9999_monthly.txt	CBA455N002f1*		
	ch4_cgo_surface-flask_2_3001-9999_monthly.txt	CGO540S002f1*		
	ch4_chr_surface-flask_2_3001-9999_monthly.txt	CHR501N002f1*		
	ch4_cmo_surface-flask_2_3001-9999_monthly.txt	CMO445N002f1*		
	ch4_cpt_surface-flask_2_3001-9999_monthly.txt	CPT134S002f1		
	ch4_crz_surface-flask_2_3001-9999_monthly.txt	CRZ146S002f1*		
	ch4_drp_ship-flask_2_3001-9999_monthly.txt	DRP859S002f1*		
	ch4_eic_surface-flask_2_3001-9999_monthly.txt	EIC327S002f1*		
	ch4_gmi_surface-flask_2_3001-9999_monthly.txt	GMI513N002f1*		
	ch4_goz_surface-flask_2_3001-9999_monthly.txt	GOZ636N002f1*		
	ch4_hba_surface-flask_2_3001-9999_monthly.txt	HBA775S002f1*		
	ch4_hpb_surface-flask_2_3001-9999_monthly.txt	HPB647N002f1*		
	ch4_hun_surface-flask_2_3001-9999_monthly.txt	HUN646N002f1*		
	ch4_ice_surface-flask_2_3001-9999_monthly.txt	ICE663N002f1*		
	ch4_itn_surface-flask_2_3001-9999_monthly.txt	ITN435N002f1*		
	ch4_izo_surface-flask_2_3001-9999_monthly.txt	IZO128N002f1*		
	ch4_key_surface-flask_2_3001-9999_monthly.txt	KEY425N002f1*		
	ch4_kum_surface-flask_2_3001-9999_monthly.txt	KUM519N002f1*		
	ch4_kzd_surface-flask_2_3001-9999_monthly.txt	KZD244N002f1*		
	ch4_kzm_surface-flask_2_3001-9999_monthly.txt	KZM243N002f1*		
	ch4_lef_surface-flask_2_3001-9999_monthly.txt	LEF445N002f1*		
	ch4_llb_surface-flask_2_3001-9999_monthly.txt	LLB454N002f1		
	ch4_lln_surface-flask_2_3001-9999_monthly.txt	LLN223N002f1*		
	ch4_lmp_surface-flask_2_3001-9999_monthly.txt	LMP635N002f1*		
	ch4_mbc_surface-flask_2_3001-9999_monthly.txt	MBC476N002f1*		
	ch4_mex_surface-flask_2_3001-9999_monthly.txt	MEX418N002f1*		
	ch4_mhd_surface-flask_2_3001-9999_monthly.txt	MHD653N002f1*		
	ch4_mid_surface-flask_2_3001-9999_monthly.txt	MID528N002f1*		
	ch4_mkn_surface-flask_2_3001-9999_monthly.txt	MKN100S002f1*		
	ch4_mlo_surface-flask_2_3001-9999_monthly.txt	MLO519N002f1*		
	ch4_mlo_surface-insitu_2_3001-9999_monthly.txt	MLO519N002i1*		
	ch4_nat_surface-flask_2_3001-9999_monthly.txt	NAT306S002f1*		
	ch4_nmb_surface-flask_2_3001-9999_monthly.txt	NMB123S002f1*		
	ch4_nwr_surface-flask_2_3001-9999_monthly.txt	NWR440N002f1*		
	ch4_opw_surface-flask_2_3001-9999_monthly.txt	OPW448N002f1*		
	ch4_oxk_surface-flask_2_3001-9999_monthly.txt	OXK650N002f1*		
	ch4_pal_surface-flask_2_3001-9999_monthly.txt	PAL667N002f1*		
	ch4_poc_ship-flask_2_3001-3001_monthly.txt	POC800N002f1*		
	ch4_poc_ship-flask_2_3001-3002_monthly.txt	POC805N002f1*		
	ch4_poc_ship-flask_2_3001-3003_monthly.txt	POC810N002f1*		
	ch4_poc_ship-flask_2_3001-3004_monthly.txt	POC815N002f1*		
	ch4_poc_ship-flask_2_3001-3005_monthly.txt	POC820N002f1*		
	ch4_poc_ship-flask_2_3001-3006_monthly.txt	POC825N002f1*		
	ch4_poc_ship-flask_2_3001-3007_monthly.txt	POC830N002f1*		
	ch4_poc_ship-flask_2_3001-3012_monthly.txt	POC805S002f1*		
	ch4_poc_ship-flask_2_3001-3013_monthly.txt	POC810S002f1*		
	ch4_poc_ship-flask_2_3001-3014_monthly.txt	POC815S002f1*		
	ch4_poc_ship-flask_2_3001-3015_monthly.txt	POC820S002f1*		
	ch4_poc_ship-flask_2_3001-3016_monthly.txt	POC825S002f1*		

	ch4_poc_ship-flask_2_3001-3017_monthly.txt ch4_poc_ship-flask_2_3001-3018_monthly.txt ch4_psa_surface-flask_2_3001-9999_monthly.txt ch4_pta_surface-flask_2_3001-9999_monthly.txt ch4_rpb_surface-flask_2_3001-9999_monthly.txt ch4_scs_ship-flask_2_3001-3101_monthly.txt ch4_scs_ship-flask_2_3001-3102_monthly.txt ch4_scs_ship-flask_2_3001-3103_monthly.txt ch4_scs_ship-flask_2_3001-3104_monthly.txt ch4_scs_ship-flask_2_3001-3105_monthly.txt ch4_scs_ship-flask_2_3001-3106_monthly.txt ch4_scs_ship-flask_2_3001-3107_monthly.txt ch4_sdz_surface-flask_2_3001-9999_monthly.txt ch4_sey_surface-flask_2_3001-9999_monthly.txt ch4_sgp_surface-flask_2_3001-9999_monthly.txt ch4_shm_surface-flask_2_3001-9999_monthly.txt ch4_smo_surface-flask_2_3001-9999_monthly.txt ch4_spo_surface-flask_2_3001-9999_monthly.txt ch4_stm_surface-flask_2_3001-9999_monthly.txt ch4_sum_surface-flask_2_3001-9999_monthly.txt ch4_syo_surface-flask_2_3001-9999_monthly.txt ch4_tap_surface-flask_2_3001-9999_monthly.txt ch4_thd_surface-flask_2_3001-9999_monthly.txt ch4_tik_surface-flask_2_3001-9999_monthly.txt ch4_ush_surface-flask_2_3001-9999_monthly.txt ch4_uta_surface-flask_2_3001-9999_monthly.txt ch4_uum_surface-flask_2_3001-9999_monthly.txt ch4_wis_surface-flask_2_3001-9999_monthly.txt ch4_wkt_surface-flask_2_3001-9999_monthly.txt ch4_wlg_surface-flask_2_3001-9999_monthly.txt ch4_zep_surface-flask_2_3001-9999_monthly.txt	POC830S002f1* POC835S002f1* PSA764S002f1* PTA438N002f1* RPB413N002f1* SCS803N002f1* SCS806N002f1* SCS809N002f1* SCS812N002f1* SCS815N002f1* SCS818N002f1* SCS821N002f1* SDZ240N002f1* SEY104S002f1* SGP436N002f1* SHM452N002f1* SMO514S002f1* SPO789S002f1* STM666N002f1* SUM672N002f1* SYO769S002f1* TAP236N002f1* THD441N002f1 TIK271N002f1* USH354S002f1* UTA439N002f1* UUM244N002f1* WIS631N002f1* WKT431N002f1* WLG236N002f1* ZEP678N002f1*		
RIVM	ch4_kmw_surface-insitu_63_9999-9999_monthly.txt	KMW653N063iz	NIST	0.9973
RSE	ch4_prs_surface-insitu_64_9999-9999_monthly.txt	PRS645N064iz*	WMO X2004	1
SAWS	ch4_cpt_surface-insitu_66_9999-1001_monthly.txt	CPT134S066iz*	WMO X2004 WMO X2004A	1 1
TU	ch4_syo_surface-insitu_70_9999-9999_monthly.txt	SYO769S070iz	TU-1987	
UBAA	ch4_snb_surface-insitu_72_9999-9999_monthly.txt	SNB647N072iz*	WMO X2004	1
UBAG	ch4_deu_surface-insitu_71_9999-9999_monthly.txt ch4_ngl_surface-insitu_71_9999-9999_monthly.txt ch4_ssl_surface-insitu_71_9999-9999_monthly.txt ch4_zgt_surface-insitu_71_9999-9999_monthly.txt ch4_zsf_surface-insitu_71_9999-9999_monthly.txt ch4_zug_surface-insitu_71_9999-9999_monthly.txt	DEU649N071iz* NGL653N071iz* SSL647N071iz* ZGT654N071iz* ZSF647N071iz* ZUG647N071iz*	WMO X2004	1
UMLT	ch4_glh_surface-insitu_75_9999-9999_monthly.txt	GLH636N075iz		
UNIURB	ch4_cmn_surface-insitu_74_9999-9999_monthly.txt	CMN644N074iz*	WMO X2004A	1
VNMHA	ch4_pdi_surface-insitu_51_9999-9999_monthly.txt	PDI221N051iz	WMO X2004	1

* Stations with an asterisk are used for the calculation of the global mean mole fractions and related quantities. The site selection procedure is described in Appendix A.

4. Nitrous Oxide (N_2O)

The Halocarbons and other Atmospheric Trace Species (HATS) Group of NOAA/ESRL maintains a set of standards for N_2O (Hall *et al.*, 2001) and serves as a CCL for N_2O. The WMO X2006 scale (Hall *et al.*, 2007) was revised and updated to WMO X2006A in 2011 to deal with drifting in secondary standards, and is now designated as the primary scale for the GAW Programme. CCL compares its standards with those of other laboratories, including ECCC and the Australian Commonwealth Scientific and Industrial Research

Organisation (CSIRO). The Karlsruhe Institute of Technology under the Institute for Meteorology and Climate Research (KIT/IMK-IFU) in Germany serves as the GAW WCC for N_2O.

The SIO-98 scale is approximately equivalent to the WMO X2006 scale, with an average difference of 0.01% over the range of 299 – 319 ppb. SIO-16 scale values can be converted to WMO X2006A via multiplication by a factor of 0.9983 (Prinn *et al.*, 2018). The WMO X2000 scale can be converted to WMO X2006 values using a factor of 0.999402 (Hall *et al.*, 2007).

Table B5. Status of the standard scales of N_2O with conversion factors.

Organi-zation	WDCGG Filename	Filename Code in Plate 3.1	Calibration Scale	Conv-ersion Factor
AEMET	n2o_izo_surface-insitu_3_9999-9999_monthly.txt	IZO128N003iz*	WMO X2006A	1
AGAGE	n2o_cgo_surface-insitu_4_2021-2021_monthly.txt n2o_mhd_surface-insitu_4_2021-2021_monthly.txt n2o_rpb_surface-insitu_4_2021-2021_monthly.txt n2o_smo_surface-insitu_4_2021-2021_monthly.txt n2o_thd_surface-insitu_4_2021-2021_monthly.txt	CGO540S004ic* MHD653N004ic* RPB413N004ic* SMO514S004ic* THD441N004ic*	SIO-16	0.9983
	n2o_adr_surface-insitu_4_2001-2004_monthly.txt n2o_cgo_surface-insitu_4_2001-2004_monthly.txt n2o_cgo_surface-insitu_4_2011-2015_monthly.txt n2o_cmo_surface-insitu_4_2001-2004_monthly.txt n2o_cmo_surface-insitu_4_2011-2015_monthly.txt n2o_mhd_surface-insitu_4_2011-2015_monthly.txt n2o_rpb_surface-insitu_4_2001-2004_monthly.txt n2o_rpb_surface-insitu_4_2011-2015_monthly.txt n2o_smo_surface-insitu_4_2001-2004_monthly.txt n2o_smo_surface-insitu_4_2011-2015_monthly.txt	ADR651N004ia* CGO540S004ia* CGO540S004ib* CMO445N004ia* CMO445N004ib* MHD653N004ib* RPB413N004ia* RPB413N004ib* SMO514S004ia* SMO514S004ib*	SIO-98	1
CSIRO	n2o_alt_surface-flask_16_9999-9999_monthly.txt n2o_cfa_surface-flask_16_9999-9999_monthly.txt n2o_cgo_surface-flask_16_9999-9999_monthly.txt n2o_cri_surface-flask_16_9999-9999_monthly.txt n2o_cya_surface-flask_16_9999-9999_monthly.txt n2o_esp_surface-flask_16_9999-9999_monthly.txt n2o_maa_surface-flask_16_9999-9999_monthly.txt n2o_mlo_surface-flask_16_9999-9999_monthly.txt n2o_mqa_surface-flask_16_9999-9999_monthly.txt n2o_sis_surface-flask_16_9999-9999_monthly.txt n2o_spo_surface-flask_16_9999-9999_monthly.txt	ALT482N016fz* CFA519S016fz* CGO540S016fz CRI215N016fz* CYA766S016fz* ESP449N016fz* MAA767S016fz* MLO519N016fz* MQA554S016fz* SIS660N016fz* SPO789S016fz	WMO X2006A	1
Empa	n2o_jfj_surface-insitu_23_9999-9999_monthly.txt	JFJ646N023iz*	WMO X2006A SIO-98	1 1
ENEA	n2o_lmp_surface-flask_24_9999-9999_monthly.txt	LMP635N024fz	WMO X2006	1
GERC	n2o_gsn_surface-insitu_52_9999-9999_monthly.txt	GSN233N052iz	WMO X2006	1
JMA	n2o_ryo_surface-insitu_1_9999-9999_monthly.txt	RYO239N001iz*	WMO X2006A	1
KMA	n2o_amy_surface-insitu_39_9999-9999_monthly.txt	AMY236N039iz	WMO X2006 KRISS	1
METRI	n2o_gsn_surface-flask_55_9999-9999_monthly.txt	GSN233N055fz	WMO X1997	
MRI	n2o_mmb_surface-insitu_48_9999-9999_monthly.txt	MMB243N048iz		
NAGOU	n2o_ngy_surface-insitu_49_9999-9999_monthly.txt	NGY235N049iz		
NIES	n2o_coi_surface-insitu_53_9999-9999_monthly.txt n2o_hat_surface-insitu_53_9999-9999_monthly.txt	COI243N053iz* HAT224N053iz*	NIES 96**	1
NILU	n2o_zep_surface-insitu_54_9999-9999_monthly.txt	ZEP678N054iz		
NIWA	n2o_arh_surface-flask_57_9999-9999_monthly.txt n2o_bhd_surface-flask_57_9999-9999_monthly.txt	ARH777S057fz BHD541S057fz*	WMO X2006A	1

NOAA	n2o_brw_surface-insitu_2_3003-9999_monthly.txt n2o_mlo_surface-insitu_2_3003-9999_monthly.txt n2o_nwr_surface-insitu_2_3003-9999_monthly.txt n2o_smo_surface-insitu_2_3003-9999_monthly.txt n2o_spo_surface-insitu_2_3003-9999_monthly.txt	BRW471N002i3* MLO519N002i3* NWR440N002i3* SMO514S002i3* SPO789S002i3*	WMO X2006	1
	n2o_abp_surface-flask_2_3001-9999_monthly.txt n2o_alt_surface-flask_2_3001-9999_monthly.txt n2o_alt_surface-flask_2_3004-9999_monthly.txt n2o_alt_surface-flask_2_3005-9999_monthly.txt n2o_amy_surface-flask_2_3001-9999_monthly.txt n2o_asc_surface-flask_2_3001-9999_monthly.txt n2o_ask_surface-flask_2_3001-9999_monthly.txt n2o_azr_surface-flask_2_3001-9999_monthly.txt n2o_bal_surface-flask_2_3001-9999_monthly.txt n2o_bhd_surface-flask_2_3001-9999_monthly.txt n2o_bkt_surface-flask_2_3001-9999_monthly.txt n2o_bme_surface-flask_2_3001-9999_monthly.txt n2o_bmw_surface-flask_2_3001-9999_monthly.txt n2o_brw_surface-flask_2_3001-9999_monthly.txt n2o_brw_surface-flask_2_3004-9999_monthly.txt n2o_brw_surface-flask_2_3005-9999_monthly.txt n2o_brw_surface-insitu_2_3002-9999_monthly.txt n2o_bsc_surface-flask_2_3001-9999_monthly.txt n2o_cba_surface-flask_2_3001-9999_monthly.txt n2o_cgo_surface-flask_2_3001-9999_monthly.txt n2o_cgo_surface-flask_2_3004-9999_monthly.txt n2o_cgo_surface-flask_2_3005-9999_monthly.txt n2o_chr_surface-flask_2_3001-9999_monthly.txt n2o_cpt_surface-flask_2_3001-9999_monthly.txt n2o_crz_surface-flask_2_3001-9999_monthly.txt n2o_drp_ship-flask_2_3001-9999_monthly.txt n2o_eic_surface-flask_2_3001-9999_monthly.txt n2o_gmi_surface-flask_2_3001-9999_monthly.txt n2o_hba_surface-flask_2_3001-9999_monthly.txt n2o_hfm_surface-flask_2_3005-9999_monthly.txt n2o_hpb_surface-flask_2_3001-9999_monthly.txt n2o_hun_surface-flask_2_3001-9999_monthly.txt n2o_ice_surface-flask_2_3001-9999_monthly.txt n2o_itn_surface-flask_2_3001-9999_monthly.txt n2o_itn_surface-flask_2_3005-9999_monthly.txt n2o_izo_surface-flask_2_3001-9999_monthly.txt n2o_key_surface-flask_2_3001-9999_monthly.txt n2o_kum_surface-flask_2_3001-9999_monthly.txt n2o_kum_surface-flask_2_3005-9999_monthly.txt n2o_kzd_surface-flask_2_3001-9999_monthly.txt n2o_kzm_surface-flask_2_3001-9999_monthly.txt n2o_lef_surface-flask_2_3001-9999_monthly.txt n2o_lef_surface-flask_2_3005-9999_monthly.txt n2o_llb_surface-flask_2_3001-9999_monthly.txt n2o_lln_surface-flask_2_3001-9999_monthly.txt n2o_lmp_surface-flask_2_3001-9999_monthly.txt n2o_mex_surface-flask_2_3001-9999_monthly.txt n2o_mhd_surface-flask_2_3001-9999_monthly.txt n2o_mhd_surface-flask_2_3005-9999_monthly.txt n2o_mid_surface-flask_2_3001-9999_monthly.txt n2o_mkn_surface-flask_2_3001-9999_monthly.txt	ABP312S002f1* ALT482N002f1 ALT482N002f4* ALT482N002f5 AMY236N002f1* ASC107S002f1* ASK123N002f1* AZR638N002f1* BAL655N002f1* BHD541S002f1 BKT500S002f1* BME432N002f1* BMW432N002f1* BRW471N002f1 BRW471N002f4* BRW471N002f5 BRW471N002i2* BSC644N002f1* CBA455N002f1* CGO540S002f1* CGO540S002f4 CGO540S002f5 CHR501N002f1* CPT134S002f1* CRZ146S002f1* DRP859S002f1* EIC327S002f1* GMI513N002f1* HBA775S002f1* HFM442N002f5* HPB647N002f1* HUN646N002f1* ICE663N002f1* ITN435N002f1 ITN435N002f5* IZO128N002f1* KEY425N002f1* KUM519N002f1* KUM519N002f5* KZD244N002f1* KZM243N002f1* LEF445N002f1* LEF445N002f5* LLB454N002f1* LLN223N002f1* LMP635N002f1* MEX418N002f1* MHD653N002f1* MHD653N002f5 MID528N002f1* MKN100S002f1*	WMO X2006A	1

	n2o_mlo_surface-flask_2_3001-9999_monthly.txt	MLO519N002f1		
	n2o_mlo_surface-flask_2_3004-9999_monthly.txt	MLO519N002f4*		
	n2o_mlo_surface-flask_2_3005-9999_monthly.txt	MLO519N002f5		
	n2o_mlo_surface-insitu_2_3002-9999_monthly.txt	MLO519N002i2*		
	n2o_nat_surface-flask_2_3001-9999_monthly.txt	NAT306S002f1*		
	n2o_nmb_surface-flask_2_3001-9999_monthly.txt	NMB123S002f1*		
	n2o_nwr_surface-flask_2_3001-9999_monthly.txt	NWR440N002f1*		
	n2o_nwr_surface-flask_2_3004-9999_monthly.txt	NWR440N002f4*		
	n2o_nwr_surface-flask_2_3005-9999_monthly.txt	NWR440N002f5		
	n2o_nwr_surface-insitu_2_3002-9999_monthly.txt	NWR440N002i2		
	n2o_oxk_surface-flask_2_3001-9999_monthly.txt	OXK650N002f1*		
	n2o_pal_surface-flask_2_3001-9999_monthly.txt	PAL667N002f1*		
	n2o_poc_ship-flask_2_3001-3001_monthly.txt	POC800N002f1*		
	n2o_poc_ship-flask_2_3001-3002_monthly.txt	POC805N002f1*		
	n2o_poc_ship-flask_2_3001-3003_monthly.txt	POC810N002f1*		
	n2o_poc_ship-flask_2_3001-3004_monthly.txt	POC815N002f1*		
	n2o_poc_ship-flask_2_3001-3005_monthly.txt	POC820N002f1*		
	n2o_poc_ship-flask_2_3001-3006_monthly.txt	POC825N002f1*		
	n2o_poc_ship-flask_2_3001-3007_monthly.txt	POC830N002f1*		
	n2o_poc_ship-flask_2_3001-3012_monthly.txt	POC805S002f1*		
	n2o_poc_ship-flask_2_3001-3013_monthly.txt	POC810S002f1*		
	n2o_poc_ship-flask_2_3001-3014_monthly.txt	POC815S002f1*		
	n2o_poc_ship-flask_2_3001-3015_monthly.txt	POC820S002f1*		
	n2o_poc_ship-flask_2_3001-3016_monthly.txt	POC825S002f1*		
	n2o_poc_ship-flask_2_3001-3017_monthly.txt	POC830S002f1*		
	n2o_psa_surface-flask_2_3001-9999_monthly.txt	PSA764S002f1*		
	n2o_psa_surface-flask_2_3005-9999_monthly.txt	PSA764S002f5		
	n2o_pta_surface-flask_2_3001-9999_monthly.txt	PTA438N002f1*		
	n2o_rpb_surface-flask_2_3001-9999_monthly.txt	RPB413N002f1*		
	n2o_sdz_surface-flask_2_3001-9999_monthly.txt	SDZ240N002f1*		
	n2o_sey_surface-flask_2_3001-9999_monthly.txt	SEY104S002f1*		
	n2o_sgp_surface-flask_2_3001-9999_monthly.txt	SGP436N002f1*		
	n2o_shm_surface-flask_2_3001-9999_monthly.txt	SHM452N002f1*		
	n2o_smo_surface-flask_2_3001-9999_monthly.txt	SMO514S002f1*		
	n2o_smo_surface-flask_2_3004-9999_monthly.txt	SMO514S002f4		
	n2o_smo_surface-flask_2_3005-9999_monthly.txt	SMO514S002f5		
	n2o_smo_surface-insitu_2_3002-9999_monthly.txt	SMO514S002i2		
	n2o_spo_surface-flask_2_3001-9999_monthly.txt	SPO789S002f1		
	n2o_spo_surface-flask_2_3004-9999_monthly.txt	SPO789S002f4*		
	n2o_spo_surface-flask_2_3005-9999_monthly.txt	SPO789S002f5		
	n2o_spo_surface-insitu_2_3002-9999_monthly.txt	SPO789S002i2*		
	n2o_stm_surface-flask_2_3001-9999_monthly.txt	STM666N002f1*		
	n2o_sum_surface-flask_2_3001-9999_monthly.txt	SUM672N002f1*		
	n2o_sum_surface-flask_2_3005-9999_monthly.txt	SUM672N002f5		
	n2o_sum_surface-insitu_2_3002-9999_monthly.txt	SUM672N002i2		
	n2o_syo_surface-flask_2_3001-9999_monthly.txt	SYO769S002f1*		
	n2o_tap_surface-flask_2_3001-9999_monthly.txt	TAP236N002f1*		
	n2o_thd_surface-flask_2_3001-9999_monthly.txt	THD441N002f1		
	n2o_thd_surface-flask_2_3005-9999_monthly.txt	THD441N002f5		
	n2o_tik_surface-flask_2_3001-9999_monthly.txt	TIK271N002f1*		
	n2o_ush_surface-flask_2_3001-9999_monthly.txt	USH354S002f1*		
	n2o_ush_surface-flask_2_3005-9999_monthly.txt	USH354S002f5		
	n2o_uta_surface-flask_2_3001-9999_monthly.txt	UTA439N002f1*		
	n2o_uum_surface-flask_2_3001-9999_monthly.txt	UUM244N002f1*		
	n2o_wis_surface-flask_2_3001-9999_monthly.txt	WIS631N002f1*		
	n2o_wkt_surface-flask_2_3001-9999_monthly.txt	WKT431N002f1*		

	n2o_wlg_surface-flask_2_3001-9999_monthly.txt n2o_zep_surface-flask_2_3001-9999_monthly.txt	WLG236N002f1* ZEP678N002f1*		
SAWS	n2o_cpt_surface-insitu_66_9999-1001_monthly.txt	CPT134S066iz*	NOAA	0.999402
UBAG	n2o_zsf_surface-insitu_71_9999-9999_monthly.txt	ZSF647N071iz*	WMO X2006A	1
	n2o_ssl_surface-insitu_71_9999-9999_monthly.txt	SSL647N071iz	SIO-98	1
UNIURB	n2o_cmn_surface-insitu_74_9999-9999_monthly.txt	CMN644N074iz*	WMO X2006A	1

* Stations with an asterisk are used for the calculation of the global mean mole fractions and related quantities. The site selection procedure is described in Appendix A.

** NIES 96 N_2O scale is approximately 0.7 ppb lower than that of WMO X2006A in the range 325 to 326 ppb. (http://www.esrl.noaa.gov/gmd/ccgg/wmorr/wmorr_results.php?rr=rr6&param=n2o)

5. Carbon Monoxide (CO)

NOAA/ESRL is the WMO/GAW CCL for carbon monoxide. Due to lack of stability of CO in high pressure cylinders, the CO scale has historically been defined by repeated sets of gravimetric standards made in 1996/1997, 1999/2000, 2006 and 2011. The CCL make revisions in the CO scale whenever new gravimetric standard sets indicate a significant drift in the scale. Scale revisions are indicated with date codes (WMO X2000, WMO X2004, WMO X2014) with the most recent made in December 2015 being WMO X2014A (WMO, 2020).

Empa serves as the WCC under GAW based on its secondary standards calibrated against the standard at NOAA/ESRL designated as the Primary Standard for GAW. Empa, as WCC for CO, has developed an audit system for CO measurements at GAW stations.

A small fraction of the data is reported in units of $\mu g/m^3$ or mg/m^3. In WDCGG analysis, these units are converted to ppb using the following formulas:

$$X_p\,[\text{ppb}] = (R \times T / M / P_0) \times 10 \times X_g\,[\mu g/m^3]$$

and

$$X_p\,[\text{ppb}] = (R \times T / M / P_0) \times 10^4 \times X_g\,[mg/m^3],$$

where

R is the molar gas constant (8.31451 [J/K/mol]),

T is the reported temperature for conversion (293.15 [K] or 298.15 [K]),

M is the molecular weight of CO (28.0101) and

P_0 is the standard pressure (1013.25 [hPa]).

It is highly desirable to report CO concentration data in mole fractions (mostly in ppb) traceable to the WMO Mole Fraction Scale.

Table B6. Status of CO standard scales.

Organi-zation	WDCGG Filename	Filename Code in Plate 5.1	Calibration Scale / Units except for using ppb	Audit Empa-WCC
AEMET	co_izo_surface-insitu_3_9999-9999_monthly.txt	IZO128N003iz	WMO X2014A	00, 04, 09, 13
AGAGE	co_cgo_surface-insitu_4_2021-2021_monthly.txt co_mhd_surface-insitu_4_2021-2021_monthly.txt	CGO540S004ic MHD653N004ic*	CSIRO-94	
ARSO	co_kvv_surface-insitu_8_9999-9999_monthly.txt	KVV646N008iz*		
BAS	co_hba_surface-insitu_9_9999-9999_monthly.txt	HBA775S009iz	WMO X2014A	
BMKG	co_bkt_surface-insitu_10_9999-9999_monthly.txt	BKT500S010iz	WMO X2000	01, 04, 07, 08, 11, 14, 19
CHMI	co_kos_surface-insitu_12_9999-9999_monthly.txt	KOS649N012iz	$\mu g/m^3$-20°C	
CSIRO	co_alt_surface-flask_16_9999-9999_monthly.txt co_cfa_surface-flask_16_9999-9999_monthly.txt co_cgo_surface-flask_16_9999-9999_monthly.txt co_cri_surface-flask_16_9999-9999_monthly.txt co_cya_surface-flask_16_9999-9999_monthly.txt co_esp_surface-flask_16_9999-9999_monthly.txt co_maa_surface-flask_16_9999-9999_monthly.txt co_mlo_surface-flask_16_9999-9999_monthly.txt	ALT482N016fz* CFA519S016fz* CGO540S016fz* CRI215N016fz* CYA766S016fz* ESP449N016fz* MAA767S016fz* MLO519N016fz	CSIRO-94	Cape Grim: 02, 16

	co_mqa_surface-flask_16_9999-9999_monthly.txt co_sis_surface-flask_16_9999-9999_monthly.txt co_spo_surface-flask_16_9999-9999_monthly.txt	MQA554S016fz* SIS660N016fz* SPO789S016fz*		
DMC	co_tll_surface-insitu_17_9999-9999_monthly.txt	TLL330S017iz	WMO X2004	
DWD	co_hpb_surface-insitu_19_9999-9999_monthly.txt	HPB647N019iz*	WMO X2004	97, 06, 11
ECCC	co_alt_surface-insitu_20_9999-9999_monthly.txt co_cdl_surface-insitu_20_9999-9999_monthly.txt co_chl_surface-insitu_20_9999-9999_monthly.txt co_chm_surface-insitu_20_9999-9999_monthly.txt co_egb_surface-insitu_20_9999-9999_monthly.txt co_esp_surface-insitu_20_9999-9999_monthly.txt co_etl_surface-insitu_20_9999-9999_monthly.txt co_fsd_surface-insitu_20_9999-9999_monthly.txt co_llb_surface-insitu_20_9999-9999_monthly.txt co_wsa_surface-insitu_20_9999-9999_monthly.txt	ALT482N020iz CDL453N020iz* CHL458N020iz CHM449N020iz* EGB444N020iz* ESP449N020iz* ETL454N020iz* FSD449N020iz* LLB454N020iz* WSA443N020iz*	WMO X2014A	Alert: 04
Empa	co_jfj_surface-insitu_23_9999-9999_monthly.txt	JFJ646N023iz*	WMO	99, 06, 15
	co_pay_surface-insitu_23_9999-9999_monthly.txt co_rig_surface-insitu_23_9999-9999_monthly.txt	PAY646N023iz* RIG647N023iz*	NPL	
INRNE	co_beo_surface-insitu_33_9999-9999_monthly.txt	BEO642N033iz*		
ISAC	co_cmn_surface-insitu_37_9999-9999_monthly.txt	CMN644N037iz	WMO X2004 WMO X2014A	12, 18
	co_cgr_surface-insitu_37_9999-9999_monthly.txt co_lmt_surface-insitu_37_9999-9999_monthly.txt	CGR637N037iz* LMT638N037iz*	WMO X2014A	
	co_eco_surface-insitu_37_9999-9999_monthly.txt	ECO640N037iz*		
JMA	co_mnm_surface-insitu_1_9999-9999_monthly.txt co_ryo_surface-insitu_1_9999-9999_monthly.txt co_yon_surface-insitu_1_9999-9999_monthly.txt	MNM224N001iz* RYO239N001iz* YON224N001iz*	WMO X2014A	
KMD	co_mkn_surface-insitu_40_9999-9999_monthly.txt	MKN100S040iz*	WMO X2000	05, 06, 08, 10, 15
LA	co_pdm_surface-insitu_43_9999-9999_monthly.txt	PDM642N043iz		
LAMP	co_puy_surface-insitu_44_9999-9999_monthly.txt	PUY645N044iz		16
LSCE	co_ams_surface-insitu_45_9999-9999_monthly.txt	AMS137S045iz		08
NIWA	co_arh_surface-flask_57_9999-9999_monthly.txt co_bhd_surface-flask_57_9999-9999_monthly.txt co_lau_surface-flask_57_9999-9999_monthly.txt	ARH777S057fz BHD541S057fz* LAU545S057fz	WMO X2014A	
NOAA	co_abp_surface-flask_2_3001-9999_monthly.txt co_alt_surface-flask_2_3001-9999_monthly.txt co_amy_surface-flask_2_3001-9999_monthly.txt co_asc_surface-flask_2_3001-9999_monthly.txt co_ask_surface-flask_2_3001-9999_monthly.txt co_azr_surface-flask_2_3001-9999_monthly.txt co_bal_surface-flask_2_3001-9999_monthly.txt co_bhd_surface-flask_2_3001-9999_monthly.txt co_bkt_surface-flask_2_3001-9999_monthly.txt co_bme_surface-flask_2_3001-9999_monthly.txt co_bmw_surface-flask_2_3001-9999_monthly.txt co_brw_surface-flask_2_3001-9999_monthly.txt co_bsc_surface-flask_2_3001-9999_monthly.txt co_cba_surface-flask_2_3001-9999_monthly.txt co_cgo_surface-flask_2_3001-9999_monthly.txt	ABP312S002f1* ALT482N002f1 AMY236N002f1* ASC107S002f1* ASK123N002f1* AZR638N002f1* BAL655N002f1* BHD541S002f1* BKT500S002f1* BME432N002f1* BMW432N002f1* BRW471N002f1* BSC644N002f1* CBA455N002f1* CGO540S002f1	WMO X2014A	

	co_chr_surface-flask_2_3001-9999_monthly.txt	CHR501N002f1*		
	co_cmo_surface-flask_2_3001-9999_monthly.txt	CMO445N002f1*		
	co_cpt_surface-flask_2_3001-9999_monthly.txt	CPT134S002f1		
	co_crz_surface-flask_2_3001-9999_monthly.txt	CRZ146S002f1*		
	co_drp_ship-flask_2_3001-9999_monthly.txt	DRP859S002f1*		
	co_eic_surface-flask_2_3001-9999_monthly.txt	EIC327S002f1*		
	co_gmi_surface-flask_2_3001-9999_monthly.txt	GMI513N002f1*		
	co_goz_surface-flask_2_3001-9999_monthly.txt	GOZ636N002f1*		
	co_hba_surface-flask_2_3001-9999_monthly.txt	HBA775S002f1*		
	co_hpb_surface-flask_2_3001-9999_monthly.txt	HPB647N002f1*		
	co_hun_surface-flask_2_3001-9999_monthly.txt	HUN646N002f1*		
	co_ice_surface-flask_2_3001-9999_monthly.txt	ICE663N002f1*		
	co_itn_surface-flask_2_3001-9999_monthly.txt	ITN435N002f1*		
	co_izo_surface-flask_2_3001-9999_monthly.txt	IZO128N002f1*		
	co_key_surface-flask_2_3001-9999_monthly.txt	KEY425N002f1*		
	co_kum_surface-flask_2_3001-9999_monthly.txt	KUM519N002f1*		
	co_kzd_surface-flask_2_3001-9999_monthly.txt	KZD244N002f1*		
	co_kzm_surface-flask_2_3001-9999_monthly.txt	KZM243N002f1*		
	co_lef_surface-flask_2_3001-9999_monthly.txt	LEF445N002f1*		
	co_llb_surface-flask_2_3001-9999_monthly.txt	LLB454N002f1		
	co_lln_surface-flask_2_3001-9999_monthly.txt	LLN223N002f1*		
	co_lmp_surface-flask_2_3001-9999_monthly.txt	LMP635N002f1*		
	co_mbc_surface-flask_2_3001-9999_monthly.txt	MBC476N002f1*		
	co_mex_surface-flask_2_3001-9999_monthly.txt	MEX418N002f1*		
	co_mhd_surface-flask_2_3001-9999_monthly.txt	MHD653N002f1*		
	co_mid_surface-flask_2_3001-9999_monthly.txt	MID528N002f1*		
	co_mkn_surface-flask_2_3001-9999_monthly.txt	MKN100S002f1*		
	co_mlo_surface-flask_2_3001-9999_monthly.txt	MLO519N002f1*		
	co_nat_surface-flask_2_3001-9999_monthly.txt	NAT306S002f1*		
	co_nmb_surface-flask_2_3001-9999_monthly.txt	NMB123S002f1*		
	co_nwr_surface-flask_2_3001-9999_monthly.txt	NWR440N002f1*		
	co_oxk_surface-flask_2_3001-9999_monthly.txt	OXK650N002f1*		
	co_pal_surface-flask_2_3001-9999_monthly.txt	PAL667N002f1*		
	co_poc_ship-flask_2_3001-3001_monthly.txt	POC800N002f1*		
	co_poc_ship-flask_2_3001-3002_monthly.txt	POC805N002f1*		
	co_poc_ship-flask_2_3001-3003_monthly.txt	POC810N002f1*		
	co_poc_ship-flask_2_3001-3004_monthly.txt	POC815N002f1*		
	co_poc_ship-flask_2_3001-3005_monthly.txt	POC820N002f1*		
	co_poc_ship-flask_2_3001-3006_monthly.txt	POC825N002f1*		
	co_poc_ship-flask_2_3001-3007_monthly.txt	POC830N002f1*		
	co_poc_ship-flask_2_3001-3012_monthly.txt	POC805S002f1*		
	co_poc_ship-flask_2_3001-3013_monthly.txt	POC810S002f1*		
	co_poc_ship-flask_2_3001-3014_monthly.txt	POC815S002f1*		
	co_poc_ship-flask_2_3001-3015_monthly.txt	POC820S002f1*		
	co_poc_ship-flask_2_3001-3016_monthly.txt	POC825S002f1*		
	co_poc_ship-flask_2_3001-3017_monthly.txt	POC830S002f1*		
	co_psa_surface-flask_2_3001-9999_monthly.txt	PSA764S002f1*		
	co_pta_surface-flask_2_3001-9999_monthly.txt	PTA438N002f1*		
	co_rpb_surface-flask_2_3001-9999_monthly.txt	RPB413N002f1*		
	co_scs_ship-flask_2_3001-3101_monthly.txt	SCS803N002f1*		
	co_scs_ship-flask_2_3001-3102_monthly.txt	SCS806N002f1*		
	co_scs_ship-flask_2_3001-3103_monthly.txt	SCS809N002f1*		
	co_scs_ship-flask_2_3001-3104_monthly.txt	SCS812N002f1*		
	co_scs_ship-flask_2_3001-3105_monthly.txt	SCS815N002f1*		
	co_scs_ship-flask_2_3001-3106_monthly.txt	SCS818N002f1*		
	co_scs_ship-flask_2_3001-3107_monthly.txt	SCS821N002f1		

	co_sdz_surface-flask_2_3001-9999_monthly.txt co_sey_surface-flask_2_3001-9999_monthly.txt co_sgp_surface-flask_2_3001-9999_monthly.txt co_shm_surface-flask_2_3001-9999_monthly.txt co_smo_surface-flask_2_3001-9999_monthly.txt co_spo_surface-flask_2_3001-9999_monthly.txt co_stm_surface-flask_2_3001-9999_monthly.txt co_sum_surface-flask_2_3001-9999_monthly.txt co_syo_surface-flask_2_3001-9999_monthly.txt co_tap_surface-flask_2_3001-9999_monthly.txt co_thd_surface-flask_2_3001-9999_monthly.txt co_tik_surface-flask_2_3001-9999_monthly.txt co_ush_surface-flask_2_3001-9999_monthly.txt co_uta_surface-flask_2_3001-9999_monthly.txt co_uum_surface-flask_2_3001-9999_monthly.txt co_wis_surface-flask_2_3001-9999_monthly.txt co_wkt_surface-flask_2_3001-9999_monthly.txt co_wlg_surface-flask_2_3001-9999_monthly.txt co_zep_surface-flask_2_3001-9999_monthly.txt	SDZ240N002f1* SEY104S002f1* SGP436N002f1* SHM452N002f1* SMO514S002f1* SPO789S002f1 STM666N002f1* SUM672N002f1* SYO769S002f1* TAP236N002f1* THD441N002f1* TIK271N002f1* USH354S002f1* UTA439N002f1* UUM244N002f1* WIS631N002f1* WKT431N002f1* WLG236N002f1* ZEP678N002f1*		
ONM	co_ask_surface-insitu_59_9999-9999_monthly.txt	ASK123N059iz		07, 15
PolyU	co_hkg_surface-insitu_61_9999-9999_monthly.txt	HKG222N061iz		
RIVM	co_kmw_surface-insitu_63_9999-9999_monthly.txt	KMW653N063iz*		
	co_ktb_surface-insitu_63_9999-9999_monthly.txt	KTB653N063iz	µg/m^3-25°C	
SAWS	co_cpt_surface-insitu_66_9999-1001_monthly.txt	CPT134S066iz*	WMO X2004 WMO X2014A CPT	98, 02, 06, 11, 15
UBAA	co_snb_surface-insitu_72_9999-9999_monthly.txt	SNB647N072iz*	NIST	98
UBAG	co_zsf_surface-insitu_71_9999-9999_monthly.txt	ZSF647N071iz*	WMO X2014 WMO X2014A	01, 06, 11
	co_ngl_surface-insitu_71_9999-9999_monthly.txt co_ssl_surface-insitu_71_9999-9999_monthly.txt	NGL653N071iz* SSL647N071iz*		
	co_zug_surface-insitu_71_9999-9999_monthly.txt	ZUG647N071iz*	mg/m^3-25°C	97, 01
UMLT	co_glh_surface-insitu_75_9999-9999_monthly.txt	GLH636N075iz*		
UNIURB	co_cmn_surface-insitu_74_9999-9999_monthly.txt	CMN644N074iz*	WMO X2014	
UYRK	co_cvo_surface-insitu_76_9999-9999_monthly.txt	CVO116N076iz*	WMO X2014	12
VNMHA	co_pdi_surface-insitu_51_9999-9999_monthly.txt	PDI221N051iz	WMO X2004	

* Stations with an asterisk are used for the calculation of the global mean mole fractions and related quantities. The site selection procedure is described in Appendix A.

APPENDIX C LIST OF OBSERVATIONAL STATIONS

Station	Country/Territory	GAW ID	Organization	Location Latitude (°)	Location Longitude (°)	Altitude (m)	Parameter
REGION I (Africa)							
Amsterdam Island	France	AMS	NOAA	37.80 S	77.54 E	70	CO_2, CH_4
Amsterdam Island	France	AMS	LSCE	37.80 S	77.54 E	70	CO_2, CH_4, CO
Ascension Island	United Kingdom of Great Britain and Northern Ireland	ASC	NOAA	7.97 S	14.40 W	91	CO_2, CH_4, N_2O, SF_6, $^{13}CH_4$, $^{13}CO_2$, $C^{18}O_2$, CO, H_2
Assekrem	Algeria	ASK	NOAA	23.27 N	5.63 E	2710	CO_2, CH_4, N_2O, SF_6, $^{13}CO_2$, $C^{18}O_2$, CO, H_2
Assekrem	Algeria	ASK	ONM	23.27 N	5.63 E	2710	CO
Cairo	Egypt	CAI	EMA	30.08 N	31.28 E	35	CO_2
Cape Point	South Africa	CPT	NOAA	34.35 S	18.49 E	230	CO_2, CH_4, N_2O, SF_6, $^{13}CO_2$, $C^{18}O_2$, CO
Cape Point	South Africa	CPT	ANSTO	34.35 S	18.49 E	230	^{222}Rn
Cape Point	South Africa	CPT	SAWS	34.35 S	18.49 E	230	CO_2, CH_4, N_2O, CO
Cape Verde Atmospheric Observatory	Cabo Verde	CVO	UYRK	16.86 N	24.87 W	10	CO
Crozet	France	CRZ	NOAA	46.43 S	51.83 E	120	CO_2, CH_4, N_2O, SF_6, $^{13}CO_2$, $C^{18}O_2$, CO, H_2
Farafra	Egypt	FRF	EMA	27.06 N	27.99 E	92	CO_2
Gobabeb	Namibia	NMB	NOAA	23.57 S	15.03 E	408	CO_2, CH_4, N_2O, SF_6, $^{13}CO_2$, $C^{18}O_2$, CO
Izaña (Tenerife)	Spain	IZO	NOAA	28.31 N	16.50 W	2373	CO_2, CH_4, N_2O, SF_6, $^{13}CO_2$, $C^{18}O_2$, CO, H_2
Izaña (Tenerife)	Spain	IZO	AEMET	28.31 N	16.50 W	2373	CO_2, CH_4, N_2O, SF_6, CO
Mahé	Seychelles	SEY	NOAA	4.67 S	55.17 E	3	CO_2, CH_4, N_2O, SF_6, $^{13}CO_2$, $C^{18}O_2$, CO, H_2
Mt. Kenya	Kenya	MKN	NOAA	0.06 S	37.30 E	3678	CO_2, CH_4, N_2O, SF_6, $^{13}CO_2$, $C^{18}O_2$, CO
Mt. Kenya	Kenya	MKN	KMD	0.06 S	37.30 E	3678	CO
REGION II (Asia)							
Anmyeon-do	Republic of Korea	AMY	NOAA	36.54 N	126.33 E	46	CO_2, CH_4, N_2O, SF_6, $^{13}CH_4$, CO
Anmyeon-do	Republic of Korea	AMY	KMA	36.54 N	126.33 E	46	CO_2, CH_4, N_2O, SF_6, CFCs, CO
Bering Island	Russian Federation	BER	MGO	55.20 N	165.98 E	13	CO_2
Cape Ochiishi	Japan	COI	NIES	43.17 N	145.50 E	49	CO_2, CH_4, N_2O, SF_6, CFCs, HCFCs, HFCs
Cape Rama	India	CRI	CSIRO	15.08 N	73.83 E	60	CO_2, CH_4, N_2O, $^{13}CO_2$, CO, H_2
Gosan	Republic of Korea	GSN	AGAGE	33.28 N	126.17 E	72	SF_6, CCl_4, CH_3CCl_3, CFCs, HCFCs, HFCs, PFCs, $CBrClF_2$, $CBrF_3$, $C_2Br_2F_4$, $CHCl_3$, CH_3Cl
Gosan	Republic of Korea	GSN	GERC	33.28 N	126.17 E	72	CO_2, CH_4, N_2O
Gosan	Republic of Korea	GSN	METRI	33.28 N	126.17 E	72	CO_2, CH_4, N_2O, CFCs
Hamamatsu	Japan	HMM	SHIZU	34.72 N	137.72 E	29	CO_2

LIST OF OBSERVATIONAL STATIONS (continued)

Station	Country/Territory	GAW ID	Organization	Location Latitude (°)	Location Longitude (°)	Altitude (m)	Parameter
Hateruma Island	Japan	HAT	NIES	24.05 N	123.81 E	10	CO_2, CH_4, N_2O, SF_6, CFCs, HCFCs, HFCs
Hok Tsui / Cape d Aguilar	Hong Kong, China	HKG	HKO	22.21 N	114.26 E	60	CO_2
Hok Tsui / Cape d Aguilar	Hong Kong, China	HKG	PolyU	22.21 N	114.26 E	60	CO
Issyk-Kul	Kyrgyzstan	ISK	KSNU	42.62 N	76.98 E	1640	CO_2, CH_4
Jeju Gosan	Republic of Korea	JGS	KMA	33.18 N	126.12 E	52	CO_2
Kaashidhoo (Male Atoll)	Maldives	KCO	NOAA	4.97 N	73.47 E	1	CO_2, CH_4, N_2O, SF_6, CO
King's Park	Hong Kong, China	HKO	HKO	22.31 N	114.17 E	65	CO_2
Kisai	Japan	KIS	SAIPF	36.08 N	139.55 E	13	CO_2
Kotelnyj Island	Russian Federation	KOT	MGO	76.00 N	137.87 E	5	CO_2
Kyzylcha	Uzbekistan	KYZ	MGO	40.87 N	66.15 E	340	CO_2
Lulin	Taiwan, Province of China	LLN	NOAA	23.47 N	120.87 E	2862	CO_2, CH_4, N_2O, SF_6, $^{13}CO_2$, $C^{18}O_2$, CO
Memanbetsu	Japan	MMB	MRI	43.92 N	144.20 E	33	N_2O
Mikawa-Ichinomiya	Japan	MKW	AICH	34.85 N	137.43 E	50	CO_2
Minamitorishima	Japan	MNM	JMA	24.29 N	153.98 E	7.1	CO_2, CH_4, CO
Mt. Dodaira	Japan	DDR	SAIPF	36.00 N	139.20 E	840	CO_2
Mt. Waliguan	China	WLG	NOAA	36.29 N	100.90 E	3810	CO_2, CH_4, N_2O, SF_6, $^{13}CH_4$, $^{13}CO_2$, $C^{18}O_2$, CO, H_2
Mt. Waliguan	China	WLG	CMA	36.29 N	100.90 E	3810	CO_2, CH_4
Nagoya	Japan	NGY	NAGOU	35.15 N	136.97 E	35	N_2O
Nepal Climate Observatory - Pyramid	Nepal	PYR	UNIURB	27.96 N	86.81 E	5079	SO_2F_2, COS, CCl_4, CH_3CCl_3, CFCs, HCFCs, HFCs, PFCs, $CBrClF_2$, $CBrF_3$, $CHCl_3$, CH_3Cl, CH_2Cl_2, CH_3I, CH_3Br, CH_2Br_2, C_2HCl_3, C_2Cl_4, $CHBr_3$
Pha Din	Viet Nam	PDI	VNMHA	21.57 N	103.52 E	1466	CO_2, CH_4, CO
Plateau Assy	Kazakhstan	KZM	NOAA	43.25 N	77.88 E	2519	CO_2, CH_4, N_2O, SF_6, $^{13}CO_2$, $C^{18}O_2$, CO, H_2
Ryori	Japan	RYO	JMA	39.03 N	141.82 E	260	CO_2, CH_4, N_2O, CCl_4, CH_3CCl_3, CFCs, CO
Sary Taukum	Kazakhstan	KZD	NOAA	44.45 N	77.57 E	412	CO_2, CH_4, N_2O, SF_6, $^{13}CO_2$, $C^{18}O_2$, CO, H_2
Shangdianzi	China	SDZ	NOAA	40.65 N	117.12 E	287	CO_2, CH_4, N_2O, SF_6, $^{13}CO_2$, $C^{18}O_2$, CO
Suita	Japan	SUI	OSAKAU	34.82 N	135.52 E	63	CO_2
Tae-ahn Peninsula	Republic of Korea	TAP	NOAA	36.73 N	126.13 E	20	CO_2, CH_4, N_2O, SF_6, $^{13}CH_4$, $^{13}CO_2$, $C^{18}O_2$, CO, H_2
Takayama	Japan	TKY	AIST	36.15 N	137.42 E	1420	CO_2
Tateno (Tsukuba)	Japan	TKB	MRI	36.06 N	140.13 E	25.2	CO_2, CH_4
Tiksi	Russian Federation	TIK	NOAA	71.59 N	128.92 E	8	CO_2, CH_4, N_2O, SF_6, $^{13}CO_2$, $C^{18}O_2$, CO
Tiksi	Russian Federation	TIK	FMI	71.59 N	128.92 E	8	CH_4
Tiksi	Russian Federation	TIK	MGO	71.59 N	128.92 E	8	CO_2, CH_4

LIST OF OBSERVATIONAL STATIONS (continued)

Station	Country/Territory	GAW ID	Organization	Location Latitude (°)	Location Longitude (°)	Altitude (m)	Parameter
Ulaan Uul	Mongolia	UUM	NOAA	44.44 N	111.09 E	992	CO_2, CH_4, N_2O, SF_6, $^{13}CO_2$, $C^{18}O_2$, CO, H_2
Urawa	Japan	URW	SAIPF	35.87 N	139.62 E	10	CO_2
Yonagunijima	Japan	YON	JMA	24.47 N	123.01 E	30	CO_2, CH_4, CO
REGION III (South America)							
Arembepe	Brazil	ABP	NOAA	12.77 S	38.17 W	0	CO_2, CH_4, N_2O, SF_6, $^{13}CO_2$, $C^{18}O_2$, CO
Arembepe	Brazil	ABP	INPE	12.77 S	38.17 W	0	CO_2, CH_4, N_2O, CO
Bird Island (South Georgia)	United Kingdom of Great Britain and Northern Ireland	SGI	NOAA	54.01 S	38.05 W	30	CO_2, CH_4
Easter Island	Chile	EIC	NOAA	27.17 S	109.42 W	41	CO_2, CH_4, N_2O, SF_6, $^{13}CO_2$, $C^{18}O_2$, CO, H_2
El Tololo	Chile	TLL	DMC	30.17 S	70.80 W	2154	CO_2, CH_4, CO
Huancayo	Peru	HUA	IGP	12.15 S	75.57 W	4575	CO_2
Natal	Brazil	NAT	NOAA	6.00 S	35.20 W	0	CO_2, CH_4, N_2O, SF_6, $^{13}CO_2$, $C^{18}O_2$, CO
Ushuaia	Argentina	USH	NOAA	54.85 S	68.31 W	18	CO_2, CH_4, N_2O, SF_6, $^{13}CO_2$, $C^{18}O_2$, CCl_4, CH_3CCl_3, CFCs, CO
REGION IV (North and Central America)							
Alert	Canada	ALT	NOAA	82.50 N	62.34 W	210	CO_2, CH_4, N_2O, SF_6, $^{13}CH_4$, $^{13}CO_2$, $C^{18}O_2$, CCl_4, CH_3CCl_3, CFCs, HCFCs, HFCs, $CBrClF_2$, CO, CH_3Cl, CH_2Cl_2, CH_3Br, C_2Cl_4, H_2
Alert	Canada	ALT	CSIRO	82.50 N	62.34 W	210	CO_2, CH_4, N_2O, $^{13}CO_2$, CO, H_2
Alert	Canada	ALT	ECCC	82.50 N	62.34 W	210	CO_2, CH_4, N_2O, $^{13}CO_2$, $C^{18}O_2$, CO
Argyle (ME)	United States of America	AMT	NOAA	45.03 N	68.68 W	50	CH_4, N_2O, SF_6, $^{13}CO_2$, $C^{18}O_2$, CO
Barrow (AK)	United States of America	BRW	NOAA	71.32 N	156.61 W	11	CO_2, CH_4, N_2O, SF_6, $^{13}CH_4$, $^{13}CO_2$, $C^{18}O_2$, CCl_4, CH_3CCl_3, CFCs, HCFCs, HFCs, $CBrClF_2$, $CBrF_3$, CO, CH_3Cl, CH_2Cl_2, CH_3Br, C_2Cl_4, H_2
Candle Lake	Canada	CDL	ECCC	53.99 N	105.12 W	591	CO_2, CH_4, CO
Cape Meares (OR)	United States of America	CMO	NOAA	45.00 N	124.00 W	30	CO_2, CH_4, $^{13}CO_2$, $C^{18}O_2$, CO, H_2
Cape Meares (OR)	United States of America	CMO	AGAGE	45.00 N	124.00 W	30	CH_4, N_2O, CCl_4, CH_3CCl_3, CFCs
Chibougamau	Canada	CHM	ECCC	49.69 N	74.34 W	383	CO_2, CH_4, CO

LIST OF OBSERVATIONAL STATIONS (continued)

Station	Country/Territory	GAW ID	Organization	Location Latitude (°)	Location Longitude (°)	Altitude (m)	Parameter
Churchill	Canada	CHL	ECCC	58.74 N	93.82 W	16	CO_2, CH_4, N_2O, $^{13}CO_2$, $C^{18}O_2$, CO
Cold Bay (AK)	United States of America	CBA	NOAA	55.20 N	162.72 W	25	CO_2, CH_4, N_2O, SF_6, $^{13}CH_4$, $^{13}CO_2$, $C^{18}O_2$, CO, H_2
East Trout Lake	Canada	ETL	ECCC	54.35 N	104.99 W	500	CO_2, CH_4, $^{13}CO_2$, $C^{18}O_2$, CO
Egbert	Canada	EGB	ECCC	44.23 N	79.78 W	255	CO_2, CH_4, CO
Estevan Point	Canada	ESP	CSIRO	49.38 N	126.54 W	7	CO_2, CH_4, N_2O, $^{13}CO_2$, CO, H_2
Estevan Point	Canada	ESP	ECCC	49.38 N	126.54 W	7	CO_2, CH_4, N_2O, $^{13}CO_2$, $C^{18}O_2$, CO
Fraserdale	Canada	FSD	ECCC	49.84 N	81.52 W	210	CO_2, CH_4, $^{13}CO_2$, $C^{18}O_2$, CO
Grifton - Georgia Station (NC)	United States of America	ITN	NOAA	35.35 N	77.38 W	505	CH_4, N_2O, SF_6, $^{13}CO_2$, $C^{18}O_2$, CCl_4, CH_3CCl_3, CFCs, CO, H_2
Harvard Forest (MA)	United States of America	HFM	NOAA	42.90 N	72.30 W	340	N_2O, SF_6, CCl_4, CH_3CCl_3, CFCs, HCFCs, HFCs, $CBrClF_2$, CH_3Cl, CH_2Cl_2, CH_3Br, C_2Cl_4
Key Biscane (FL)	United States of America	KEY	NOAA	25.67 N	80.20 W	3	CO_2, CH_4, N_2O, SF_6, $^{13}CO_2$, $C^{18}O_2$, CO, H_2
Kitt Peak (AZ)	United States of America	KPA	NOAA	31.97 N	111.60 W	2083	CH_4
La Jolla (CA)	United States of America	SIO	NOAA	32.83 N	117.27 W	14	CH_4
Lac La Biche (Alberta)	Canada	LLB	NOAA	54.95 N	112.47 W	548	CO_2, CH_4, N_2O, SF_6, $^{13}CH_4$, $^{13}CO_2$, $C^{18}O_2$, CO
Lac La Biche (Alberta)	Canada	LLB	ECCC	54.95 N	112.47 W	548	CO_2, CH_4, CO
Mex High Altitude Global Climate Observation Center	Mexico	MEX	NOAA	18.99 N	97.31 W	4560	CO_2, CH_4, N_2O, SF_6, $^{13}CH_4$, $^{13}CO_2$, $C^{18}O_2$, CO
Moody (TX)	United States of America	WKT	NOAA	31.32 N	97.62 W	723	CH_4, N_2O, SF_6, $^{13}CO_2$, $C^{18}O_2$, CO
Mould Bay	Canada	MBC	NOAA	76.25 N	119.35 W	58	CO_2, CH_4, $^{13}CO_2$, $C^{18}O_2$, CO, H_2
Niwot Ridge - T-van (CO)	United States of America	NWR	NOAA	40.05 N	105.59 W	3523	CO_2, CH_4, N_2O, SF_6, $^{13}CH_4$, $^{13}CO_2$, $C^{18}O_2$, CCl_4, CH_3CCl_3, CFCs, HCFCs, HFCs, $CBrClF_2$, CO, CH_3Cl, CH_2Cl_2, CH_3Br, C_2Cl_4, H_2, $^{14}CO_2$
Olympic Peninsula (WA)	United States of America	OPW	NOAA	48.25 N	124.42 W	488	CO_2, CH_4
Park Falls (WI)	United States of America	LEF	NOAA	45.93 N	90.27 W	868	CO_2, CH_4, N_2O, SF_6, $^{13}CO_2$, $C^{18}O_2$, CCl_4, CH_3CCl_3, CFCs, HCFCs, HFCs, $CBrClF_2$, CO, CH_3Cl, CH_2Cl_2, CH_3Br,

LIST OF OBSERVATIONAL STATIONS (continued)

Station	Country/Territory	GAW ID	Organization	Location Latitude (°)	Location Longitude (°)	Altitude (m)	Parameter
							C_2Cl_4, H_2
Point Arena (CA)	United States of America	PTA	NOAA	38.95 N	123.73 W	17	CO_2, CH_4, N_2O, SF_6, $^{13}CO_2$, $C^{18}O_2$, CO
Ragged Point	Barbados	RPB	NOAA	13.17 N	59.43 W	45	CO_2, CH_4, N_2O, SF_6, $^{13}CO_2$, $C^{18}O_2$, CO, H_2
Ragged Point	Barbados	RPB	AGAGE	13.17 N	59.43 W	45	CH_4, N_2O, SF_6, SO_2F_2, NF_3, CCl_4, CH_3CCl_3, CFCs, HCFCs, HFCs, PFCs, $CBrClF_2$, $CBrF_3$, $C_2Br_2F_4$, $CHCl_3$, CH_3Cl, CH_2Cl_2, CH_3Br, C_2Cl_4
Sable Island	Canada	WSA	ECCC	43.93 N	60.01 W	2	CO_2, CH_4, N_2O, $^{13}CO_2$, $C^{18}O_2$, CO
Shemya Island	United States of America	SHM	NOAA	52.72 N	174.10 E	40	CO_2, CH_4, N_2O, SF_6, $^{13}CO_2$, $C^{18}O_2$, CO, H_2
Southern Great Plains E13 (OK)	United States of America	SGP	NOAA	36.60 N	97.50 W	318	CO_2, CH_4, N_2O, SF_6, $^{13}CO_2$, $C^{18}O_2$, CO
St. Croix	United States of America	AVI	NOAA	17.75 N	64.75 W	3	CO_2, CH_4
St. David's Head	United Kingdom of Great Britain and Northern Ireland	BME	NOAA	32.37 N	64.65 W	30	CO_2, CH_4, N_2O, SF_6, $^{13}CO_2$, $C^{18}O_2$, CO, H_2
Trinidad Head (CA)	United States of America	THD	NOAA	41.05 N	124.15 W	107	CO_2, CH_4, N_2O, SF_6, $^{13}CO_2$, $C^{18}O_2$, CCl_4, CH_3CCl_3, CFCs, HCFCs, HFCs, $CBrClF_2$, $CBrF_3$, CO, CH_3Cl, CH_2Cl_2, CH_3Br, C_2Cl_4
Trinidad Head (CA)	United States of America	THD	AGAGE	41.05 N	124.15 W	107	CH_4, N_2O, SF_6, SO_2F_2, NF_3, CCl_4, CH_3CCl_3, CFCs, HCFCs, HFCs, PFCs, $CBrClF_2$, $CBrF_3$, $C_2Br_2F_4$, $CHCl_3$, CH_3Cl, CH_2Cl_2, CH_3Br, C_2Cl_4
Tudor Hill (Bermuda)	United Kingdom of Great Britain and Northern Ireland	BMW	NOAA	32.27 N	64.88 W	30	CO_2, CH_4, N_2O, SF_6, $^{13}CO_2$, $C^{18}O_2$, CO, H_2
Wendover (UT)	United States of America	UTA	NOAA	39.90 N	113.72 W	1320	CO_2, CH_4, N_2O, SF_6, $^{13}CO_2$, $C^{18}O_2$, CO, H_2
West Branch (Iowa)	United States of America	WBI	NOAA	41.72 N	91.35 W	242	$C^{18}O_2$
REGION V (South-West Pacific)							
Baring Head	New Zealand	BHD	NOAA	41.41 S	174.87 E	85	CO_2, CH_4, N_2O, SF_6, $^{13}CH_4$, $^{13}CO_2$, $C^{18}O_2$, CO
Baring Head	New Zealand	BHD	NIWA	41.41 S	174.87 E	85	CO_2, CH_4, N_2O, $^{13}CH_4$, CO, $^{14}CO_2$
Bukit Kototabang	Indonesia	BKT	NOAA	0.20 S	100.32 E	864	CO_2, CH_4, N_2O, SF_6, $^{13}CO_2$, $C^{18}O_2$, CO
Bukit Kototabang	Indonesia	BKT	BMKG	0.20 S	100.32 E	864	CO_2, CH_4, CO

LIST OF OBSERVATIONAL STATIONS (continued)

Station	Country/Territory	GAW ID	Organization	Location Latitude (°)	Location Longitude (°)	Altitude (m)	Parameter
Cape Ferguson	Australia	CFA	CSIRO	19.28 S	147.06 E	2	CO_2, CH_4, N_2O, $^{13}CO_2$, CO, H_2
Cape Grim	Australia	CGO	NOAA	40.68 S	144.69 E	94	CO_2, CH_4, N_2O, SF_6, $^{13}CH_4$, $^{13}CO_2$, $C^{18}O_2$, CCl_4, CH_3CCl_3, CFCs, HCFCs, HFCs, $CBrClF_2$, $CBrF_3$, CO, CH_3Cl, CH_2Cl_2, CH_3Br, C_2Cl_4, H_2
Cape Grim	Australia	CGO	AGAGE	40.68 S	144.69 E	94	CH_4, N_2O, SF_6, SO_2F_2, NF_3, CCl_4, CH_3CCl_3, CFCs, HCFCs, HFCs, PFCs, $CBrClF_2$, $CBrF_3$, $C_2Br_2F_4$, CO, $CHCl_3$, CH_3Cl, CH_2Cl_2, CH_3Br, C_2Cl_4, H_2
Cape Grim	Australia	CGO	ANSTO	40.68 S	144.69 E	94	^{222}Rn
Cape Grim	Australia	CGO	CSIRO	40.68 S	144.69 E	94	CO_2, CH_4, N_2O, $^{13}CO_2$, CO, H_2
Cape Kumukahi (HI)	United States of America	KUM	NOAA	19.52 N	154.82 W	3	CO_2, CH_4, N_2O, SF_6, $^{13}CH_4$, $^{13}CO_2$, $C^{18}O_2$, CCl_4, CH_3CCl_3, CFCs, HCFCs, HFCs, $CBrClF_2$, $CBrF_3$, CO, CH_3Cl, CH_2Cl_2, CH_3Br, C_2Cl_4, H_2
Christmas Island	Kiribati	CHR	NOAA	1.70 N	157.17 W	3	CO_2, CH_4, N_2O, SF_6, $^{13}CO_2$, $C^{18}O_2$, CO, H_2
Danum Valley	Malaysia	DMV	MMD	4.98 N	117.84 E	426	CO_2
Guam (Mariana Island)	United States of America	GMI	NOAA	13.43 N	144.78 E	2	CO_2, CH_4, N_2O, SF_6, $^{13}CO_2$, $C^{18}O_2$, CO, H_2
Gunn Point	Australia	GPA	CSIRO	12.25 S	131.05 E	25	CO_2, CH_4, N_2O, $^{13}CO_2$, CO, H_2
Kaitorete Spit	New Zealand	NZL	NOAA	43.83 S	172.63 E	3	CH_4
Lauder	New Zealand	LAU	NIWA	45.04 S	169.68 E	370	CH_4, CO
Macquarie Island	Australia	MQA	CSIRO	54.50 S	158.94 E	6	CO_2, CH_4, N_2O, $^{13}CO_2$, CO, H_2
Mauna Loa (HI)	United States of America	MLO	NOAA	19.54 N	155.58 W	3397	CO_2, CH_4, N_2O, SF_6, $^{13}CH_4$, $^{13}CO_2$, $C^{18}O_2$, CCl_4, CH_3CCl_3, CFCs, HCFCs, HFCs, $CBrClF_2$, $CBrF_3$, CO, CH_3Cl, CH_2Cl_2, CH_3Br, C_2Cl_4, H_2
Mauna Loa (HI)	United States of America	MLO	CSIRO	19.54 N	155.58 W	3397	CO_2, CH_4, N_2O, $^{13}CO_2$, CO, H_2
Samoa (Cape Matatula)	United States of America	SMO	NOAA	14.25 S	170.56 W	77	CO_2, CH_4, N_2O, SF_6, $^{13}CH_4$, $^{13}CO_2$, $C^{18}O_2$, CCl_4, CH_3CCl_3, CFCs, HCFCs, HFCs, $CBrClF_2$, $CBrF_3$, CO, CH_3Cl, CH_2Cl_2, CH_3Br, C_2Cl_4, H_2

LIST OF OBSERVATIONAL STATIONS (continued)

Station	Country/Territory	GAW ID	Organization	Location Latitude (°)	Location Longitude (°)	Altitude (m)	Parameter
Samoa (Cape Matatula)	United States of America	SMO	AGAGE	14.25 S	170.56 W	77	CH_4, N_2O, SF_6, SO_2F_2, NF_3, CCl_4, CH_3CCl_3, CFCs, HCFCs, HFCs, PFCs, $CBrClF_2$, $CBrF_3$, $C_2Br_2F_4$, $CHCl_3$, CH_3Cl, CH_2Cl_2, CH_3Br, C_2Cl_4
Sand Island	United States of America	MID	NOAA	28.22 N	177.37 W	4	CO_2, CH_4, N_2O, SF_6, $^{13}CO_2$, $C^{18}O_2$, CO, H_2
REGION VI (Europe)							
Adrigole	Ireland	ADR	AGAGE	51.68 N	9.73 W	50	N_2O, CCl_4, CH_3CCl_3, CFCs
BEO Moussala	Bulgaria	BEO	INRNE	42.18 N	23.59 E	2925	CO_2, CO
Baltic Sea	Poland	BAL	NOAA	55.50 N	16.67 E	7	CO_2, CH_4, N_2O, SF_6, $^{13}CH_4$, $^{13}CO_2$, $C^{18}O_2$, CO, H_2
Begur	Spain	BGU	LSCE	41.97 N	3.23 E	13	CO_2, CH_4
Brotjacklriegel	Germany	BRT	UBAG	48.82 N	13.22 E	1016	CO_2
Capo Granitola	Italy	CGR	ISAC	37.67 N	12.65 E	5	CO_2, CH_4, CO
Constanta (Black Sea)	Romania	BSC	NOAA	44.17 N	28.68 E	3	CO_2, CH_4, N_2O, SF_6, $^{13}CO_2$, $C^{18}O_2$, CO, H_2
Deuselbach	Germany	DEU	UBAG	49.77 N	7.05 E	480	CO_2, CH_4
Diabla Gora / Puszcza Borecka	Poland	DIG	IOEP	54.15 N	22.07 E	157	CO_2
Dwejra Point	Malta	GOZ	NOAA	36.05 N	14.18 E	30	CO_2, CH_4, $^{13}CO_2$, $C^{18}O_2$, CO, H_2
Finokalia	Greece	FIK	LSCE	35.34 N	25.67 E	150	CO_2, CH_4
Fundata	Romania	FDT	INMH	45.43 N	25.27 E	1384	CO_2
Gartow	Germany	GAT	DWD	53.07 N	11.44 E	69	CO_2, CH_4, CO
Giordan Lighthouse	Malta	GLH	UMLT	36.07 N	14.22 E	167	CO_2, CH_4, CO, ^{222}Rn
Hegyhatsal	Hungary	HUN	NOAA	46.95 N	16.65 E	248	CO_2, CH_4, N_2O, SF_6, $^{13}CO_2$, $C^{18}O_2$, CO, H_2
Hegyhatsal	Hungary	HUN	HMS	46.95 N	16.65 E	248	CO_2
Hohenpeissenberg	Germany	HPB	NOAA	47.80 N	11.01 E	985	CO_2, CH_4, N_2O, SF_6, $^{13}CO_2$, $C^{18}O_2$, CO
Hohenpeissenberg	Germany	HPB	DWD	47.80 N	11.01 E	985	CO_2, CH_4, CO, ^{222}Rn
Ile Grande	France	LPO	LSCE	48.80 N	3.58 W	20	CO_2, CH_4
Jungfraujoch	Switzerland	JFJ	AGAGE	46.55 N	7.99 E	3580	SF_6, SO_2F_2, NF_3, CCl_4, CH_3CCl_3, CFCs, HCFCs, HFCs, PFCs, $CBrClF_2$, $CBrF_3$, $C_2Br_2F_4$, $CHCl_3$, CH_3Cl, CH_2Cl_2, CH_3Br, C_2HCl_3, C_2Cl_4
Jungfraujoch	Switzerland	JFJ	Empa	46.55 N	7.99 E	3580	CO_2, CH_4, N_2O, SF_6, CO
Jungfraujoch	Switzerland	JFJ	KUP	46.55 N	7.99 E	3580	CO_2
K-Puszta	Hungary	KPS	HMS	46.97 N	19.58 E	125	CO_2
Kloosterburen	Netherlands	KTB	RIVM	53.40 N	6.42 E	0	CO
Kollumerwaard	Netherlands	KMW	RIVM	53.33 N	6.27 E	0	CO_2, CH_4, CO
Kosetice Observatory	Czech Republic	KOS	CHMI	49.58 N	15.08 E	534	CH_4, CO
Krvavec	Slovenia	KVV	ARSO	46.30 N	14.53 E	1740	CO

LIST OF OBSERVATIONAL STATIONS (continued)

Station	Country/Territory	GAW ID	Organization	Location Latitude (°)	Location Longitude (°)	Altitude (m)	Parameter
Lamezia Terme	Italy	LMT	ISAC	38.88 N	16.23 E	6	CO_2, CH_4, CO
Lampedusa	Italy	LMP	NOAA	35.52 N	12.63 E	45	CO_2, CH_4, N_2O, SF_6, $^{13}CO_2$, $C^{18}O_2$, CO
Lampedusa	Italy	LMP	ENEA	35.52 N	12.63 E	45	CO_2, CH_4, N_2O, SF_6, CCl_4, CH_3CCl_3, CFCs, HCFCs, HFCs, $CBrClF_2$, $CBrF_3$, $CHCl_3$, CH_3Cl, CH_2Cl_2, CH_3I, CH_3Br, CH_2Br_2
Lecce Environmental-Climate Observatory	Italy	ECO	ISAC	40.34 N	18.12 E	36	CO_2, CH_4, CO
Lerwick	United Kingdom of Great Britain and Northern Ireland	SIS	CSIRO	60.13 N	1.18 W	84	CO_2, CH_4, N_2O, $^{13}CO_2$, CO, H_2
Lindenberg	Germany	LIN	DWD	52.22 N	14.12 E	112	CO_2, CH_4
Mace Head	Ireland	MHD	NOAA	53.33 N	9.90 W	5	CO_2, CH_4, N_2O, SF_6, $^{13}CH_4$, $^{13}CO_2$, $C^{18}O_2$, CCl_4, CH_3CCl_3, CFCs, HCFCs, HFCs, $CBrClF_2$, CO, CH_3Cl, CH_2Cl_2, CH_3Br, C_2Cl_4, H_2
Mace Head	Ireland	MHD	AGAGE	53.33 N	9.90 W	5	CH_4, N_2O, SF_6, SO_2F_2, NF_3, CCl_4, CH_3CCl_3, CFCs, HCFCs, HFCs, PFCs, $CBrClF_2$, $CBrF_3$, $C_2Br_2F_4$, CO, $CHCl_3$, CH_3Cl, CH_2Cl_2, CH_3Br, C_2HCl_3, C_2Cl_4, H_2
Mace Head	Ireland	MHD	LSCE	53.33 N	9.90 W	5	CO_2, CH_4
Monte Cimone	Italy	CMN	AGAGE	44.17 N	10.68 E	2165	SO_2F_2, CCl_4, CH_3CCl_3, CFCs, HCFCs, HFCs, PFCs, $CBrClF_2$, $CBrF_3$, $CHCl_3$, CH_3Cl, CH_2Cl_2, CH_3Br, C_2Cl_4
Monte Cimone	Italy	CMN	IAFMS	44.17 N	10.68 E	2165	CO_2, CH_4
Monte Cimone	Italy	CMN	ISAC	44.17 N	10.68 E	2165	CO, H_2
Monte Cimone	Italy	CMN	UNIURB	44.17 N	10.68 E	2165	CH_4, N_2O, SF_6, CO
Monte Curcio	Italy	CUR	IIA	39.32 N	16.42 E	1796	CO_2, CH_4, CO
Neuglobsow	Germany	NGL	UBAG	53.14 N	13.03 E	62	CO_2, CH_4, CO
Ocean Station Charlie	United States of America	STC	NOAA	54.00 N	35.00 W	0	CO_2
Ocean Station Charlie	United States of America	STC	MGO	54.00 N	35.00 W	0	CO_2
Ocean Station M	Norway	STM	NOAA	66.00 N	2.00 E	4	CO_2, CH_4, N_2O, SF_6, $^{13}CO_2$, $C^{18}O_2$, CO, H_2
Ochsenkopf	Germany	OXK	NOAA	50.03 N	11.81 E	1185	CO_2, CH_4, N_2O, SF_6, $^{13}CO_2$, $C^{18}O_2$, CO
Pallas	Finland	PAL	NOAA	67.97 N	24.12 E	560	CO_2, CH_4, N_2O, SF_6, $^{13}CO_2$, $C^{18}O_2$, CO
Pallas	Finland	PAL	FMI	67.97 N	24.12 E	560	CO_2, CH_4
Payerne	Switzerland	PAY	Empa	46.81 N	6.94 E	490	CO
Pic du Midi	France	PDM	LA	42.94 N	0.14 E	2877	CO
Pic du Midi	France	PDM	LSCE	42.94 N	0.14 E	2877	CO_2, CH_4

LIST OF OBSERVATIONAL STATIONS (continued)

Station	Country/Territory	GAW ID	Organization	Location Latitude (°)	Location Longitude (°)	Altitude (m)	Parameter
Plateau Rosa	Italy	PRS	RSE	45.94 N	7.71 E	3480	CO_2, CH_4
Puy de Dôme	France	PUY	LAMP	45.77 N	2.97 E	1465	CO
Puy de Dôme	France	PUY	LSCE	45.77 N	2.97 E	1465	CO_2, CH_4
Ridge Hill	United Kingdom of Great Britain and Northern Ireland	RGL	UNIVBRIS	52.00 N	2.54 W	204	CO_2, CH_4, N_2O, SF_6
Rigi	Switzerland	RIG	Empa	47.07 N	8.46 E	1031	CO
Schauinsland	Germany	SSL	UBAG	47.90 N	7.92 E	1205	CO_2, CH_4, N_2O, SF_6, CO
Sede Boker	Israel	WIS	NOAA	31.13 N	34.88 E	400	CO_2, CH_4, N_2O, SF_6, $^{13}CO_2$, $C^{18}O_2$, CO, H_2
Serreta (Terceira)	Portugal	AZR	NOAA	38.77 N	27.38 W	40	CO_2, CH_4, N_2O, SF_6, $^{13}CH_4$, $^{13}CO_2$, $C^{18}O_2$, CO, H_2
Sonnblick	Austria	SNB	UBAA	47.05 N	12.96 E	3106	CO_2, CH_4, CO
Storhofdi	Iceland	ICE	NOAA	63.40 N	20.28 W	118	CO_2, CH_4, N_2O, SF_6, $^{13}CO_2$, $C^{18}O_2$, CO, H_2
Summit	Denmark	SUM	NOAA	72.58 N	38.48 W	3238	CO_2, CH_4, N_2O, SF_6, $^{13}CH_4$, $^{13}CO_2$, $C^{18}O_2$, CCl_4, CH_3CCl_3, CFCs, HCFCs, HFCs, $CBrClF_2$, CO, CH_3Cl, CH_2Cl_2, CH_3Br
Summit	Denmark	SUM	INSTAAR	72.58 N	38.48 W	3238	CH_4
Tacolneston Tall Tower	United Kingdom of Great Britain and Northern Ireland	TAC	NOAA	52.52 N	1.14 E	56	CO_2, CH_4, N_2O, SF_6, CO
Tacolneston Tall Tower	United Kingdom of Great Britain and Northern Ireland	TAC	UNIVBRIS	52.52 N	1.14 E	56	CO_2, CH_4, N_2O, SF_6, SO_2F_2, CH_3CCl_3, CFCs, HCFCs, HFCs, PFCs, $CBrClF_2$, $CBrF_3$, CO, $CHCl_3$, CH_3Cl, CH_2Cl_2, CH_3Br, C_2HCl_3, C_2Cl_4, H_2
Teriberka	Russian Federation	TER	MGO	69.20 N	35.10 E	40	CO_2, CH_4
Waldhof-Langenbrügge	Germany	WAL	UBAG	52.80 N	10.76 E	74	CO_2
Wank	Germany	WNK	IMKIFU	47.51 N	11.14 E	1780	CO_2
Westerland	Germany	WES	UBAG	54.92 N	8.31 E	12	CO_2
Zeppelin Mountain (Ny Ålesund)	Norway	ZEP	NOAA	78.91 N	11.89 E	475	CO_2, CH_4, N_2O, SF_6, $^{13}CH_4$, $^{13}CO_2$, $C^{18}O_2$, CO, H_2
Zeppelin Mountain (Ny Ålesund)	Norway	ZEP	AGAGE	78.91 N	11.89 E	475	SF_6, SO_2F_2, NF_3, CH_3CCl_3, CFCs, HCFCs, HFCs, PFCs, $CBrClF_2$, $CBrF_3$, $C_2Br_2F_4$, $CHCl_3$, CH_3Cl, CH_2Cl_2, CH_3Br, C_2Cl_4
Zeppelin Mountain (Ny Ålesund)	Norway	ZEP	ITM	78.91 N	11.89 E	475	CO_2
Zeppelin Mountain (Ny Ålesund)	Norway	ZEP	NILU	78.91 N	11.89 E	475	N_2O, CFCs
Zingst	Germany	ZGT	UBAG	54.44 N	12.72 E	1	CO_2, CH_4
Zugspitze-Gipfel	Germany	ZUG	IMKIFU	47.42 N	10.99 E	2962	CO_2
Zugspitze-Gipfel	Germany	ZUG	UBAG	47.42 N	10.99 E	2962	CO_2, CH_4, CO

LIST OF OBSERVATIONAL STATIONS (continued)

Station	Country/Territory	GAW ID	Organization	Location Latitude (°)	Location Longitude (°)	Altitude (m)	Parameter
Zugspitze-Schneefernerhaus	Germany	ZSF	DWD	47.42 N	10.98 E	2671	^{222}Rn, ^{7}Be
Zugspitze-Schneefernerhaus	Germany	ZSF	UBAG	47.42 N	10.98 E	2671	CO_2, CH_4, N_2O, SF_6, CO

LIST OF OBSERVATIONAL STATIONS (continued)

Station	Country/Territory	GAW ID	Organization	Location Latitude (°)	Location Longitude (°)	Altitude (m)	Parameter
ANTARCTICA							
Arrival Heights	New Zealand	ARH	NIWA	77.83 S	166.66 E	184	CH_4, N_2O, $^{13}CH_4$, CO
Casey	Australia	CYA	CSIRO	66.28 S	110.52 E	51	CO_2, CH_4, N_2O, $^{13}CO_2$, CO, H_2
Halley	United Kingdom of Great Britain and Northern Ireland	HBA	NOAA	75.57 S	25.50 W	30	CO_2, CH_4, N_2O, SF_6, $^{13}CO_2$, $C^{18}O_2$, CO, H_2
Halley	United Kingdom of Great Britain and Northern Ireland	HBA	BAS	75.57 S	25.50 W	30	CO
Jubany	Argentina	JBN	IAA	62.24 S	58.67 W	15	CO_2
King Sejong	Republic of Korea	KSG	KMA	62.22 S	58.78 W	0	CO_2
Mawson	Australia	MAA	CSIRO	67.60 S	62.87 E	20	CO_2, CH_4, N_2O, $^{13}CO_2$, CO, H_2
McMurdo	United States of America	MCM	NOAA	77.85 S	166.67 E	11	CH_4
Palmer Station	United States of America	PSA	NOAA	64.77 S	64.05 W	10	CO_2, CH_4, N_2O, SF_6, $^{13}CO_2$, $C^{18}O_2$, CCl_4, CH_3CCl_3, CFCs, HCFCs, HFCs, $CBrClF_2$, CO, CH_3Cl, CH_2Cl_2, CH_3Br, H_2
South Pole	United States of America	SPO	NOAA	90.00 S	24.80 W	2841	CO_2, CH_4, N_2O, SF_6, $^{13}CH_4$, $^{13}CO_2$, $C^{18}O_2$, CCl_4, CH_3CCl_3, CFCs, HCFCs, HFCs, $CBrClF_2$, $CBrF_3$, CO, CH_3Cl, CH_2Cl_2, CH_3Br, C_2Cl_4, H_2
South Pole	United States of America	SPO	CSIRO	90.00 S	24.80 W	2841	CO_2, CH_4, N_2O, $^{13}CO_2$, CO, H_2
Syowa	Japan	SYO	NOAA	69.01 S	39.58 E	18.4	CO_2, CH_4, N_2O, SF_6, $^{13}CO_2$, $C^{18}O_2$, CO, H_2
Syowa	Japan	SYO	TU	69.01 S	39.58 E	18.4	CO_2, CH_4
MOBILE							
Aircraft (Western North Pacific)	Japan	AOA	JMA				CO_2, CH_4, N_2O, CO
Aircraft (off the coast of Sendai Plain)	Japan	PIP	TU				CH_4
Aircraft (over Bass Strait and Cape Grim)	Australia	AIA	CSIRO				CO_2, CH_4, N_2O, $^{13}CO_2$, CO, H_2
Aircraft (over Japan and surroundings)	Japan	OAS	MRI				CH_4, N_2O, SF_6, CFCs
Aircraft: Orleans	France	ORL	LSCE				CO_2, CH_4
Alligator liberty, M/V	Japan	ALL	JMA				CO_2
Atlantic Ocean	United States of America	AOC	NOAA				CO_2, CH_4
CONTRAIL	Japan	EOM	NIES				CO_2, CH_4

LIST OF OBSERVATIONAL STATIONS (continued)

Station	Country/Territory	GAW ID	Organization	Location Latitude (°)	Location Longitude (°)	Location Altitude (m)	Parameter
CONTRAIL	Japan	EOM	TU				$^{13}CH_4$, CH_3D
Drake Passage	United States of America	DRP	NOAA				CO_2, CH_4, N_2O, SF_6, $^{13}CO_2$, $C^{18}O_2$, CO
INSTAC	Japan	INS	MRI				CO_2, CH_4, $^{13}CO_2$
Keifu Maru, R/V	Japan	KEF	JMA				CO_2, CFCs, TIC
Kofu Maru, R/V	Japan	KOF	JMA				CO_2
MRI Research, Hakuho Maru, R/V	Japan	HKH	MRI				CO_2, CH_4
MRI Research, Kaiyo Maru, R/V	Japan	KIY	MRI				CO_2, CO
MRI Research, Natushima, R/V	Japan	NTU	MRI				CO_2, CH_4
MRI Research, Ryofu Maru, R/V	Japan	RFM	MRI				CO_2, CH_4
MRI Research, Ship observations	Japan	MRI	MRI				CH_4
MRI Research, Wellington Maru, R/V	Japan	WLT	MRI				CO_2
Mirai, R/V	Japan	MMR	MRI				CO_2
Mirai, R/V	Japan	MMR	JAMSTEC				CO_2
NOPACCS - Hakurei Maru -	Japan	HAK	NEDO				TIC
Northern and western Pacific	Japan	NWP	TU				N_2O
Pacific Ocean	United States of America	POC	NOAA				CO_2, CH_4, N_2O, SF_6, $^{13}CO_2$, $C^{18}O_2$, CO, H_2
Pacific Ocean	New Zealand	BSL	NIWA				CH_4, $^{13}CH_4$
Pacific-Atlantic Ocean	United States of America	PAO	NOAA				CO_2, CH_4, N_2O, SF_6, CO
Ryofu Maru, R/V	Japan	RYF	JMA				CO_2, CH_4, N_2O, CFCs, TIC
Santarem	Brazil	SAN	INPE				CO_2, CH_4, N_2O, SF_6, CO
Ship between Ishigaki Island and Hateruma Island	Japan	SIH	TU				CO_2
South China Sea	United States of America	SCS	NOAA				CO_2, CH_4, $^{13}CO_2$, $C^{18}O_2$, CO, H_2
Soyo Maru, R/V	Japan	SOY	FRA				CO_2
WEST COSMIC - Hakurei Maru No.2 -	Japan	HRM	NEDO				TIC
Wakataka-Maru	Japan	WAK	FRA				CO_2
Western Pacific	United States of America	WPC	NOAA				CO_2, CH_4, N_2O, SF_6, $^{13}CH_4$, $^{13}CO_2$, $C^{18}O_2$, CO
over Japan between Sendai and Fukuoka	Japan	TDA	TU				CH_4

APPENDIX D LIST OF CONTRIBUTORS

Station Country/Territory	Name	Address
REGION I (Africa)		
Mt. Kenya (Kenya)	Constance Okuku	Kenya Meteorological Department MT KENYA GAW STATION P.O. Box 192 10400 NANYUKI Kenya
	Jörg Klausen	Federal Office of Meteorology and Climatology MeteoSwiss 8058 ZH,Zürich-Flughafen Operation Center 1, Switzerland
	Stephan Henne	Swiss Federal Laboratories for Materials Science and Technology Ueberlandstrasse 129 8600 Duebendorf, Switzerland
Izaña (Tenerife) (Spain)	Emilio Cuevas	State Meteorological Agency of Spain C/ La Marina, 20, Planta 6, 38001 Santa Cruz de Tenerife, Spain
Cape Point (South Africa)	Alastair Williams	ANSTO, Locked Bag 2001 Kirrawee DC, NSW 2232 Australia
	Scott Chambers	ANSTO, Locked Bag 2001 Kirrawee DC, NSW 2232 Australia
Assekrem (Algeria)	Sidi Baika	Office National de la Meteorologie POBox 31 Tamanrasset 11000, Algeria
Cairo Farafra (Egypt)	AbdElhamid Gouda Elawadi	Department of Air Pollution Study Egyptian Meteorological Authority P.O.Box:11784 Cairo, Egypt
	Zeinab Salah	Egyptian Meteorological Authority Al-Khalifa El-Maamoun St. Kobry Al-Qubba Cairo, Egypt P.O.Box: 11784
Amsterdam Island (France)	Michel Ramonet	LSCE - CEA Saclay - Orme des Merisiers - 91191 Gif-sur-Yvette, France
	Jean Sciare	LSCE - CEA Saclay - Orme des Merisiers - Bat.701 91191 Gif-sur-Yvette, France
Cape Point (South Africa)	Thumeka Mkololo	SAWS, c/o CSIR (Environmentek), P.O. Box 320,Stellenbosch 7599, South Africa
	Casper Labuschagne	SA Weather Service c/o CSIR (Environmentek) P.O. Box 320,Stellenbosch 7599, South Africa
	Lynwill Martin	SAWS, c/o CSIR (Environmentek), P.O. Box 320,Stellenbosch 7599, South Africa

LIST OF CONTRIBUTORS (continued)

Station Country/Territory	Name	Address
	Warren Joubert	SAWS c/o CSIR (Environmentek) P.O. Box 320,Stellenbosch 7599, South Africa
Cape Verde Atmospheric Observatory (Cabo Verde)	Katie Read	Department of Chemistry University of York, Heslington York YO10 5DD United Kingdom
	Lucy Carpenter	Department of Chemistry University of York, Heslington York YO10 5DD United Kingdom
REGION II (Asia)		
Hamamatsu (Japan)	Mitsuo Toda	Shizuoka University 3-5-1 Jyohoku, Hamamatsu 432-8561, Japan
Cape Ochiishi Hateruma Island (Japan)	Yasunori TOHJIMA	National Institute for Environmental Studies Center for Global Environmental Research 16-2, Onogawa, Tsukuba-shi, Ibaraki 305-8506, Japan
	Hitoshi MUKAI	National Institute for Environmental Studies Center for Global Environmental Research 16-2, Onogawa, Tsukuba-shi, Ibaraki 305-8506, Japan
	Takuya Saito	National Institute for Environmental Studies 16-2 Onogawa, Tsukuba 305-8506, Japan
Memanbetsu Tateno (Tsukuba) (Japan)	Kazuhiro Tsuboi	Meteorological Research Institute 1-1, Nagamine Tsukuba Ibaraki 305-0052
Minamitorishima Ryori Yonagunijima (Japan)	Kazuyuki SAITO	Japan Meteorological Agency 1-3-4 Otemachi Chiyoda-ku Tokyo 100-8122
Bering Island Kotelnyj Island Tiksi (Russian Federation) Kyzylcha (Uzbekistan)	Nina Paramonova	Voeikov Main Geophysical Observatory St. Petersburg, Karbyshev Street 7, Russian Federation, 194021
Mt. Waliguan (China)	ZHANG Yong	China Meteorological Administration 46 Zhongguancun S. Ave., Haidian Dist., Beijing, 100081, China

LIST OF CONTRIBUTORS (continued)

Station Country/Territory	Name	Address
Kisai Mt. Dodaira Urawa (Japan)	Yosuke MUTO	Center for Environmental Science in Saitama 914 Kamitanadare,Kazo,Saitama,Japan
Gosan (Republic of Korea)	Haeyoung Lee	National Institute of Meteorological Sciences/Korea Meteorological Administration 33 Seohobuk-ro, Seogwipo, Jeju, 63568 Rep.of Korea
	Park Hyo-Jin	Climate Change Monitoring Division, Korea Meteorological Administration 61 Yeouidaebang-ro 16 gil, Dongjak-gu, Seoul, 07062, Republic of Korea
Tiksi (Russian Federation)	Ed Dlugokencky	NOAA ESRL GML 325 Broadway R/GML-1 Boulder, CO 80305-3328
	Viktor Ivakhov	Voeikov Main Geophysical Observatory St. Petersburg, Karbyshev Street 7, Russian Federation, 194021
	Tuomas Laurila	Finnish Meteorological Institute P.O. BOX 503 FI-00101 HELSINKI FINLAND
Takayama (Japan)	Shohei Murayama	AIST Tsukuba West, 16-1 Onogawa, Tsukuba, Ibaraki 305-8569, Japan
Hok Tsui / Cape d Aguilar King's Park (Hong Kong, China)	David H.Y. Lam	Hong Kong Observatory 134A Nathan Road, Kowloon, Hong Kong.
	Olivia S.M. Lee	Hong Kong Observatory 134A Nathan Road, Kowloon, Hong Kong.
Nepal Climate Observatory - Pyramid (Nepal)	Jgor Arduini	University of Urbino, Dep. of Pure and Applied Sciences (DISPEA) piazza Rinascimento 6, 61029 Urbino - Italy
Jeju Gosan (Republic of Korea)	Haeyoung Lee	National Institute of Meteorological Sciences/Korea Meteorological Administration 33 Seohobuk-ro, Seogwipo, Jeju, 63568 Rep.of Korea
Anmyeon-do (Republic of Korea)	Haeyoung Lee	National Institute of Meteorological Sciences/Korea Meteorological Administration 33 Seohobuk-ro, Seogwipo, Jeju, 63568 Rep.of Korea
	Sumin Kim	National Institute of Meteorological Sciences 33, Seohobuk-ro, Seoqwipo. Jeju, 63568, Rep. of KOREA
Hok Tsui / Cape d Aguilar (Hong Kong, China)	Ka Se Lam	The Hong Kong Polytechnic University Hung Hom, Kowloon, Hong Kong, China

LIST OF CONTRIBUTORS (continued)

Station Country/Territory	Name	Address
Pha Din (Viet Nam)	Martin Steinbacher	Swiss Federal Laboratories for Materials Science and Technology Ueberlandstrasse 129 CH-8600 Duebendorf Switzerland
	Nguyen Nhat Anh	Viet Nam Meteorological and Hydrological Administration No. 8 Phao Dai Lang street 100000 Ha Noi Viet Nam
Issyk-Kul (Kyrgyzstan)	V. Sinyakov	Kyrgyz National University Manas Street 101, Bishkek, 720033, Kyrgyz Republic
Gosan (Republic of Korea)	Jiyoung Kim	National Institute of Environmental Research Environmental Research Complex Hwangyeong-ro 42, Seo-gu, Incheon, 22689
	Eunjung Kim	National Institute of Environmental Research Environmental Research Complex Hwangyeong-ro 42, Seo-gu, Incheon, 22689
Suita (Japan)	Tomohiro Oda	Universities Space Research Association Global Modeling and Assimilation Office NASA Goddard Space Flight Center 8800 Greenbelt Road, Greenbelt, Maryland 20771
	Takashi Machimura	Osaka University Green Engieering Lab Division of Sustainable Energy and Environmental Engineering 2-1 Yamadaoka, Suita, Osaka 565-0871 Japan
Nagoya (Japan)	A. Matsunami	Research Center for Advanced Energy Conversion, Nagoya University Furo-cho, Chikusaku, Nagoya 464-8603, Japan
Mikawa-Ichinomiya (Japan)	Koji Ohno	Aichi Air Environment Division 1-2 Sannomaru-3chome, Naka-ku, Nagoya, Aichi 460-8501, Japan
REGION III (South America)		
El Tololo (Chile)	Martin Steinbacher	Swiss Federal Laboratories for Materials Science and Technology Ueberlandstrasse 129 CH-8600 Duebendorf Switzerland
	Gaston Torres	Dirección Meteorológica de Chile Av. Portales 3450, Estación Central - Santiago
Huancayo (Peru)	Mutsumi Ishitsuka	Observatorio de Huancayo, Instituto Geofisico del Peru Apartado 46, Huancayo, Peru

LIST OF CONTRIBUTORS (continued)

Station Country/Territory	Name	Address
Arembepe (Brazil)	Luciana Vanni Gatti	National Institute in Space Research Atmospheric Chemistry Laboratory Av. Prof. Lineu Prestes, 2242 Cidade Universitaria, Sao Paulo, SP- BRAZIL CEP 05508-900
REGION IV (North and Central America)		
Alert Churchill East Trout Lake Estevan Point Fraserdale Sable Island (Canada)	Lin Huang	Environment and Climate Change Canada Climate Research Division 4905 Dufferin Street, Toronto, Ontario CANADA M3H 5T4
	Doug Worthy	Environment and Climate Change Canada Climate Research Division 4905 Dufferin Street, Toronto, Ontario CANADA M3H 5T4
Candle Lake Chibougamau Egbert Lac La Biche (Alberta) (Canada)	Doug Worthy	Environment and Climate Change Canada Climate Research Division 4905 Dufferin Street, Toronto, Ontario CANADA M3H 5T4
REGION V (South-West Pacific)		
Cape Grim (Australia)	Alastair Williams	ANSTO, Locked Bag 2001 Kirrawee DC, NSW 2232 Australia
	Scott Chambers	ANSTO, Locked Bag 2001 Kirrawee DC, NSW 2232 Australia
Cape Grim (Australia)	Paul Krummel	CSIRO Oceans and Atmosphere - Climate Science Centre 107-121 Station Street Aspendale Victoria, 3195 Australia
	Ray Langenfelds	CSIRO Oceans and Atmosphere - Climate Science Centre 107-121 Station Street Aspendale Victoria, 3195 Australia
	Zoë Loh	CSIRO Oceans and Atmosphere - Climate Science Centre 107-121 Station Street Aspendale Victoria, 3195 Australia
Lauder (New Zealand)	Sylvia Nichol	NIWA - Wellington Private Bag 14901, Kilbirnie, Wellington, 6241 301 Evans Bay Parade, Hataitai, Wellington 6021
	Gordon Brailsford	NIWA - Wellington Private Bag 14901, Kilbirnie, Wellington, 6241 301 Evans Bay Parade, Hataitai, Wellington 6021

LIST OF CONTRIBUTORS (continued)

Station Country/Territory	Name	Address
Baring Head (New Zealand)	Jocelyn Turnbull	GNS Science
	Sylvia Nichol	NIWA - Wellington Private Bag 14901, Kilbirnie, Wellington, 6241 301 Evans Bay Parade, Hataitai, Wellington 6021
	Gordon Brailsford	NIWA - Wellington Private Bag 14901, Kilbirnie, Wellington, 6241 301 Evans Bay Parade, Hataitai, Wellington 6021
Danum Valley (Malaysia)	Ahmad Fairudz Jamaluddin	Malaysian Meteorological Department Jalan Sultan, 46667, Petaling Jaya, Selangor MALAYSIA
	Mohan Kumar Sammathuria	Malaysian Meteorological Department Jalan Sultan, 46667, Petaling Jaya, Selangor MALAYSIA
Bukit Kototabang (Indonesia)	Martin Steinbacher	Swiss Federal Laboratories for Materials Science and Technology Ueberlandstrasse 129 CH-8600 Duebendorf Switzerland
	Okaem, Tanti Tritama	Agency for Meteorology, Climatology and Geophysics Jl. Raya Bukittinggi-Medan Km. 17 Palupuh, District Agam, West Sumatera, Indonesia PO BOX 11 Bukittinggi 26100
	Nahas, Alberth Christian	Agency for Meteorology, Climatology and Geophysics Jl. Raya Bukittinggi-Medan Km. 17 Palupuh, District Agam, West Sumatera, Indonesia PO BOX 11 Bukittinggi 26100
	Reza Mahdi	Agency for Meteorology, Climatology and Geophysics Stasiun Pemantau Atmosfer Global Bukit Kototabang Jl Raya Bukittinggi-Medan Km 17 Palupuh 26100, Bukittinggi
REGION VI (Europe)		
Diabla Gora / Puszcza Borecka (Poland)	Zdzislaw Przadka	Institute of Environmental Protection - NRI Kolektorska 4, 01-692 Warsaw, Poland
	Anna Degorska	Institute of Environmental Protection - NRI Kolektorska 4 01-692 Warsaw, Poland
	Krzysztof Skotak	Institute of Environmental Protection - NRI Kolektorska 4, 01-692 Warsaw, Poland
Monte Curcio (Italy)	Mariantonia Bencardino	CNR-Institute of Atmospheric Pollution Research c/o UNICAL-Polifunzionale 87036 Rende, Italy
BEO Moussala (Bulgaria)	Ivo Kalapov	Institute for Nuclear Research and Nuclear Energy Tsarigradsko shose Blvd. 1784 Sofia Bulgaria

LIST OF CONTRIBUTORS (continued)

Station Country/Territory	Name	Address
Kloosterburen Kollumerwaard (Netherlands)	Ronald Spoor	National Institute of Public Health and the Environment PO Box 1 3720 BA Bilthoven the Netherlands
Schauinsland (Germany)	Frank Meinhardt	German Environment Agency Umweltbundesam Messstation Schauinsland Schauinslandweg 2 79254 Oberried-Hofsgrund
Brotjacklriegel Deuselbach Neuglobsow Waldhof-Langenbrügge Westerland Zingst Zugspitze-Gipfel (Germany)	Ludwig Ries	German Environment Agency Umweltbundesamt, Umweltforschungsstation Schneefernerhaus, Zugspitze 5, 82475 Zugspitze
Zugspitze-Schneefernerhaus (Germany)	Cedric Couret	German Environment Agency Umweltbundesamt, Umweltforschungsstation Schneefernerhaus, Zugspitze 5, 82475 Zugspitze
Jungfraujoch (Switzerland)	Markus Leuenberger	University of Bern Physics Institute, Climate and Environmental Physics Sidlerstrasse 5, CH-3012 Bern
Tacolneston Tall Tower (United Kingdom of Great Britain and Northern Ireland)	Simon O'Doherty	Atmospheric Chemistry Research Group School of Chemistry University of Bristol Cantocks Close BS8 1TS Bristol United Kingdom
	Kieran Stanley	Atmospheric Chemistry Research Group School of Chemistry University of Bristol Cantocks Close BS8 1TS Bristol United Kingdom
	Daniel Say	Atmospheric Chemistry Research Group School of Chemistry University of Bristol Cantocks Close BS8 1TS Bristol United Kingdom
Ridge Hill (United Kingdom of Great Britain and Northern Ireland)	Simon O'Doherty	Atmospheric Chemistry Research Group School of Chemistry University of Bristol Cantocks Close BS8 1TS Bristol United Kingdom
	Daniel Say	Atmospheric Chemistry Research Group School of Chemistry University of Bristol Cantocks Close BS8 1TS Bristol United Kingdom
Sonnblick (Austria)	Wolfgang Spangl	Federal Environment Agency Austria Spittelauer Lände 5 A-1090 Wien
	Iris Buxbaum	Federal Environment Agency Austria Spittelauer Lände 5 A-1090 Wien

LIST OF CONTRIBUTORS (continued)

Station Country/Territory	Name	Address
	Andreas Wolf	Federal Environment Agency Austria Spittelauer Lände 5 A-1090 Wien
Ocean Station Charlie (United States of America)	Nina Paramonova	Voeikov Main Geophysical Observatory St. Petersburg, Karbyshev Street 7, Russian Federation, 194021
Teriberka (Russian Federation)	Nina Paramonova	Voeikov Main Geophysical Observatory St. Petersburg, Karbyshev Street 7, Russian Federation, 194021
	Viktor Ivakhov	Voeikov Main Geophysical Observatory St. Petersburg, Karbyshev Street 7, Russian Federation, 194021
Jungfraujoch (Switzerland)	Martin Steinbacher	Swiss Federal Laboratories for Materials Science and Technology Ueberlandstrasse 129 CH-8600 Duebendorf Switzerland
	Thomas Seitz	Swiss Federal Laboratories for Materials Science and Technology Überlandstrasse 129 CH-8600 Dübendorf Switzerland
Payerne Rigi (Switzerland)	Thomas Seitz	Swiss Federal Laboratories for Materials Science and Technology Überlandstrasse 129 CH-8600 Dübendorf Switzerland
Puy de Dôme (France)	Meyerfeld Yves	Laboratoire d'Aérologie 14 avenue Edouard Belin 31400 - TOULOUSE
	Pichon Jean-Marc	Laboratoire de Météorologie Physique LaMP 4 av. Blaise Pascal TSA 60026 CS 60026 63178 Aubière
Monte Cimone (Italy)	Luigi Caracciolo di Torchiarolo	Italian Air Force Meteorological Service Aeronautica Militare Comando Squadra Aerea Reparto di Meteorologia Viale dell'Universita' 4 - 00185 Roma
Pallas (Finland)	Juha Hatakka	Finnish Meteorological Institute Erik Palmenin aukio 1 FI-00560 Helsinki, Finland
Monte Cimone (Italy)	Jgor Arduini	University of Urbino, Dep. of Pure and Applied Sciences (DISPEA) piazza Rinascimento 6, 61029 Urbino - Italy

LIST OF CONTRIBUTORS (continued)

Station Country/Territory	Name	Address
Hegyhatsal K-Puszta (Hungary)	Laszlo Haszpra	Research Centre for Astronomy and Earth Sciences
Plateau Rosa (Italy)	Daniela Heltai	Ricerca sul Sistema Energetico - RSE S.p.A. via Rubattino 54, 20134 Milano, Italy
	Francesco Apadula	Ricerca sul Sistema Energetico - RSE S.p.A. via Rubattino 54, 20134 Milano, Italy
	Andrea Lanza	Ricerca sul Sistema Energetico - RSE S.p.A. via Rubattino 54, 20134 Milano, Italy
Giordan Lighthouse (Malta)	Martin Saliba	University of Malta Department of Geosciences Tal-Qroqq Msida, MSD 2080
	Francelle Azzopardi	University of Malta Department of Geosciences Tal-Qroqq Msida, MSD 2080
	Raymond Ellul	University of Malta Department of Geosciences Tal-Qroqq Msida, MSD 2080
Kosetice Observatory (Czech Republic)	Adéla Holubová	Czech Hydrometeorological Institute Na sabatce 2050/17, 143 06 Praha 412-Komorany
Fundata (Romania)	Florin Nicodim	National Meteorological Administration Sos. Bucuresti-Ploiesti nr. 97, 71552 Bucharest, Romania
Zeppelin Mountain (Ny Ålesund) (Norway)	Hans-Christen	Department of Applied Environmental Science (ITM) Stockholm University SE-10691 Stockholm
	Birgitta Noone	Department of Applied Environmental Science (ITM) Stockholm University SE-10691 Stockholm
Krvavec (Slovenia)	Marijana Murovec	Ministrstvo za okolje in prostor / Ministry of Environment and Spatial Planning Agencija RS za okolje / Slovenian Environment Agency Urad za stanje okolja / State of environment Office Sektor za kakovost zraka / Air Quality Division Vojkova 1b, 1001 Ljubljana, p.p
	Janja Turšič	Ministrstvo za okolje in prostor / Ministry of Environment and Spatial Planning Agencija RS za okolje / Slovenian Environment Agency Urad za stanje okolja / State of environment Office Sektor za kakovost zraka / Air Quality Division Vojkova 1b, 1001 Ljubljana, p.p

LIST OF CONTRIBUTORS (continued)

Station Country/Territory	Name	Address
	Mateja Gjerek	Ministrstvo za okolje in prostor / Ministry of Environment and Spatial Planning Agencija RS za okolje / Slovenian Environment Agency Urad za stanje okolja / State of environment Office Sektor za kakovost zraka / Air Quality Division Vojkova 1b, 1001 Ljubljana, p.p
Summit (Denmark)	Jacques Hueber	INSTAAR, Univ. of Colorado 1560, 30th Street UCB 450 Boulder, CO 80309 U.S.A.
	Detlev Helmig	INSTAAR, Univ. of Colorado 1560, 30th Street UCB 450 Boulder, CO 80309 U.S.A.
Lampedusa (Italy)	Salvatore Chiavarini	ENEA-UTPRA Via Anguillarese, 301 00123 Rome, Italy
	Damiano Sferlazzo	Italian National Agency for New Technologies, Energy and Sustainable Economic Development Laboratory for Observations and Measurements for Environment and Climate Station for Climate Observations Contrada Capo Grecale 92010 Lampedusa Italy
	Alcide di Sarra	Italian National Agency for New Technologies, Energy and Sustainable Economic Development Laboratory for Observations and Measurements for Environment and Climate Via Anguillarese, 301 00123 Rome, Italy
	Salvatore Piacentino	Italian National Agency for New Technologies, Energy and Sustainable Economic Development Laboratory for Observations and Measurements for Environment and Climate Via Principe di Granatelli 24, 90139 Palermo, Italy
	Tatiana Di Iorio	Italian National Agency for New Technologies, Energy and Sustainable Economic Development Laboratory for Observations and Measurements for Environment and Climate Via Anguillarese 301, 00123 Rome, Italy
	Francesco Monteleone	Italian National Agency for New Technologies, Energy and Sustainable Economic Development Laboratory for Observations and Measurements for Environment and Climate Via Principe di Granatelli 24, 90139 Palermo, Italy
Lamezia Terme (Italy)	Daniel Gullì	National Research Council, Institute of Atmospheric Sciences and Climate Area Industriale Comp. 15, 88046 Lamezia Terme
	Claudia Calidonna	National Research Council, Institute of Atmospheric Sciences and Climate Area Industriale Comp. 15, 88046 Lamezia Terme
	Ivano Ammoscato	National Research Council, Institute of Atmospheric Sciences and Climate Area Industriale Comp. 15, 88046 Lamezia Terme

LIST OF CONTRIBUTORS (continued)

Station Country/Territory	Name	Address
Lecce Environmental-Climate Observatory (Italy)	Adelaide Dinoi	National Research Council, Institute of Atmospheric Sciences and Climate Str. Prv. Lecce-Monteroni km 1.2 73100 Lecce
Capo Granitola (Italy)	Paolo Cristofanelli	ISAC-CNR, VIa Gobetti 101 - 40129 Bologna, Italy
	Ignazio Fontana	Istituto per lo studio degli impatti Antropici e Sostenibilità in ambiente marino via del Mare n. 3 - 91021 Torretta Granitola (TP) - Italy
	Giorgio Tranchida	Istituto per lo studio degli impatti Antropici e Sostenibilità in ambiente marino via del Mare n. 3 - 91021 Torretta Granitola (TP) - Italy
	Giovanni Giacalone	Istituto per lo studio degli impatti Antropici e Sostenibilità in ambiente marino via del Mare n. 3 - 91021 Torretta Granitola (TP) - Italy
Monte Cimone (Italy)	Jgor Arduini	University of Urbino, Dep. of Pure and Applied Sciences (DISPEA) piazza Rinascimento 6, 61029 Urbino - Italy
	Michela Maione	University of Urbino, Dep. of Pure and Applied Sciences (DISPEA) Istituto di Scienze Chimiche piazza Rinascimento 6, 61029 Urbino - Italy
	Paolo Cristofanelli	ISAC-CNR, VIa Gobetti 101 - 40129 Bologna, Italy
Finokalia (Greece)	Michel Ramonet	LSCE - CEA Saclay - Orme des Merisiers - 91191 Gif-sur-Yvette, France
Mace Head (Ireland)		
Begur (Spain)		
Ile Grande Pic du Midi Puy de Dôme (France)		
Pic du Midi (France)	Meyerfeld Yves	Laboratoire d'Aérologie 14 avenue Edouard Belin 31400 - TOULOUSE
	Gheusi Francois	Laboratoire d'Aérologie 14 avenue Eduard Belin 31400 Toulouse
Zugspitze-Schneefernerhaus (Germany)	Gabriele Frank	Deutscher Wetterdienst, German Meteorological Service Frankfurter Str. 135 63067 Offenbach Germany

LIST OF CONTRIBUTORS (continued)

Station Country/Territory	Name	Address
Hohenpeissenberg (Germany)	Dagmar Kubistin	German Meteorological Service Albin-Schwaiger-Weg 10 D-82383 Hohenpeissenberg Germany
	Robert Holla	German Meteorological Service Albin-Schwaiger-Weg 10 D-82383 Hohenpeissenberg Germany
	Matthias Lindauer	German Meteorological Service Albin-Schwaiger-Weg 10 82383 Hohenpeissenberg
	Christian Plass-Dulmer	German Meteorological Service Albin-Schwaiger-Weg 10 D-82383 Hohenpeissenberg Germany
	Jennifer Müller-Williams	German Meteorological Service Albin-Schwaiger-Weg 10 D-82383 Hohenpeissenberg Germany
Gartow Lindenberg (Germany)	Dagmar Kubistin	German Meteorological Service Albin-Schwaiger-Weg 10 D-82383 Hohenpeissenberg Germany
	Matthias Lindauer	German Meteorological Service Albin-Schwaiger-Weg 10 82383 Hohenpeissenberg
	Christian Plass-Dulmer	German Meteorological Service Albin-Schwaiger-Weg 10 D-82383 Hohenpeissenberg Germany
	Jennifer Müller-Williams	German Meteorological Service Albin-Schwaiger-Weg 10 D-82383 Hohenpeissenberg Germany
Wank Zugspitze-Gipfel (Germany)	Thomas Trickl	Fraunhofer-Institute for Atmospheric Environmental Research Kreuzeckbahnstr. 19 82467 Garmisch-Partenkirchen
Zeppelin Mountain (Ny Ålesund) (Norway)	Ove Hermansen	Norwegian Institute for Air Research P. O. Box 100 Instituttveien 18, N-2027 Kjeller, Norway
ANTARCTICA		
Syowa (Japan)	Shuji Aoki	Tohoku University Aoba 6-3, Aramaki, Aoba-ku, Sendai 980-8578
	Shinji Morimoto	Tohoku University Aoba 6-3, Aramaki, Aoba-ku, Sendai 980-8578
	Daisuke Goto	National Institute of Polar Research 10-3 Midori-cho, Tachikawa, Tokyo 190-8518

LIST OF CONTRIBUTORS (continued)

Station Country/Territory	Name	Address
Jubany (Argentina)	Horacio Rodriguez	Direcion Nacional del Antartico- Istituto Antartico Argentino, Buenos Aires, Argentina Dto. Ciencias de la Atmósfera Instituto Antártico Argentino DIRECCION NACIONAL DEL ANTARTICO Cerrito 1248 (1010) Capital Federal ARGENTINA
	Angelo Viola	National Research Council, Institute of Atmospheric Sciences and Climate via fosso del Cavaliere 100, Italy
King Sejong (Republic of Korea)	Haeyoung Lee	National Institute of Meteorological Sciences/Korea Meteorological Administration 33 Seohobuk-ro, Seogwipo, Jeju, 63568 Rep.of Korea
	Taejin Choi	Division of Polar Climate Research, KOPRI Get-Pearl Tower, 12 Gaetbeol-ro, Yeonsu-gu, Incheon, 406-840, Republic of Korea
Arrival Heights (New Zealand)	Sylvia Nichol	NIWA - Wellington Private Bag 14901, Kilbirnie, Wellington, 6241 301 Evans Bay Parade, Hataitai, Wellington 6021
	Gordon Brailsford	NIWA - Wellington Private Bag 14901, Kilbirnie, Wellington, 6241 301 Evans Bay Parade, Hataitai, Wellington 6021
Halley (United Kingdom of Great Britain and Northern Ireland)	Anna Jones	British Antarctic Survey
MOBILE		
CONTRAIL (Japan)	Hidekazu Matsueda	Meteorological Research Institute Nagamine 1-1, Tsukuba, Ibaraki 305-0052, Japan
	Toshinobu Machida	National Institute for Environmental Studies 16-2 Onogawa, Tsukuba 305-8506, Japan
	Yosuke Niwa	National Institute for Environmental Studies 16-2 Onogawa, Tsukuba 305-8506, Japan
Northern and western Pacific (Japan)	Shuji Aoki	Tohoku University Aoba 6-3, Aramaki, Aoba-ku, Sendai 980-8578
	Kentaro Ishijima	Oceanography and Geochemistry Research Department Meteorological Research Institute Japan Meteorological Agency 1-1 Nagamine, Tsukuba, Ibaraki 305-0052, Japan
	Shinji Morimoto	Tohoku University Aoba 6-3, Aramaki, Aoba-ku, Sendai 980-8578

LIST OF CONTRIBUTORS (continued)

Station Country/Territory	Name	Address
Aircraft (off the coast of Sendai Plain) over Japan between Sendai and Fukuoka (Japan)	Shuji Aoki	Tohoku University Aoba 6-3, Aramaki, Aoba-ku, Sendai 980-8578
	Taku Umezawa	National Institute for Environmental Studies 16-2 Onogawa, Tsukuba 305-8506, Japan
	Shinji Morimoto	Tohoku University Aoba 6-3, Aramaki, Aoba-ku, Sendai 980-8578
Ship between Ishigaki Island and Hateruma Island (Japan)	Shuji Aoki	Tohoku University Aoba 6-3, Aramaki, Aoba-ku, Sendai 980-8578
	Shinji Morimoto	Tohoku University Aoba 6-3, Aramaki, Aoba-ku, Sendai 980-8578
CONTRAIL (Japan)	Shuji Aoki	Tohoku University Aoba 6-3, Aramaki, Aoba-ku, Sendai 980-8578
	Taku Umezawa	National Institute for Environmental Studies 16-2 Onogawa, Tsukuba 305-8506, Japan
Soyo Maru, R/V Wakataka-Maru (Japan)	Tsuneo Ono	Fisheries Research Agency Hokkaido National Fisheries Research Institute 116 Katsurakoi, Kushiro 085-0802, Japan
Mirai, R/V (Japan)	Akihiko Murata	Physical and Chemical Oceanography Research Group, Global Ocean Observation Research Center, Research Institute for Global Change (RIGC) Japan Agency for Marine-Earth Science and Technology (JAMSTEC), 2-15, Natsushima, Yokosuka, Kanagawa, Japan 237-0061
Mirai, R/V (Japan)	Hisayuki Yoshikawa-Inoue	Hokkaido University Laboratory of Marine and Atmospheric GeochemistryGraduate School of Environmental Earth Science N10W5, Kita-ku, Sapporo 060-0810, Japan
MRI Research, Wellington Maru, R/V (Japan)	Masao Ishii	Meteorological Research Institute Nagamine 1-1, Tsukuba, Ibaraki 305-0052, Japan
Aircraft (over Japan and surroundings) (Japan)	Kazuhiro Tsuboi	Meteorological Research Institute 1-1, Nagamine Tsukuba Ibaraki 305-0052
INSTAC MRI Research, Hakuho Maru, R/V	Hidekazu Matsueda	Meteorological Research Institute Nagamine 1-1, Tsukuba, Ibaraki 305-0052, Japan
MRI Research, Kaiyo Maru, R/V MRI Research, Natushima, R/V MRI Research, Ryofu Maru, R/V	Masao Ishii	Meteorological Research Institute Nagamine 1-1, Tsukuba, Ibaraki 305-0052, Japan

LIST OF CONTRIBUTORS (continued)

Station Country/Territory	Name	Address
MRI Research, Ship observations (Japan)	Kazuhiro Tsuboi	Meteorological Research Institute 1-1, Nagamine Tsukuba Ibaraki 305-0052
Alligator liberty, M/V Keifu Maru, R/V Kofu Maru, R/V Ryofu Maru, R/V (Japan)	ENYO Kazutaka KADONO Koji	Japan Meteorological Agency 1-3-4 Ote-machi, Chiyoda-ku, Tokyo 100-8122 Japan Meteorological Agency 1-3-4 Ote-machi, Chiyoda-ku, Tokyo 100-8122
Aircraft (Western North Pacific) (Japan)	Kazuyuki SAITO	Japan Meteorological Agency 1-3-4 Otemachi Chiyoda-ku Tokyo 100-8122
NOPACCS - Hakurei Maru - WEST COSMIC - Hakurei Maru No.2 - (Japan)	General Environmental Technos	The General Environmental Technos Co., Ltd. (Old:Kansai Environmental Engineering Center, Co., Ltd.) 1-3-5, Azuchi machi, Chuo-ku, Osaka 541-0052, Japan
Santarem (Brazil)	Luciana Vanni Gatti	National Institute in Space Research Atmospheric Chemistry Laboratory Av. Prof. Lineu Prestes, 2242 Cidade Universitaria, Sao Paulo, SP- BRAZIL CEP 05508-900
Pacific Ocean (New Zealand)	Sylvia Nichol	NIWA - Wellington Private Bag 14901, Kilbirnie, Wellington, 6241 301 Evans Bay Parade, Hataitai, Wellington 6021
	Gordon Brailsford	NIWA - Wellington Private Bag 14901, Kilbirnie, Wellington, 6241 301 Evans Bay Parade, Hataitai, Wellington 6021
Aircraft: Orleans (France)	Michel Ramonet	LSCE - CEA Saclay - Orme des Merisiers - 91191 Gif-sur-Yvette, France

LIST OF CONTRIBUTORS (continued)

Station Country/Territory	Name	Address
NOAA /ESRL Flask Network		
Ushuaia (Argentina) Cape Grim (Australia) Ragged Point (Barbados) Arembepe Natal (Brazil) Alert Lac La Biche (Alberta) Mould Bay (Canada) Easter Island (Chile) Mt. Waliguan Shangdianzi (China) Hohenpeissenberg Ochsenkopf (Germany) Summit (Denmark) Assekrem (Algeria) Izaña (Tenerife) (Spain) Pallas (Finland) Amsterdam Island Crozet (France) Ascension Island Bird Island (South Georgia) Halley St. David's Head Tacolneston Tall Tower Tudor Hill (Bermuda) (United Kingdom of Great Britain and Northern Ireland) Hegyhatsal (Hungary)	Pieter Tans* Kirk Thoning* (CO_2) Ed Dlugokencky* Colm Sweeney* (CO_2, CH_4, N_2O and SF_6) Sylvia Michel** James White** Bruce H Vaughn** ($^{13}CH_4$, $^{13}CO_2$ and $C^{18}O_2$) Arlyn Andrews* (CO) Gabrielle Petron* (CO and H_2) Scott Lehman** Jocelyn Turnbull ($^{14}CO_2$)	(*) NOAA/ESRL R/GMD1 325 Broadway Boulder, CO 80305-3337 (**) Institute of Arctic and Alpine Research University of Colorado Campus Box 450 Boulder, CO 80309-0450 USA

LIST OF CONTRIBUTORS (continued)

Station Country/Territory	Name	Address
Bukit Kototabang (Indonesia)		
Mace Head (Ireland)		
Sede Boker (Israel)		
Storhofdi (Iceland)		
Lampedusa (Italy)		
Syowa (Japan)		
Mt. Kenya (Kenya)		
Christmas Island (Kiribati)		
Anmyeon-do Tae-ahn Peninsula (Republic of Korea)		
Plateau Assy Sary Taukum (Kazakhstan)		
Ulaan Uul (Mongolia)		
Dwejra Point (Malta)		
Kaashidhoo (Male Atoll) (Maldives)		
Mex High Altitude Global Climate Observation Center (Mexico)		
Gobabeb (Namibia)		
Ocean Station M Zeppelin Mountain (Ny Ålesund) (Norway)		
Baring Head Kaitorete Spit (New Zealand)		
Baltic Sea (Poland)		
Serreta (Terceira) (Portugal)		

LIST OF CONTRIBUTORS (continued)

Station Country/Territory	Name	Address
Constanta (Black Sea) (Romania)		
Tiksi (Russian Federation)		
Mahé (Seychelles)		
Lulin (Taiwan, Province of China)		
Argyle (ME) Atlantic Ocean Barrow (AK) Cape Kumukahi (HI) Cape Meares (OR) Cold Bay (AK) Drake Passage Grifton - Georgia Station (NC) Guam (Mariana Island) Key Biscane (FL) Kitt Peak (AZ) La Jolla (CA) Mauna Loa (HI) McMurdo Moody (TX) Niwot Ridge - T-van (CO) Ocean Station Charlie Olympic Peninsula (WA) Pacific Ocean Pacific-Atlantic Ocean Palmer Station Park Falls (WI) Point Arena (CA) Samoa (Cape Matatula) Sand Island Shemya Island South China Sea South Pole Southern Great Plains E13 (OK) St. Croix Trinidad Head (CA) Wendover (UT) West Branch (Iowa) Western Pacific (United States of America)		
Cape Point (South Africa)		
NOAA /ESRL HATS Network		
Ushuaia (Argentina) Cape Grim (Australia)	Debra J. Mondeel J. David Nance James W. Elkins Bradley D. Hall Geoffrey S. Dutton	Halocarbons and Other Atmosphere Trace Species Group (HATS)/NOAA/ESRL R/GMD1 325 Broadway Boulder, CO 80305-3337

LIST OF CONTRIBUTORS (continued)

Station Country/Territory	Name	Address
	Stephen A. Montzka	
Alert (Canada)		
Summit (Denmark)		
Mace Head (Ireland)		
Barrow (AK) Cape Kumukahi (HI) Grifton - Georgia Station (NC) Harvard Forest (MA) Mauna Loa (HI) Niwot Ridge - T-van (CO) Palmer Station Park Falls (WI) Samoa (Cape Matatula) South Pole Trinidad Head (CA) (United States of America)		

LIST OF CONTRIBUTORS (continued)

Station Country/Territory	Name	Address
CSIRO Flask Network		
Aircraft (over Bass Strait and Cape Grim) Cape Ferguson Cape Grim Casey Gunn Point Macquarie Island Mawson (Australia)	Zoë Loh Ray Langenfelds Paul Krummel	Commonwealth Scientific and Industrial Research Organisation (CSIRO) CSIRO Oceans and Atmosphere - Climate Science Centre Private Bag 1, Aspendale, Vic, Australia 3195
Alert Estevan Point (Canada)		
Lerwick (United Kingdom of Great Britain and Northern Ireland)		
Cape Rama (India)		
Mauna Loa (HI) South Pole (United States of America)		
ALE/GAGE/AGAGE Network		
Cape Grim (Australia)	Ray Wang Simon O'Doherty Dickon Young Paul Krummel Ray F. Weiss Stefan Reimann Martin Vollmer Chris Lunder Michela Maione Jgor Arduini	Advanced Global Atmospheric Gases Experiment Massachusetts Institute of Technology, Center for Global Change Science Building 54-1312 Cambridge, MA 02139-2307
Ragged Point (Barbados)		
Jungfraujoch (Switzerland)		
Adrigole Mace Head (Ireland)		
Monte Cimone (Italy)		
Gosan (Republic of Korea)		
Zeppelin Mountain (Ny Ålesund) (Norway)		
Cape Meares (OR) Samoa (Cape Matatula) Trinidad Head (CA) (United States of America)		

APPENDIX E LIST OF ABBREVIATIONS

ORGANIZATIONS:

AEMET	State Meteorological Agency of Spain (Spain)
AGAGE	Advanced Global Atmospheric Gases Experiment Science Team
AICH	Aichi Air Environment Division (Japan)
AIST	National Institute of Advanced Industrial Science and Technology (Japan)
AMERIFLUX	AmeriFlux Network (USA)
ANSTO	Australian Nuclear Science and Technology Organisation (Australia)
ARSO	Slovenian Environment Agency (Slovenia)
BAS	British Antarctic Survey (United Kingdom)
BLG	Bowling Lab Group, Terrestrial Biogeochemistry, Department of Biology, University of Utah (USA)
BMKG	Agency for Meteorology, Climatology and Geophysics (Indonesia)
CALTECH	California Institute of Technology, Division of Geological and Planetary Science (USA)
CHMI	Czech Hydrometeorological Institute (Czech Republic)
CMA	China Meteorological Administration (China)
CSIRO	Commonwealth Scientific and Industrial Research Organisation (Australia)
DMC	Dirección Meteorológica de Chile (Chile)
DWD	German Meteorological Service (Germany)
ECCC	Environment and Climate Change Canada (Canada)
ECN	Energy Research Centre of the Netherlands (Netherlands)
EMA	Egyptian Meteorological Authority (Egypt)
Empa	Swiss Federal Laboratories for Materials Science and Technology (Switzerland)
ENEA	Italian National Agency for New Technology, Energy and the Environment (Italy)
FMI	Finnish Meteorological Institute (Finland)
FRA	Fisheries Research Agency (Japan)
GAGE	Global Atmospheric Gases Experiment
GAW	Global Atmosphere Watch (WMO)
GERC	National Institute of Environmental Research (Republic of Korea)
HATS	Halocarbons and other Atmospheric Trace Species Group, NOAA/ESRL (USA)
HKO	Hong Kong Observatory (Hong Kong, China)
HMS	Hungarian Meteorological Service (Hungary)
HU	Hokkaido University (Japan)
IAA	Dirección Nacional del Antártico - Instituto Antartico Argentino, Buenos Aires, Argentina (Argentina)
IAFMC	Italian Air Force Mountain Centre (Italy)
IAFMS	Italian Air Force Meteorological Service (Italy)
ICOS	Integrated Carbon Observation System (European Union)
IGP	Instituto Geofísico del Perú (Peru)
IIA	CNR - Institute of Atmospheric Pollution Research (Italy)
IMKIFU	Fraunhofer - Institute for Atmospheric Environmental Research (Germany)
INMH	National Meteorological Administration (Romania)
INPE	National Institute in Space Research (Brazil)
INRNE	Institute for Nuclear Research and Nuclear Energy (Bulgaria)
INSTAAR	Institute of Arctic and Alpine Research, University of Colorado (USA)

IOEP	Institute of Environmental Protection - NRI (Poland)
ISAC	National Research Council, Institute of Atmospheric Sciences and Climate (Italy)
ITM	Department of Applied Environmental Science, Stockholm University (Sweden)
JAMSTEC	Japan Agency for Marine - Earth Science and Technology (Japan)
JMA	Japan Meteorological Agency (Japan)
KIT	Karlsruhe Institute of Technology (Germany)
KMA	Korea Meteorological Administration (Republic of Korea)
KMD	Kenya Meteorological Department (Kenya)
KRISS	Korea Research Institute of Standards and Science (Republic of Korea)
KSNU	Kyrgyz National University (Kyrgyzstan)
KUP	Physics Institute, Climate and Environmental Physics, University of Bern (Switzerland)
LA	Laboratoire d'Aérologie (France)
LAMP	Laboratoire de Météorologie Physique (France)
LSCE	Laboratoire des Sciences du Climat et de l'Environnement (France)
METRI	National Institute of Meteorological Research, KMA (Republic of Korea)
MGO	Voeikov Main Geophysical Observatory (Russian Federation)
MMD	Malaysian Meteorological Department (Malaysia)
MPI-BGC	Max-Planck Institute (MPI) for Biogeochemistry in Jena (Germany)
MRI	Meteorological Research Institute (Japan)
NAGOU	Nagoya University (Japan)
NCAR	U.S. National Center For Atmospheric Research (USA)
NEDO	New Energy and Industrial Technology Development Organization (Japan)
NEON	National Ecological Observatory Network (USA)
NIES	National Institute for Environmental Studies (Japan)
NILU	Norwegian Institute for Air Research (Norway)
NIST	National Institute of Standards and Technology (USA)
NIWA	National Institute of Water & Atmospheric Research Ltd. (New Zealand)
NOAA	National Oceanic and Atmospheric Administration (USA)
NOAA-CSD	Chemical Sciences Division, NOAA (USA)
NOAA/ESRL	Earth System Research Laboratory, NOAA (USA)
NPL	National Physical Laboratory (United Kingdom)
ONM	Office National de la Météorologie (Algeria)
OSAKAU	Osaka University (Japan)
PolyU	The Hong Kong Polytechnic University (Hong Kong, China)
PSU	Penn State University (USA)
RHUL	Royal Holloway University London (United Kingdom)
RIVM	National Institute of Public Health and the Environment (Netherlands)
RSE	Ricerca sul Sistema Energetico - RSE S.p.A. (Italy)
RUG	University of Groningen (RUG), Centre for Isotope Research (CIO) (Netherlands)
SAIPF	Center for Environmental Science in Saitama (Japan)
SAWS	South African Weather Service (South Africa)
SHIZU	Shizuoka University (Japan)
SIO	Scripps Institution of Oceanography (USA)
TU	Tohoku University (Japan)
UBAA	Federal Environment Agency Austria (Austria)
UBAG	German Environment Agency (Germany)
UBAG-SCHAU	Umweltbundesamt, Station Schauinsland (Germany)

UBAG/ZUG	Umweltbundesamt, Zugspitze GAW Station (Germany)
UEA	University of East Anglia (United Kingdom)
UHEI-IUP	University of Heidelberg, Institut für Umweltphysik (Germany)
UMLT	University of Malta (Malta)
UNIURB	University of Urbino, Dep. of Pure and Applied Sciences (DISPEA) (Italy)
UNIVBRIS	Atmospheric Chemistry Research Group School of Chemistry University of Bristol (United Kingdom)
UYRK	University of York (United Kingdom)
VNMHA	Viet Nam Meteorological and Hydrological Administration (Viet Nam)
WCC-Empa	World Calibration Centre (Empa)
WDCGG	World Data Centre for Greenhouse Gases (WMO)
WMO	World Meteorological Organization

ATMOSPHERIC SPECIES:

Be	beryllium
CCl_4	tetrachloromethane (carbon tetrachloride)
C_2Cl_4	tetrachloroethene (tetrachloroethylene)
CFC-11	trichlorofluoromethane (chlorofluorocarbon-11, CCl_3F)
CFC-12	dichlorodifluoromethane (chlorofluorocarbon-12, CCl_2F_2)
CFC-113	1,1,2-trichloro-1,2,2-trifluoroethane (chlorofluorocarbon-113, CCl_2FCClF_2)
CFCs	chlorofluorocarbons
CH_4	methane
$CHBr_3$	tribromomethane (bromoform)
CH_2Br_2	dibromomethane (methylene bromide)
CH_3Br	bromomethane (methyl bromide)
CH_3CCl_3	1,1,1-trichloroethane (methyl chloroform)
CH_3D	deuterated methane
CH_3I	iodomethane (methyl iodide)
$CHCl_3$	trichloromethane (chloroform)
CH_2Cl_2	dichloromethane (methylene chloride)
CH_3Cl	chloromethane (methyl chloride)
C_2HCl_3	trichloroethene (trichloroethylene)
CO	carbon monoxide
CO_2	carbon dioxide
COS	carbon oxide sulfide (carbonyl sulfide)
H_2	hydrogen
Halon-1211	bromochlorodifluoromethane ($CBrClF_2$)
Halon-1301	bromotrifluoromethane ($CBrF_3$)
Halon-2402	1,2-dibromo-1,1,2,2-tetrafluoroethane ($CBrF_2CBrF_2$)
HCFC-141b	1,1-dichloro-1-fluoroethane (hydrochlorofluorocarbon-141b, CH_3CCl_2F)
HCFC-142b	1-chloro-1,1-difluoroethane (hydrochlorofluorocarbon-142b, CH_3CClF_2)
HCFC-22	chlorodifluoromethane (hydrochlorofluorocarbon-22, $CHClF_2$)
HCFCs	hydrochlorofluorocarbons
HFC-134a	1,1,1,2-tetrafluoroethane (hydrofluorocarbon-134a, CH_2FCF_3)
HFC-152a	1,1-difluoroethane (hydrofluorocarbon-152a, CHF_2CH_3)
HFCs	hydrofluorocarbons
N_2O	nitrous oxide
NF_3	nitrogen trifluoride
PFCs	perfluorocarbons
Rn	radon

SF_6	sulfur hexafluoride
SO_2F_2	sulfuryl fluoride

UNITS:

ppm	parts per million
ppb	parts per billion
ppt	parts per trillion

Others:

TIC	total inorganic carbon
M/V	merchant vessel
R/V	research vessel

APPENDIX F LIST OF WMO/WDCGG PUBLICATIONS

DATA REPORTING MANUAL:

WDCGG No. 1	January	1991

WMO WDCGG DATA REPORT:

			(period of data accepted)				
WDCGG No. 2 Part A	October	1992	October	1990	~	August	1992
WDCGG No. 2 Part B	October	1992	October	1990	~	August	1992
WDCGG No. 3	October	1993	September	1992	~	March	1993
WDCGG No. 5	March	1994	April	1993	~	September	1993
WDCGG No. 6	September	1994	September	1993	~	March	1994
WDCGG No. 7	March	1995	April	1994	~	December	1994
WDCGG No. 9	September	1995	January	1995	~	June	1995
WDCGG No.10	March	1996	July	1995	~	December	1995
WDCGG No.11	September	1996	January	1996	~	June	1996
WDCGG No.12	March	1997	July	1996	~	November	1996
WDCGG No.14	September	1997	December	1996	~	June	1997
WDCGG No.16	March	1998	July	1997	~	December	1997
WDCGG No.17	September	1998	January	1998	~	June	1998
WDCGG No.18	March	1999	July	1998	~	December	1998
WDCGG No.20	September	1999	January	1999	~	June	1999
WDCGG No.21	March	2000	July	1999	~	December	1999
WDCGG No.23	September	2000	January	2000	~	June	2000
WDCGG No.25	March	2001	July	2000	~	December	2000

WMO WDCGG DATA CATALOGUE:

WDCGG No. 4	December	1993
WDCGG No.13	March	1997
WDCGG No.19	March	1999
WDCGG No.24	March	2001

WMO WDCGG DATA SUMMARY:

WDCGG No. 8	October	1995
WDCGG No.15	March	1998
WDCGG No.22	March	2000
WDCGG No.26	March	2002
WDCGG No.27	March	2003
WDCGG No.28	March	2004
WDCGG No.29	March	2005
WDCGG No.30	March	2006
WDCGG No.31	March	2007
WDCGG No.32	March	2008
WDCGG No.33	March	2009
WDCGG No.34	March	2010
WDCGG No.35	March	2011
WDCGG No.36	March	2012
WDCGG No.37	March	2013
WDCGG No.38	March	2014
WDCGG No.39	March	2015
WDCGG No.40	March	2016
WDCGG No.41	March	2017
WDCGG No.42	October	2018
WDCGG No.43	March	2020

WMO WDCGG CD-ROM: (period of data accepted)

CD-ROM No. 1	March	1995	October	1990	~	December	1994
CD-ROM No. 2	March	1996	October	1990	~	June	1995
CD-ROM No. 3	March	1997	October	1990	~	June	1996
CD-ROM No. 4	March	1998	October	1990	~	December	1997
CD-ROM No. 5	March	1999	October	1990	~	December	1998
CD-ROM No. 6	March	2000	October	1990	~	December	1999
CD-ROM No. 7	March	2001	October	1990	~	December	2000
CD-ROM No. 8	March	2002	October	1990	~	January	2002
CD-ROM No. 9	March	2003	October	1990	~	December	2002
CD-ROM No.10	March	2004	October	1990	~	December	2003
CD-ROM No.11	March	2005	October	1990	~	December	2004
CD-ROM No.12	March	2006	October	1990	~	December	2005
CD-ROM No.13	March	2007	October	1990	~	November	2006
CD-ROM No.14	March	2008	October	1990	~	November	2007

WMO WDCGG DVD: (period of data accepted)

DVD No. 1	March	2009	October	1990	~	November	2008
DVD No. 2	March	2010	October	1990	~	November	2009
DVD No. 3	March	2011	October	1990	~	November	2010
DVD No. 4	March	2012	October	1990	~	November	2011
DVD No. 5	March	2013	October	1990	~	November	2012
DVD No. 6	March	2014	October	1990	~	November	2013
DVD No. 7	March	2015	October	1990	~	November	2014
DVD No. 8	March	2016	October	1990	~	November	2015

REFERENCES

References

Aoki, S., T. Nakazawa, S. Murayama, and S. Kawaguchi, Measurements of atmospheric methane at the Japanese Antarctic station, Syowa, *Tellus*, **44B**, 273–281, 1992.

Bousquet, P., P. Ciais, J. B. Miller, E. J. Dlugokencky, D. A. Hauglustaine, C. Prigent, G. R. Van der Werf, P. Peylin, E.-G. Brunke, C. Carouge, R. L. Langenfelds, J. Lathière, F. Papa, M. Ramonet, M. Schmidt, L. P. Steele, S. C. Tyler, and J. White, Contribution of anthropogenic and natural sources to atmospheric methane variability, *Nature*, **443**, 439-443, https://doi.org/10.1038/nature05132, 2006.

Cleveland, W. S., and S. J. Devlin, Locally weighted regression: an approach to regression analysis by local fitting, *J. Amer. Statist. Assn.*, **83**, 596–610, 1988.

Conway, T. J., P. P. Tans, L. S. Waterman, K. W. Thoning, D. R. Kitzis, K. A. Masarie, and N. Zhang, Evidence for interannual variability of the carbon cycle from the National Oceanic and Atmospheric Administration/Climate Monitoring and Diagnostics Laboratory global air sampling network, *J. Geophys. Res.*, **99**, 22831–22855, 1994.

Dlugokencky, E. J., L. P. Steele, P. M. Lang, and K. A. Masarie, The growth rate and distribution of atmospheric methane, *J. Geophys. Res.*, **99**, 17021–17043, 1994.

Dlugokencky, E. J., B. P. Walter, K. A. Masarie, P. M. Lang, and E. S. Kasischke, Measurements of an anomalous global methane increase during 1998, *Geophys. Res. Lett.*, **28**, 499–502, 2001.

Dlugokencky, E. J., R. C. Myers, P. M. Lang, K. A. Masarie, A. M. Crotwell, K. W. Thoning, B. D. Hall, J. W. Elkins, and L. P. Steele, Conversion of NOAA atmospheric dry air CH_4 mole fractions to a gravimetrically prepared standard scale, *J. Geophys. Res.*, **110**, D18306, https://doi.org/10.1029/2005JD006035, 2005.

Duchon, C. E., Lanczos filtering in one and two dimensions, *J. Appl. Meteor.*, **18**, 1016-1022, 1979.

Friedlingstein, P., M. W. Jones, M. O'Sullivan, R. M. Andrew, J. Hauck, G. P. Peters, W. Peters, J. Pongratz, S. Sitch, C. Le Quéré, D. C. E. Bakker, J. G. Canadell, P. Ciais, R. B. Jackson, P. Anthoni, L. Barbero, A. Bastos, V. Bastrikov, M. Becker, L. Bopp, E. Buitenhuis, N. Chandra, F. Chevallier, L. P. Chini, K. I. Currie, R. A. Feely, M. Gehlen, D. Gilfillan, T. Gkritzalis, D. S. Goll, N. Gruber, S. Gutekunst, I. Harris, V. Haverd, R. A. Houghton, G. Hurtt, T. Ilyina, A. K. Jain, E. Joetzjer, J. O. Kaplan, E. Kato, K. Klein Goldewijk, J. Ivar Korsbakken, P. Landschützer, S. K. Lauvset, N. Lefèvre, A. Lenton, S. Lienert, D. Lombardozzi, G. Marland, P. C. McGuire, J. R. Melton, N. Metzl, D. R. Munro, J. E. M. S. Nabel, S. Nakaoka, C. Neill, A. M. Omar, T. Ono, A. Peregon, D. Pierrot, B. Poulter, G. Rehder, L. Resplandy, E. Robertson, C. Rödenbeck, R. Séférian, J. Schwinger, N. Smith, P. P. Tans, H. Tian, B. Tilbrook, F. N. Tubiello, G. R. van der Werf, A. J. Wiltshire, and S. Zaehle, Global Carbon Budget 2019, *Earth Syst. Sci. Data*, **11**, 1783–1838, https://doi.org/10.5194/essd-11-1783-2019, 2019.

Haan, D., and D. Raynaud, Ice core record of CO variations during the last two millennia: atmospheric implications and chemical interactions within the Greenland ice, *Tellus*, **50B**, 253–262, 1998.

Hall, B. D. (ed.), J. W. Elkins, J. H. Butler, S. A. Montzka, T. M. Thompson, L. Del Negro, G. S. Dutton, D. F. Hurst, D. B. King, E. S. Kline, L. Lock, D. MacTaggart, D. Mondeel, F. L. Moore, J. D. Nance, E. A. Ray, and P. A. Romashkin, Halocarbons and Other Atmospheric Trace Species, Section 5 in Climate Monitoring and Diagnostics Laboratory Summary Report No. 25, 1998–1999, R. S. Schnell, D. B. King, and R. M. Rosson (eds.), NOAA-CMDL, Boulder, CO., USA, 2001.

Hall, B. D., G. S. Dutton, and J. W. Elkins, The NOAA nitrous oxide standard scale for atmospheric observations, *J. Geophys. Res.*, **112**, D09305, https://doi.org/10.1029/2006JD007954, 2007.

IPCC, Climate Change 2013: The Physical Science Basis. Contribution of Working Group I to the Fifth Assessment Report of the Intergovernmental Panel on Climate Change [Stocker, T. F., D. Qin, G.-K. Plattner, M. Tignor, S. K. Allen, J. Boschung, A. Nauels, Y. Xia, V. Bex, and P. M. Midgley (eds.)]. Cambridge University Press, Cambridge, United Kingdom and New York, NY, USA, 2013.

Montzka S. A., G. S. Dutton, P. Yu, E. Ray, R. W. Portmann, J. S. Daniel, L. Kuijpers, B. D. Hall, D. Mondeel, C. Siso, J. D. Nance, M. Rigby, A. J. Manning, L. Hu, F. Moore, B. R. Miller, and J. W. Elkins, An unexpected and persistent increase in global emissions of ozone-depleting CFC-11, *Nature*, **557**, 413–417, https://doi.org/10.1038/s41586-018-0106-2, 2018.

Novelli, P. C., K. A. Masarie, and P. M. Lang, Distributions and recent changes of carbon monoxide in the lower troposphere, *J. Geophys. Res.*, **103**, 19015–19033, 1998.

Novelli, P. C., K. A. Masarie, P. M. Lang, B. D. Hall, R. C. Myers, and J. W. Elkins, Reanalysis of tropospheric CO trends: Effects of the 1997–1998 wildfires, *J. Geophys. Res.*, **108**, 4464, https://doi.org/10.1029/2002JD003031, 2003.

Prinn, R. G., R. F. Weiss, J. Arduini, T. Arnold, H. L. DeWitt, P. J. Fraser, A. L. Ganesan, J. Gasore, C. M. Harth, O. Hermansen, J. Kim, P. B. Krummel, S. Li, Z. M. Loh, C. R. Lunder, M. Maione, A. J. Manning, B. R. Miller, B. Mitrevski, J. Mühle, S. O'Doherty, S.

Park, S. Reimann, M. Rigby, T. Saito, P. K. Salameh, R. Schmidt, P. G. Simmonds, L. P. Steele, M. K. Vollmer, R. H. Wang, B. Yao, Y. Yokouchi, D. Young, and L. Zhou, History of chemically and radiatively important atmospheric gases from the Advanced Global Atmospheric Gases Experiment (AGAGE), *Earth Syst. Sci. Data*, **10**, 985–1018, https://doi.org/10.5194/essd-10-985-2018, 2018.

Tian, H., R. Xu, J. G. Canadell, R. L. Thompson, W. Winiwarter, P. Suntharalingam, E. A. Davidson, P. Ciais, R. B. Jackson, G. Janssens-Maenhout, M. J. Prather, P. Regnier, N. Pan, S. Pan, G. P. Peters, H. Shi, F. N. Tubiello, S. Zaehle, F. Zhou, A. Arneth, G. Battaglia, S. Berthet, L. Bopp, A. F. Bouwman, E. T. Buitenhuis, J. Chang, M. P. Chipperfield, S. R. S. Dangal, E. Dlugokencky, J. W. Elkins, B. D. Eyre, B. Fu, B. Hall, A. Ito, F. Joos, P. B. Krummel, A. Landolfi, G. G. Laruelle, R. Lauerwald, W. Li, S. Lienert, T. Maavara, M. MacLeod, D. B. Millet, S. Olin, P. K. Patra, R. G. Prinn, P. A. Raymond, D. J. Ruiz, G. R. van der Werf, N. Vuichard, J. Wang, R. F. Weiss, K. C. Wells, C. Wilson, J. Yang, and Y. Yao, A comprehensive quantification of global nitrous oxide sources and sinks, *Nature*, **586**, 248–256, https://doi.org/10.1038/s41586-020-2780-0, 2020.

WMO, Technical Report of Global Analysis Method for Major Greenhouse Gases by the World Data Center for Greenhouse Gases, GAW Report No. 184, WMO TD No. 1473, 2009.

WMO, WMO Global Atmosphere Watch (GAW) Implementation Plan: 2016-2023, GAW Report No.228, 2017.

WMO, WMO Greenhouse Gas Bulletin No.15, 2019.

WMO, 20th WMO/IAEA Meeting on Carbon Dioxide, Other Greenhouse Gases and Related Measurement Techniques (GGMT-2019), GAW Report No.255, 2020.

Worthy, D. E. J., I. Levin, N. B. A. Trivett, A. J. Kuhlmann, J. F. Hopper, and M. K. Ernst, Seven years of continuous methane observations at a remote boreal site in Ontario, Canada, *J. Geophys. Res.*, **103**, 15995–16007, 1998.

Zhao, C. L., P. P. Tans, and K. W. Thoning, A high precision manometric system for absolute calibrations of CO_2 in dry air, *J. Geophys. Res.*, **102**, 5885–5894, 1997.